MODELING CLIMATE CHANGE IMPACTS ON THE YIELD AND QUALITY OF CROPS

based on leaf photosynthesis with the acclimation to elevated CO_2

by Christian Jörg Biernath

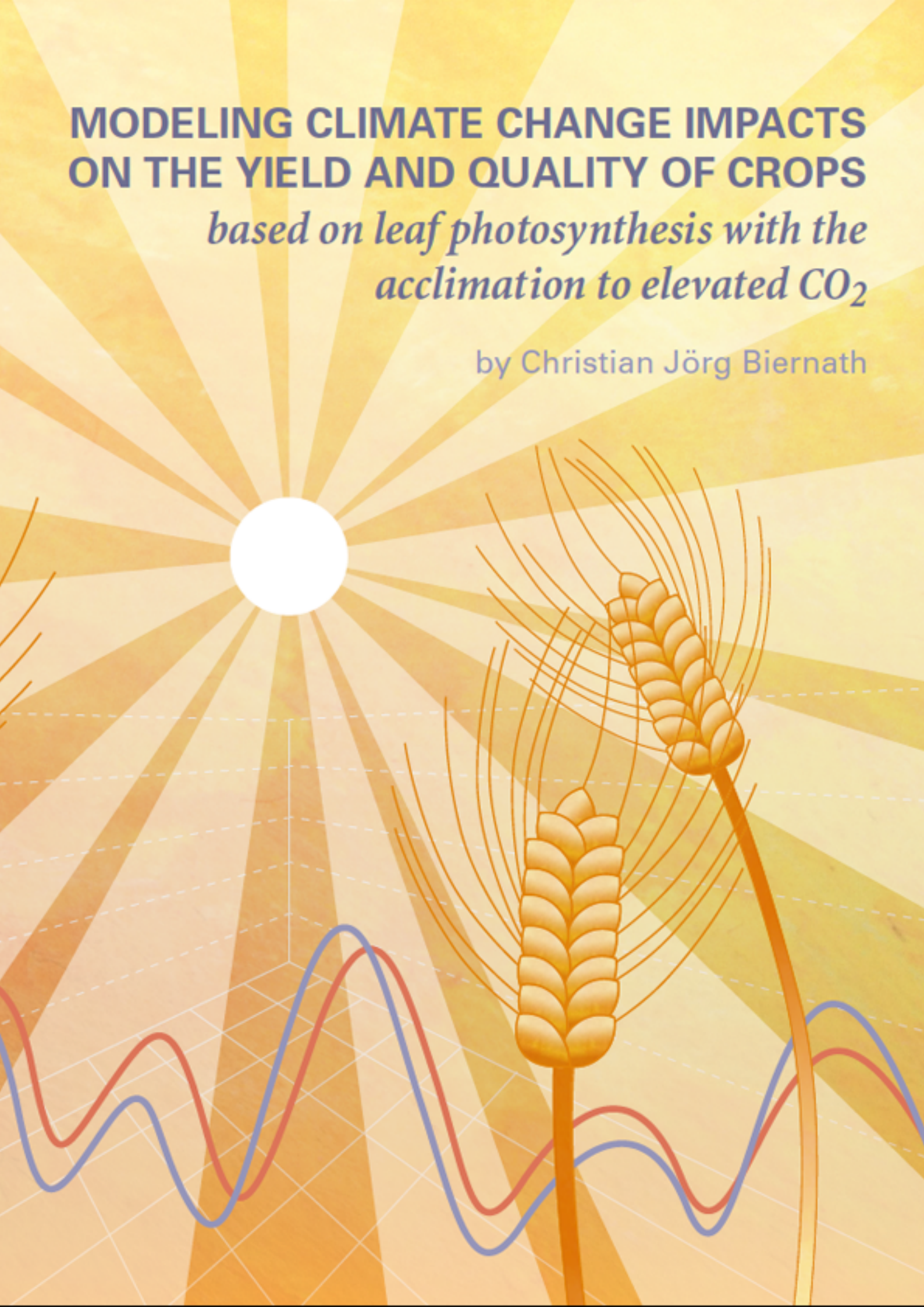

TECHNISCHE UNIVERSITÄT MÜNCHEN

Lehrstuhl für Bodenökologie

Modeling climate change impacts on the yield and quality of crops based on leaf photosynthesis with the acclimation to elevated CO_2

Christian Jörg Biernath

Vollständiger Abdruck der von der Fakultät Wissenschaftszentrum Weihenstephan für Ernährung, Landnutzung und Umwelt der Technischen Universität München zur Erlangung des akademischen Grades eines

Doktors der Naturwissenschaften

genehmigten Dissertation.

Vorsitzender: Univ.-Prof. Dr. U. Schmidhalter

Prüfer der Dissertation:

1. Univ.-Prof. Dr. J. C. Munch
2. Priv.-Doz. Dr. E. Priesack
   (Georg-August-Universität Göttingen)
3. Univ.-Prof. Dr. A. Fangmeier
   (Universität Hohenheim)

Die Dissertation wurde am 19.09.2012 bei der Technischen Universität München eingereicht und durch die Fakultät Wissenschaftszentrum Weihenstephan für Ernährung, Landnutzung und Umwelt der Technischen Universität München am 04.03.2013 angenommen.

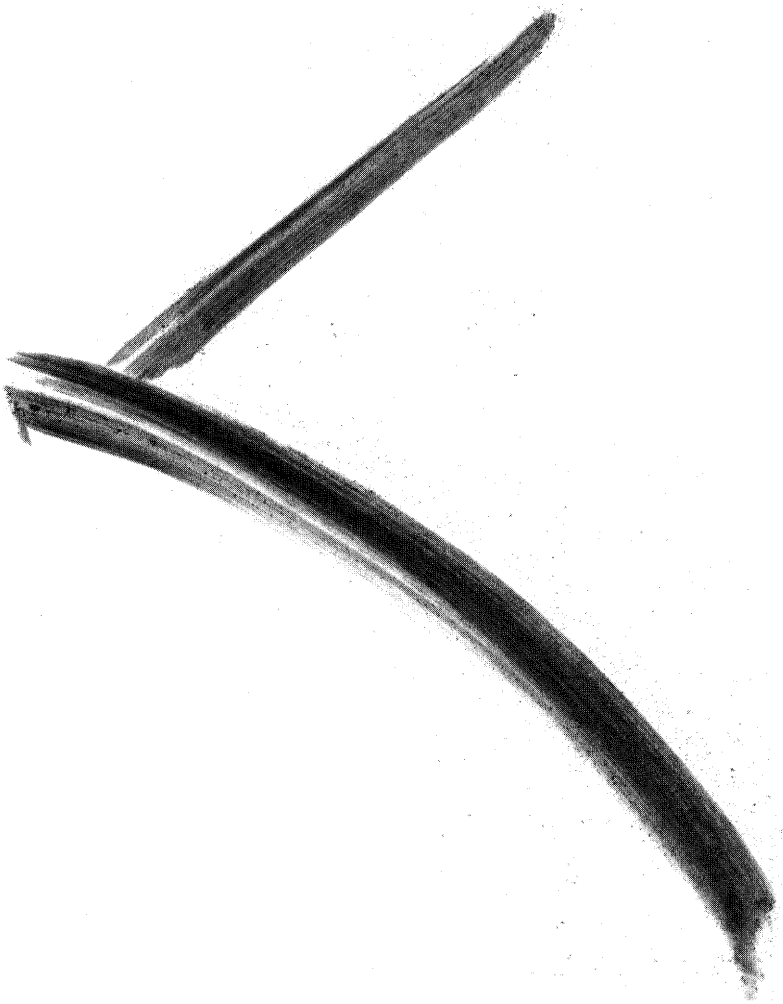

Inhaltsverzeichnis

Zusammenfassung

Diese Arbeit wurde im Rahmen des PAK-346 “Struktur und Funktionen von Agrarlandschaften unter dem Einfluss des globalen Klimawandels – Prozessverständnis und Prognosen auf der regionalen Skala” durchgeführt, welches von der Deutschen Forschungsgemeinschaft (DFG) finanziert wurde. Ziel der vorliegenden Arbeit war es das Wachstum von Kulturpflanzen hinsichtlich der Bestandesakklimation an die fortschreitende CO_2-Anreicherung der Atmosphäre mit Hilfe von Computermodellen zu simulieren. Zugrundeliegende Datensätze für die Simulationen und die Modellentwicklung bezüglich der Akklimation eines Pflanzenbestandes an eine erhöhte atmosphärische CO_2-Konzentration wurden im Rahmen der PAK-346 (Högy et al., 2012) und IMPETUS Projekte (Schütz und Fangmeier, 2001) erhoben und von Projektpartnern des PAK-346 zur Verfügung gestellt. Datenaufnahme und Entwicklung des in *Kapitel* 4 beschriebenen Lichtmodells wurden von Bittner et al. im Rahmen des DFG-Graduiertenkollegs 1086 “Die Bedeutung der Biodiversität für Stoffkreisläufe und biotische Interaktionen in temperaten Laubwäldern” geleistet.

Die vorliegende Arbeit fokussiert auf das Wachstum von Kulturpflanzenbeständen unter der Annahme, dass die oberirdischen Pflanzenteile eine homogene Grenzschicht zwischen Bodenoberfläche und Atmosphäre bilden. Die Arbeit leistet einen Beitrag zum Verständnis des Bestandeswachstums von Kulturpflanzen unter erhöhter atmosphärischer CO_2-Konzentration. Es zeigte sich, dass der Komplexitätsgrad des Lichtmodells entscheidend für die Simulation von Wachstumsdynamiken ist, wenn diese Dynamiken von der Interaktion mehrerer Umweltfaktoren abhängen (z.B. pflanzenverfügbares Wasser und atmosphärische CO_2-Konzentration). Ferner zeigt sich die Notwendigkeit Bestandesakklimation an steigende atmosphärische CO_2-Konzentrationen als dynamischen Prozess zu verstehen, der die Physiologie sowohl auf biochemischer als auch auf morphologischer Ebene beeinflusst. Aufgrund der starken Verflechtung beider Ebenen beim Akklimationsprozess können diese Ebe-

nen nicht isoliert betrachtet werden. Der pflanzeninterne Stickstoffkreislauf sollte so modelliert werden, dass ein Zielkonflikt zwischen der Verwendung des mobilen Stickstoffs für das Wachstum und für die Optimierung des Photosyntheseapparates ermöglicht wird. Bei den Simulationen des Pflanzenwachstums unter erhöhter CO_2-Konzentration zeigte sich eine erhöhte Effizienz des photosynthetisch aktiven Stickstoffs durch eine ökonomische Stickstoffumverteilung innerhalb des Bestandes. Die Akklimation führt zu einem stärker reduzierten Wurzelsystem, niedrigeren Wasser- und Nährstoffaufnahmen, sowie weiteren $\frac{Kohlenstoff}{Stickstoff}$-Verhältnissen in den bodennahen Blättern des Bestandes (verfrühte Seneszenz) und im Korn als dies bei einer Equilibriumannahme für die Tiefenverteilung photosynthetisch aktiven Stickstoffs im Bestand der Fall wäre.

Die Arbeit ist in zwei Hauptteile untergliedert, die Modellevaluation in *Abschnitt* 1 und die Modellentwicklung in *Abschnitt* 2. In *Abschnitt* 1 wurde das Potential verschiedener Pflanzenwachstumsmodelle für Kulturpflanzenbestände analysiert um das Wachstum von Sommerweizen (*Triticum aestivum* L.) unter verschiedenen atmosphärischen CO_2-Konzentrationen und unterschiedlichen Bodenbedingungen zu simulieren. Die Ergebnisse aus *Abschnitt* 1 bildeten die Grundlage für die Modellentwicklung in *Abschnitt* 2, in dem das Pflanzenwachstumsmodell GECROS (Yin and van Laar, 2005) um ein dynamisches Umsatzmodell des photosynthetisch aktiven Stickstoffs (Rubisco, N_p) nach einem Modellansatz von Thornley (1998, 2004) erweitert wurde. Im Sinne dieses Modells unterliegen Synthese und Abbau des photosynthetisch aktiven Stickstoffs einem kontinuierlichen Kreislauf, bei dem der N_P-Aufbau vom Lichtangebot und der Verfügbarkeit von Aminosäuren abhängt und der Abbau direkt proportional zum N_P-Gehalt in Abhängigkeit von der Blatttemperatur erfolgt. Die durch den N_P-Abbau freiwerdenden Aminosäuren werden vor der N_P-Neusynthese einem pflanzeninternen Stickstoffkreislauf zur Verfügung gestellt. Es entsteht dadurch ein Zielkonflikt einerseits zwischen i) der Verwendung der Aminosäuren für die N_P-Neusynthese und dessen effizienterer Umverteilung in die Blätter und andererseits ii) der Verwendung der Aminosäuren für den Aufbau neuer Biomasse. Beide Strategien können prinzipiell die Photosyntheseleistung der Pflanze optimieren, da im ersten Fall das Licht im Bestand besser genutzt wird und im zweiten Fall die assimilierende Oberfläche vergrößert wird, über die Licht absorbiert werden kann. Die Akklimation homogener Pflanzenbestände an eine CO_2-angereicherte Atmosphäre wird im Rahmen dieser Arbeit folglich sowohl durch eine Akklimation des Photosyntheseapparates als auch einer strukturellen Anpassung

durch Biomassenzuwachs modelliert. Erstmals wurde dafür das theoretische Modell von Thornley (1998, 2004) zur Beschreibung der Akklimation der Pflanze an eine erhöhte atmosphärische CO_2-Konzentration durch eine dynamische Umverteilung des Stickstoffs alternativ für Wachstum und Photosynthese mit dem mechanistischen Farquhar-Photosynthesemodell (Farquhar et al., 1980) gekoppelt. Das neue Photosynthesemodell wurde in das Pflanzenzenwachstumsmodell GECROS eingebaut und als Pflanzenwachstumsmodellkomponente im Agrarökosystemmodellframework Expert-N (Priesack et al., 2006, Priesack, 2006) ausgeführt. Die Funktionalität des neuen Modells wurde anhand von Messdaten aus CO_2-Anreicherungsversuchen getestet.

Als integrales Element eines Pflanzenwachstumsmodells kann das Modell auch bei steigender atmosphärischer CO_2-Konzentration für Ertragsprognosen, Dünge- und Bewässerungsempfehlungen im Rahmen der landwirtschaftlichen Praxis verwendet werden. Ein weiteres Einsatzgebiet des Modells ist die Pflanzenzüchtung. Die Stärken des GECROS Modells, Interaktionen von Genotyp, Boden, Klima und Management abzubilden, wurden bezüglich der Akklimation an zukünftige Klimate mit erhöhter atmosphärischer CO_2-Konzentration erweitert. Zum einen ermöglicht dies die Simulation des Wachstums vorhandener Kulturpflanzenarten und -sorten unter zukünftigen Klimabedingungen. Zum anderen ließen sich an die CO_2-angereicherten Klimate der kommenden Jahrzehnte (IPCC, 2012) angepasste Modellgenotypen generieren, und bezüglich der Ertragserwartungen und -qualität unter einer Vielzahl von Bodenbedingungen virtuell testen. Diese Modellgenotypen können dazu beitragen, die Kosten für aufwändige Züchtungsversuche unter multifaktoriellen Bedingungen zu reduzieren und so das klassische Potenzial der Pflanzenzüchtung erweitern.

Die Anwendung des neuen Modells auf Sommerweizendaten eines Mini-FACE Versuchs führte bei erhöhter atmosphärischer CO_2-Konzentration zu einer effizienteren Umverteilung des photosynthetisch aktiven Stickstoffs innerhalb des Bestandes im Vergleich zu Simulationen mit dem unmodifizierten GECROS Modell, welches grundsätzlich eine exponentielle N_P-Verteilung über die Bestandestiefe basierend auf dem Gesamtstickstoffgehalt der grünen Blätter annimmt. Darüber hinaus zeigt sich, dass die Blatttemperatur den N_P-Abbau und folglich die Akklimation des Bestandes an eine erhöhte atmosphärische CO_2-Konzentration beeinflusst. Detaillierte Kenntnisse über N_P-Abbauraten und den Einfluss der Blatttemperatur würden die Parametrisierung des neuen Modells unterstützen und die Qualität der Simulationsergebnisse erhöhen. Allerdings muss dabei berücksichtigt werden, dass

die Aggregierung aller photosynthetisch aktiven Proteine (z.B. Rubisco, Thyllakoide und sonstige lösliche Proteine) in N_P eine Vereinfachung der Physiologie darstellt, deren Abbauraten sich bezüglich der Temperatur möglicherweise unterscheiden. Auch gilt es zu berücksichtigen, dass art- und sortenspezifische Unterschiede bezüglich des Blatttemperatureffekts auf die N_P-Umsatzraten möglich sind. Das neue Modell zeigt, dass die effizientere Nutzung des assimilierten Stickstoffs unter CO_2-angereicherten Bedingungen die Ausbildung geringerer Wurzelbiomassen erlaubt, da relativ weniger Nährstoffe aufgenommen werden müssen, um mehr oberirdische Biomasse zu produzieren. Dieses Ergebnis basiert auf der Modellannahme, dass das $\frac{Spross}{Wurzel}$-Biomasseverhältnis dem $\frac{Kohlenstoff}{Stickstoff}$-Verhältnis in der Gesamtpflanze entspricht (Priesack und Gayler, 2009). Die vom Modell prognostizierte Verschiebung des $\frac{Spross}{Wurzel}$-Biomasseverhältnisses zugunsten des Sprosses bei atmosphärischer CO_2-Anreicherung würde somit zu geringeren Kohlenstoffeinträgen in die Böden führen, als dies Modelle ohne dynamisches Photosyntheseakklimationsmodell für das Kulturpflanzenwachstum unter der prognostizierten Erhöhung der atmosphärischen CO_2-Konzentrationen der kommenden Jahrzehnte (IPCC, 2012) vorhersagen würden.

Es zeigt sich, dass Pflanzenwachstumsmodelle entscheidend verbessert werden können, wenn die Lichtabsorption durch eine dynamische Rubiscoverteilung im Bestand abgebildet wird. Entscheidende Vorarbeiten, die die Bedeutung einer adäquaten Modellierung der Lichtverteilung im Bestand belegen, wurden im Rahmen des Modellvergleichs in *Kapitel* 2 dieser Arbeit gelegt. Die Arbeit von S. Bittner (2012, *Kapitel* 4), an der C. J. Biernath im Rahmen der vorliegenden Arbeit als Koautor beteiligt war, weist Wege auf, die Lichtverteilung im Bestand adäquat abzubilden, um Kerngrößen des Pflanzenwachstums zu simulieren. Da sich Lichtverteilung und N_P-Verteilung im Bestand interaktiv beeinflussen, sind die Arbeiten aus *Kapitel* 3 und *Kapitel* 4 dieser Arbeit die Basis für zukünftige Forschungsarbeiten, in denen ein Verfahren zur Berechnung der Licht- und N_P-Verteilung im Bestand implementiert und getestet werden kann, das die dynamische Abhängigkeit von Licht- und N_P-Verteilung abbildet. Da sich Licht- und Rubiscoverteilungen unmittelbar gegenseitig bedingen (Lichtextinktion, -streuung und -transmissivität hängen im Wesentlichen auch vom N_P-Gehalt der Blätter ab) ist zu erwarten, dass durch diesen Ansatz eine weitere Verbesserung des Prozessverständnisses bezüglich der Akklimation von Pflanzen an variable Umweltbedingungen erzielt werden könnte.

Summary

This thesis was part of the joint research project PAK-346 “Structure and Functions of Agricultural Landscapes under Global Climate Change – Processes and Projections on a Regional Scale” funded by the German research foundation (DFG). The aim of the study was to simulate crop acclimation with atmospheric CO_2 enrichment using computer models. The underlying data sets for model development, model calibration, and simulations, were collected within the frameworks of the PAK-346 (Högy et al., 2012) and IMPETUS (Schütz and Fangmeier, 2001) projects and were provided by the project partners of PAK-346. The data collection and development of the light model (Bittner et al., 2012) that is described in *chapter* 4 was part of the DFG research training group 1086 “The role of biodiversity for biogeochemical cycles and biotic interactions in temperate deciduous forests”.

The present study focuses on the growth of crop canopies. The basic assumption of the study is that the above-ground biomass is a homogenous layer between the soil surface and the atmosphere. The study contributes to understanding the mechanisms of canopy growth under atmospheric CO_2 enrichment. It was shown that the degree of complexity of the light model was essential to simulate the growth dynamics if these dynamics depend on the interactions of various environmental factors (such as the water available to plant and the atmospheric CO_2 enrichment). Moreover, the results of the study demonstrate the need to describe canopy acclimation to atmospheric CO_2 enrichment as a dynamic process that affects both the morphological and physiological levels of the plant. Because both levels are strongly interwoven during the acclimation process, both levels should not be described independent from each other. Therefore, the plant internal nitrogen cycle needs to be modeled in such a way that a trade-off for the use of newly assimilated or remobilized nitrogen occurs between the canopy growth and optimization of the photosynthetic apparatus. The simulations showed that plant acclimation increased the efficiency

of the photosynthetic apparatus through a more economical redistribution of the photosynthetic active nitrogen within the canopy. The consequences were a reduced root system, lower water and nutrient assimilation, and a wider $\frac{carbon}{nitrogen}$ ratio in the lower leaves of the canopy (early senescence) and in yield.

The work consists of two main parts: the model evaluation in *section* 1 and the model development in *section* 2. In *section* 1, the potential of various crop growth models to simulate spring wheat (*Triticum aestivum* L.) growth for various soil properties and at different atmospheric CO_2 concentration levels is examined. The results of *section* 1 formed the basis for the model development in *section* 2, whereby the GECROS crop growth and development model (Yin and van Laar, 2005) was extended using a dynamic turnover model of the photosynthetic active nitrogen (Rubisco, N_P) following a nitrogen turnover model that was suggested by Thornley (1998, 2004). In the sense of this model, the N_P dynamics in the green leaves follow a continuous cycle of synthesis and degradation: synthesis depends on the availability of amino acids and the intercepted amount of light, and degradation is directly proportional to the N_P content and may be affected by the leaf temperature. After the degradation of N_P the remobilized amino acids are provided to the plant's internal nitrogen cycle, and this allocation causes a trade-off in the use of amino acids i) either for N_P synthesis and its efficient redistribution within the canopy to optimize the photosynthetic apparatus or ii) for growth. In principle, either strategy can improve the carbon assimilation rates of the plant. The first case would increase the efficiency of light use, whereas the second case would increase the green leaf area for light harvesting. Within the context of this work, the acclimation of homogenous canopies to atmospheric CO_2 enrichment is described as inextricably linked to the acclimation of both the photosynthetic apparatus and the growth of crop organs. To achieve this result for the first time, the theoretical model of Thornley, describing crop acclimation to elevated CO_2 by the dynamic redistribution of nitrogen alternatively for photosynthesis and growth was coupled to the mechanistic Farquhar (1980) photosynthesis model. The new photosynthesis model was integrated into GECROS, which could optionally be selected as the crop model for the agro-ecosystem model framework Expert-N (Priesack et al., 2006; Priesack, 2006), and tested using the spring wheat growth data from atmospheric CO_2 enrichment experiments.

As an integral element of a crop growth model, the new photosynthesis model can be used for simulations applied for research, for the forecast of yields, and to obtain

recommendations of fertilizer applications and irrigation in agricultural practice. Moreover, the model could possibly be used for plant breeding. The strengths of the GECROS model to simulate the dynamic interactions of the genotype, soil, climate, and management have now been extended to canopy acclimation to atmospheric CO_2 enrichment. First, it is now possible to simulate crop growth of recent crop species and varieties with respect to the proposed climate changes, including atmospheric CO_2 enrichment for the coming decades (IPCC, 2012). Second, virtual model genotypes could be generated and tested to analyze the potential crop growth and yield traits against a wide range of regional soil characteristics and climate change scenarios. This procedure could reduce the need for costly and labor-intensive multifactorial plant breeding experiments and could thus increase the potential of classical plant breeding techniques.

The application of the new model to the spring wheat data derived from a Mini-FACE experiment showed a more economical redistribution of N_P within the canopy compared with the simulations using the unmodified GECROS model, which assumes an exponentially declining N_P distribution with canopy depth, as based on the total leaf nitrogen content. The more economical use of assimilated nitrogen allows a reduction of root biomass under elevated atmospheric CO_2 conditions because comparably fewer nutrients need to be assimilated to produce more above-ground biomass. This result is based on the model assumption in GECROS that the $\frac{shoot}{root}$ ratio of biomass equals the $\frac{carbon}{nitrogen}$ ratio of the entire plant (Priesack and Gayler, 2009). The simulations of wider $\frac{shoot}{root}$ ratios of plant biomass predict a reduced carbon sequestration into the soil in an enriched atmospheric CO_2 environment compared with the simulations derived from models without a dynamic crop acclimation model. Moreover, the simulations showed that the leaf temperature could affect the N_P degradation and, thus, crop acclimation to atmospheric CO_2 enrichment. The quality of the simulations could be improved with detailed knowledge about the mechanisms of N_P turnover. For example, knowledge about the N_P degradation response to leaf temperature, which is most likely crop or variety specific, would reduce the parameterization effort.

It has been shown that the acclimation modeling of crop growth can be improved if the light absorption and carbon assimilation in the canopy is described as a dynamic process of the N_P redistribution within the canopy (*chapter* 3). A preliminary step to show the importance of adequately modeling the light distribution within the canopy was the model comparison study in *chapter* 2. The work of S. Bittner (sub-

mitted; *chapter* 4), in which C. J. Biernath was involved as a co-author, indicates new ways to simulate light extinction and distribution mechanistically within the canopy to model the key parameters of crop growth. Because light and N_P distributions affect one another (light extinction, scattering, and transmissivity are directly affected by the N_P content), the work presented in *chapter* 3 and *chapter* 4 provide a basis for future research to implement and evaluate the dynamic dependence of the light and N_P distributions in the canopy. Such a model could further improve our understanding of crop acclimation to changing environmental conditions.

1 Einleitung

1.1 Abhängigkeit landwirtschaftlicher Erträge von der Umwelt

Die Ernährung der bis 2050 auf mindestens 8 Mrd. Menschen anwachsenden Weltbevölkerung (BpB, 2010) kann nur gewährleistet werden, wenn die landwirtschaftlichen Erträge - bei gleichbleibender oder verbesserter Qualität - im selben Maße oder stärker steigen als durchschnittlich um 2,2% pro Jahr (Anstieg der weltweiten Getreideerträge von 1961 bis 2010, FAOSTAT, 2012). Die Qualität, also die biochemische Zusammensetzung, des Ernteprodukts bestimmt, ob agrarische Rohstoffe für den tierischen und menschlichen Verzehr geeignet sind, den Nährwert, die Koch-, Back-, Brau- und Mahleigenschaften, ob sie sich zu qualitativ hochwertigeren Produkten veredeln lassen und die optische Erscheinung (Wang et al., 2011). Ferner bestimmt die biochemische Zusammensetzung auch die sensorischen Eigenschaften und die Lagerungsfähigkeit der Produkte.

Die Quantität und Qualität von Erträgen ist in erster Linie maßgeblich vom Klima und den Bodeneigenschaften abhängig. Darüber hinaus können Erträge und deren Qualität durch adequates landwirtschaftliches Management positiv beeinflusst werden. Mögliche Maßnahmen sind die Bekämpfung von Pathogenen und von Ackerbegleitflora, Bodenbearbeitung, Bewässerungstechniken und Pflanzenzüchtung. Die Möglichkeit, mit Hilfe des Haber-Boschverfahrens Mineraldünger in fast unbegrenzter Menge zu produzieren, der Einsatz chemischer Pestizide auf Grundlage massiven Einsatzes fossiler Energien und Fortschritte auf dem Gebiet der Pflanzenzüchtung revolutionierten die Landwirtschaft nach dem zweiten Weltkrieg. Zusammen mit fortschreitender Technisierung wurde die globale Nahrungsmittelproduktion im Zuge der sogenannten “grünen Revolution” bis Mitte der 1990er Jahre um das 3,5fache gesteigert (Kindell und Pimentel, 1994). Im gleichen Zeitraum stieg die Nutzung fos-

siler Energien für die landwirtschaftliche Produktion um das 50-100fache an (Kindell und Pimentel, 1994). Kindell und Pimentel (1994) zeigen, dass in den USA 10 Joule fossiler Energien eingesetzt werden um ein Joule Nahrungsmittel zu produzieren, wenn man die gesamte Produktionskette inklusive Transport und Verpackung der fertigen Nahrungsmittel berücksichtigt. Somit sind das hohe Niveau und die niedrigen Preise landwirtschaftlicher Produktion an die Verfügbarkeit fossiler Energien geknüpft.

Einige Umweltfaktoren, die das Pflanzenwachstum beeinflussen, z.B. die Zusammensetzung atmosphärischer Gase oder die Sonneneinstrahlung, lassen sich unter Freilandbedingungen nur schwer manipulieren. Die atmosphärische CO_2-Konzentration steigt seit Beginn der Industrialisierung durch die Nutzung exzessiver Mengen fossiler Energien in Industrie, Hochertragslandwirtschaft und in allen menschlichen Lebensbereichen, an. Diese Anreicherung der Atmosphäre mit CO_2 und weiteren klimarelevanten Gasen wird im allgemeinen für die derzeit beobachtete beschleunigte Klimaveränderung, die sich in einer steigenden globalen Jahresmitteltemperatur, veränderter atmosphärischer Zirkulation und sich regional stark verschiebender Häufigkeit und Dauer von Niederschlagsereignissen und Niederschlagsmengen äußert, verantwortlich gemacht (Siegenthaler et al., 2005). Auf Pflanzen wirkt sich eine CO_2-Anreicherung der Atmosphäre direkt und indirekt aus: i) direkt, da Pflanzen Zucker aus atmosphärischem CO_2 photosynthetisch assimilieren und eine höhere atmosphärische CO_2-Konzentration den Diffusionsgradienten zwischen Atmosphäre und den Mesophyllzellen im Blatt erhöht und ii) indirekt, da das Pflanzenwachstum von Temperaturen und Niederschlägen abhängt. Diese Veränderungen dürften sich auch auf die Menge und Qualität landwirtschaftlicher Erträge auswirken und folglich die menschliche Ernährung beeinflussen (Stafford, 2007). Die Mechanismen des CO_2-Effekts auf das Pflanzenwachstum sind allerdings noch nicht ausreichend untersucht.

1.2 Atmosphärische CO_2-Anreicherung

Die Hauptbestandteile der heutigen, irdischen Atmosphäre sind H_2O und Ar, sowie N_2 und O_2. Diese vier Komponenten machen zusammen mehr als 99,9% aus. Weitere zumeist als Spurengase bezeichnete Gase sind CO_2, Ne, He, CH_4, K_r, CO_2, Xe, O_3, N_2O, NH_3, SO_2, NO, NO_2, H_2 und organische Halogenverbindungen. Einige dieser Gase werden als Treibhausgase bezeichnet, deren Abundanz den Wärmehaushalt

der Erde beeinflusst (Kraus, 2004, Manier, 2004). Somit hat die Zusammensetzung der Atmosphäre einen entscheidenden Einfluss auf das Klima (Collins et al., 2006, Myhre et al., 1998, Revelle und Suess, 1957).

Zu den Treibhausgasen zählen H_2O, CO_2, N_2O, CH_4 und organische Halogenverbindungen. Dabei führt eine Anreicherung eines Treibhausgases gewöhnlich zu einer Erhöhung der mittleren globalen Temperatur der bodennahen Luftschicht. Diese Gase lassen die eintreffende Sonnenstrahlung passieren, reflektieren jedoch die von der Erde abgestrahlte Wärmestrahlung (Ramaswamy et al., 2011). Auf Basis der klassischen Theorie des Treibhauseffektes erhöht dieser natürliche Treibhauseffekt die Strahlungsgleichgewichtstemperatur der Erde von -18°C auf die mit +15°C geschätzte mittlere Temperatur der bodennahen Luftschicht der Erde (Kraus, 2004, Schönwiese, 1995, Firor, 1993, Kondratyev und Moskalenko, 1984). Im Laufe der letzten 10000 Jahre schwankte die mittlere Temperatur der bodennahen Luftschicht so um maximal ±1°C (KSK 2020Plus, 2011). Eine Anreicherung der Atmosphäre mit Treibhausgasen hat eine Erhöhung der mittleren globalen Temperatur der bodennahen Luftschicht zur Folge und eine positive Rückkopplung aufgrund der temperaturabhängig erhöhten Wasserdampfbildung über den Ozeanen, wodurch der Treibhauseffekt zusätzlich verstärkt wird (Firor, 1993).

Durch photosynthetische Kohlenstofffixierung wurde der Ur-Erdatmosphäre, die nahezu ausschließlich aus CO_2 bestand, kontinuierlich CO_2 entzogen und zeitweise auf eine Konzentration unter 0,03% (≡ 300 ppm) abgereichert (Abbildung 1.1A). Fixierter Kohlenstoff wird nach dem Absterben der Pflanzen nicht unmittelbar in die Atmosphäre zurückgeführt, sondern temperatur- und ökosystemabhängig mehr oder weniger lang in Nahrungsnetzen, Böden, Seen und kohlenstoffreichen geologischen Lagerstätten konserviert. Diese Abreicherung der atmosphärischen CO_2-Konzentration lässt sich nach Schlitter und Wildner (2001) in mehrere Phasen gliedern. Vor ca. 5-3,5 Mrd. Jahren war die Hauptkomponente der Atmosphäre unseres Planeten CO_2. In dieser Zeit entwickelte sich die Kohlenstoffassimilation und das Enzym Rubisco, durch dessen Aktivität der Atmosphäre zunehmend CO_2 entzogen wurde. So wurde bereits vor dem Auftreten der ersten Landpflanzen die Atmosphäre auf unter 10% CO_2 abgereichert und gleichzeitig mit O_2 angereichert. Die Evolution der Landpflanzen im Silur vor ca. 440-400 Mio. Jahren führte zu einer weiteren Abreicherung auf ca. 0,5% (≡ 5000 ppm). Mit der Ausbreitung der Farnwälder vor 350 Mio. Jahren reduzierte sich die CO_2-Konzentration auf 2000 ppm. Während der Gondwanavereisung sank die CO_2-Konzentration erstmals auf unter

300 ppm, um nach dem Ende der Kaltzeit wieder auf ca. 2000 ppm anzusteigen. Die Evolution der Blütenpflanzen vor ca. 135 Mio. Jahren drückte die atmosphärische CO_2-Konzentration auf unter 1000 ppm. Schließlich pendelte sich die atmosphärische CO_2-Konzentration mit der Entwicklung der Gramineen zwischen 180 und 330 ppm ein. Messungen verschiedener Forschergruppen zeigen deutliche teils kontroverse Schwankungen der atmosphärischen CO_2-Konzentration seit dem Beginn der Günzkaltzeit vor 640000 Jahren. Diese Unterschiede beruhen zumeist auf unterschiedlichen Messmethoden (McElwain et al., 2002, Tans, 2012, Etheridge et al., 1998, Beck, 2007). Dem allgemeinen Trend der ansteigenden atmosphärischen CO_2-Konzentration im Laufe der letzten 12000 Jahre widersprechen sie nicht (Abbildung 1.1A).

Neben eines Wandels der Landnutzung (wie Rodung von Wäldern, Trockenlegung von Feuchtgebieten und einer Ausdehnung der Haltung von Wiederkäuern) seit dem Ende der letzten Eiszeit ist in heutiger Zeit die Nutzung und Verbrennung fossiler Energien für die zunehmende Anreicherung der Atmosphäre mit klimarelevanten Gasen verantwortlich. Dieser Energieverbrauch wird durch die Industrialisierung angetrieben, die die Grundlage für die moderne Hochertragslandwirtschaft ("Grüne Revolution") ist, wodurch eine rasant wachsende Weltbevölkerung begünstigt wird. Die weltweiten CO_2-Emissionen stiegen von 1990 bis 2010 von 21 Gigatonnen auf 29,5 Gigatonnen pro Jahr (Dana1981 und Abraham, 2011) und die CO_2-Konzentration der Atmosphäre reicherte sich in diesem Zeitraum um ca. 40 ppm auf 393 ppm an (Tans, 2012). Von prä-industriellen, geschätzten 280 ppm beobachtet man seit ca. 200 Jahren einen beschleunigten Anstieg der CO_2-Konzentration (Siegenthaler et al., 2005), welche bereits im Jahr 2015 ein Niveau von 400 ppm erreichen kann. Dieser Wert ist möglicherweise der höchste seit dem Auftreten der ersten Gräser vor rund 55-60 Mio. Jahren (Jacobs et al., 1999). Laut IPCC (2012) sind bis zum Jahr 2030 Konzentrationen je nach Emissionsszenario bezüglich fossiler Energien zwischen 420 und 450 ppm zu erwarten. Eine weitere Anreicherung auf 500 ppm und höher wird bis zum Jahr 2050 erwartet (Weber und Zimmermann, 2004). Prognosen bis zum Ende des 21. Jahrhunderts reichen je nach Emmisoinsszenario von 440 ppm bis zu 950 ppm (IPCC, 2012; Abbildung 1.1B).

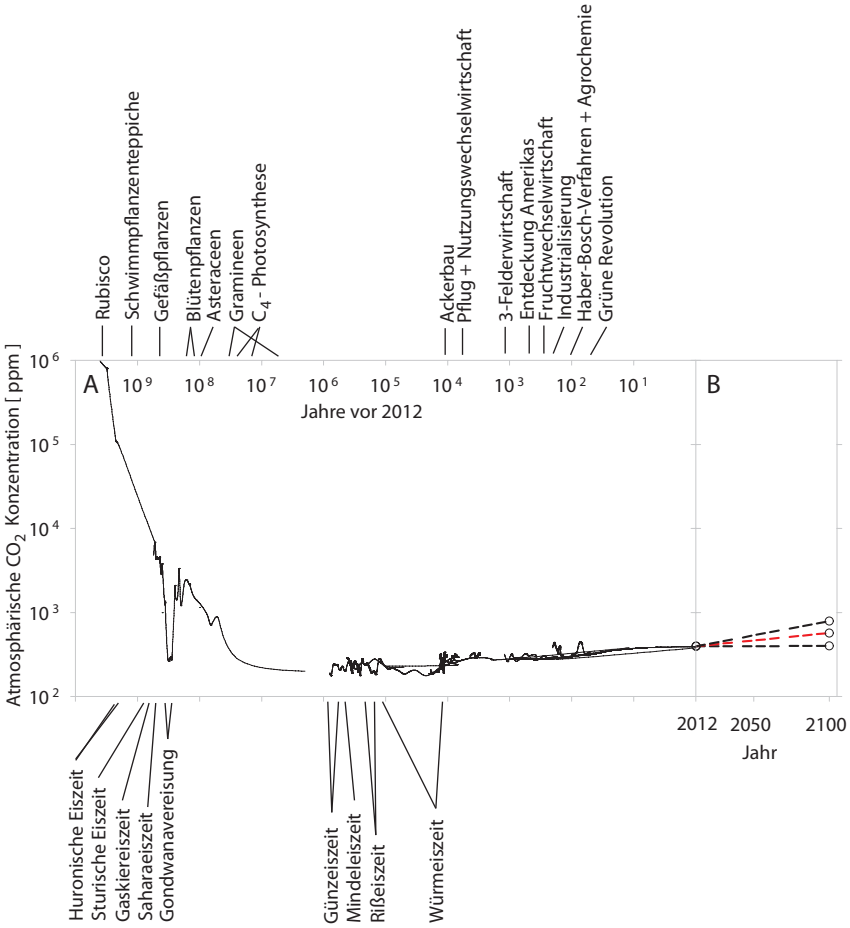

Abbildung 1.1: A: Geschätzte Dynamik der CO_2-Konzentration der Erdatmosphäre. Kurvenverläufe sind aus Arbeiten diverser Autoren extrahiert. B: Prognose auf Grundlage unterschiedlicher CO_2-Emissionsszenarien bis zum Jahr 2100 (vereinfachte Darstellung mit linearer Interpolation zwischen 2012 und 2100, nach Barker et al., 2007). Die gestrichelte rote Linie ist das Szenario mit der größten Eintrittswahrscheinlichkeit. Die gestrichelten Linien dienen lediglich der Visualisierung und repräsentieren keine prognostizierten Szenariendynamiken. Die Y-Achsen sind logarithmisch skaliert. Die X-Achse in A ist logarithmisch und in B linear skaliert. Beschriftungen unter der Abbildung indizieren die ungefähren Zeiträume für Kaltzeiten, Beschriftungen über der Abbildung indizieren entscheidende Entwicklungen und ungefähre Entwicklungszeitspannen der Photosynthese, sowie der Landwirtschaft. Kurvenverläufe atmosphärischer CO_2-Konzentration wurden aus Schlitter und Wildner (2001), Tans (2012), Etheridge et al. (1998), Barnola et al. (2011), Petit et al. (1999), Beck (2007), Dudley (1998), Wagner et al. (2004) und McElwain et al. (2002) abgeleitet. Eiszeiten nach Hoffman et al. (1998), Narbonne (2008) und Ibetsberger (2004). Evolution der Pflanzen nach Schlitter und Wildner (2001), Beerling (2005), Sage (2004), Evolution der Landwirtschaft nach Köcher-Schulz (2012) und Anonym (2012).

Während die Auswirkungen des Klimawandels auf globale und regionale Temperaturen, Niederschläge und die Windgeschwindigkeit kontrovers diskutiert werden, gilt eine weitere CO_2-Anreicherung der Atmosphäre im Laufe des 21. Jahrhunderts als sicher (IPCC, 2012). Die direkten Auswirkungen der Erhöhung dieser CO_2-Konzentration auf das Wachstum und die Ertragsqualität agrarischer Kulturpflanzen mit Hilfe physikalischer Modelle zu untersuchen ist Ziel der vorliegenden Arbeit. Indirekte Wirkungen über die Erhöhung der Temperatur aufgrund des Treibhauseffektes und der damit verbundenen Klimaveränderung werden nicht berücksichtigt.

1.3 Interaktionen der Pflanze mit der Umwelt

Lebewesen sind von ihrer Umwelt abgegrenzte Stoffsysteme. Sie haben Stoff- und Energiewechsel und treten damit in Wechselwirkung mit ihrer Umwelt, um zu wachsen, sich zu differenzieren und um sich fortzupflanzen (Grolle, 2010). Die Wechselwirkung eines Lebewesens mit der Umwelt ist nichts anderes als die optimale Nutzung der in dieser Umwelt zur Verfügung stehenden energetischen und stofflichen Ressourcen im Rahmen der physiologischen und biochemischen Möglichkeiten dieses Organismus. Landpflanzen sind weitgehend immobil an einen Standort und die dort vorherrschenden Umweltbedingungen gebunden und können auf Veränderungen lediglich durch Akklimation, nicht aber durch einen Standortwechsel antworten (Chai et al., 2005). Nährstoffe und Wasser werden vorwiegend über das Wurzelsystem aus dem Boden aufgenommen. Die Interaktion mit der Atmosphäre erfolgt oberirdisch über grüne Pflanzenteile (vorwiegend Blätter). In den Blättern ernten Lichtsammelkomplexproteine die auftreffende Strahlung und über die Stomata werden sowohl Wasserdampf (Transpiration) abgegeben als auch CO_2 für die Photosynthese aufgenommen. Somit sind Pflanzen Reaktoren zwischen Boden und Atmosphäre deren aktiver Interaktionsraum für Stoffaustausch sich auf den durchwurzelten Boden und die oberirdisch von grünen Pflanzenteilen erschlossene Atmosphäre beschränken.

1.3.1 Primärproduktion

Alle Lebewesen, die Energie einfangen und zusammen mit stofflichen Ressourcen als chemische Energie in organischer Biomasse speichern, nennt man Primärproduzenten. Zu den Primärproduzenten zählen alle Organismen, die mittels Photosynthese oder Chemosynthese Kohlenstoff fixieren, also grüne Pflanzen (inklusive der Algen und Flechten), einige Bakterien, Archaen und Protisten (Reece et al., 2010). Die Rate dieser Speicherung durch Primärproduzenten an einem bestimmten Ort über eine bestimmte Zeit ist die Bruttoprimärproduktion. Einen Teil dieser Bruttoprimärproduktion investieren die Pflanzen umgehend wieder für Zellatmung (Wachstumsatmung) und die Erhaltung der existierenden Gewebe (Erhaltungsatmung; Amthor und Baldocchi, 2001). Die darüber hinaus fixierte chemische Energie (Masse der Photosynthate) ist die Nettoprimärproduktion. Hauptbestandteil organischer Biomasse ist Kohlenstoff, welcher durch die Photosynthese mit Hilfe des Enzyms Rubisco aus atmosphärischem CO_2 in Form von Zuckern gebunden wird. Aus von Wurzeln aufgenommenen Nährstoffen und photosynthetisch assimilierten Zuckern werden Aminosäuren synthetisiert, welche in der Pflanze transportiert und für die Synthese von DNA, strukturellen Komponenten und Proteinen bereitgestellt werden. Einzelkomponenten pflanzlicher Biomasse benötigen eine Mindestmenge an Makro- und Mikronährstoffen, um optimal zu funktionieren. Demzufolge führt ein relativer Mangel an Nährstoffen auch zu einer Reduktion der Primärproduktion. Je nach Nährstoffangebot kann chemische Energie in pflanzlicher Biomasse in unterschiedlicher Qualität gespeichert werden. Da die biochemische Zusammensetzung eine Auswirkung auf die Haltbarkeit, Weiterverarbeitungseigenschaften und auf den Nährwert hat, ist sie ein Qualitätsmerkmal des Ertrages. Im konventionellen Bäckerhandwerk nimmt die Backqualität von Weizen mit steigendem Proteingehalt im Korn zu (Berg et al., 2003). Da mit dem Proteingehalt der Stickstoffgehalt in Relation zum Kohlenstoffgehalt steigt, entspricht ein höherer Proteingehalt gewöhnlich einem engeren $\frac{Kohlenstoff}{Stickstoff}$-Verhältnis.

Für die Photosynthese spielt neben Nährstoffen, Wasser, CO_2 und Lichtangebot die Gewebetemperatur eine entscheidende Rolle, da Proteine durch zu hohe oder zu niedrige Temperaturen in ihrer Funktion eingeschränkt werden oder irreversibel denaturieren können. Zwischen den Extremen, die den Funktionsverlust der Proteine zur Folge haben, liegt ein Temperaturbereich, der Bruttoprimärproduktion ermöglicht. Dauerhaft wird pflanzliches Leben erst ermöglicht, sobald die Bruttopri-

märproduktion größer als die Respiration ist. Die meisten Enzyme entfalten ihren optimalen Wirkungsgrad zwischen 25 und 40°C (Smrcka and Szarek, 1986). In diesem Temperaturbereich ist die Nettoprimärproduktion am Größten.

1.3.2 Photosynthesetypen

Grundsätzlich unterscheidet man bei Landpflanzen drei Haupttypen der Photosynthese - C_3, C_4 und CAM. Der C_3-Metabolismus wird dabei als der Grundtyp der Photosynthese betrachtet, da dieser Typus in 90% aller Landpflanzen realisiert ist (Taub, 2010). Der Zeitraum der Entwicklung des C_4-Metabolismus wird im allgemeinen vor ca. 50 Mio. Jahren mit der Entwicklung der Gramineen angenommen (Schlitter und Wildner, 2001). Überraschenderweise ist dieser Metabolismus allerdings nicht nur in Gräsern, sondern ähnlich der Karnivorie in einer weiten Bandbreite phylogenetisch nicht zusammenhängender Spezies des Pflanzenreichs anzutreffen (Honda, 2010, AGP III, 2009). So kommt der C_4-Metabolismus unter anderem sogar in Vertretern der Blaualgen und Dinoflagellaten vor (von Sengbusch, 2003). Aufgrund dessen erscheint es nicht abwegig, dass die Befähigung, beide Photosynthesewege zu beschreiten, im pflanzlichen Genom grundsätzlich vorhanden sein könnte.

Weitverbreitet ist die Ansicht, dass der C_4-Typus eine Anpassung an eine sehr niedrige atmosphärische CO_2-Konzentration ist, wie sie zur Zeit der Gramineenentwicklung vor ca. 50 Mio. Jahren vorlag. Da die Optimumtemperaturen des C_4-Metabolismus zwischen 30 und 40°C liegen und damit doppelt so hoch wie bei C_3-Pflanzen sind (Heß, 1999) und die CO_2-Vorfixierung in Form von Oxalacetaten wesentlich energieaufwändiger ist, haben sich C_4-Pflanzen in natürlichen terrestrischen Ökosystemen nur in Klimaten mit sehr hohen Temperaturen bei gleichzeitig niedriger atmosphärischer CO_2-Konzentration gegenüber den C_3-Pflanzen durchgesetzt. Allerdings vermuten Schopfer und Brennicke (2010), dass dieser Vorteil schon bei einer Verdopplung bis Verdreifachung der atmosphärischen CO_2-Konzentration, also ab ca. 750 ppm, verloren gehen könnte.

Die drei Haupttypen der Photosynthese unterscheiden sich bezüglich der räumlichen bzw. zeitlichen Fixierung des Kohlenstoffs. In C_3-Pflanzen diffundiert atmosphärisches CO_2 entlang eines Konzentrationsgefälles in die Stomatahöhle und von dort weiter in die Mesophyllzellen, wo die Kohlenstofffixierung mit Hilfe des Rubiscoenzyms im Calvinzyklus abläuft. Das erste dabei entstehende Produkt ist ein

Molekül mit drei Kohlenstoffatomen; daher die Bezeichnung C_3-Pflanze. Im Gegensatz dazu wird CO_2 bei C_4-Pflanzen in den Mesophyllzellen als Oxalacetat (vier Kohlenstoffatome) vorfixiert, über die Plasmodesmen in die Bündelschneidezellen transportiert und dort rubisconah freigesetzt, woraufhin der Calvin-Zyklus ablaufen kann (Taub, 2010). Dies stellt einen effizienteren Mechanismus bei niedrigen CO_2-Konzentrationen dar, da durch die Vorfixierung CO_2 nicht mit O_2 um den Bindungsplatz im reaktiven Zentrum von Rubisco konkurrieren muss. Somit werden a) geringere Rubiscomengen benötigt und b) findet nahezu keine Photorespiration statt (Jones, 2011). C_4-Pflanzen reichern durch eine räumlich getrennte CO_2-Vorfixierung aktiv ATP-abhängig CO_2 in den Mesophyllzellen an und sind so weniger von der tatsächlichen atmosphärischen CO_2-Konzentration abhängig wie C_3-Pflanzen. Der CAM-Typus ähnelt dem C_4-Typus und ist eine Anpassung an sehr trockene Klimate bei der CO_2-Aufnahme und Photosynthese nicht nur räumlich sondern auch zeitlich getrennt ablaufen. Diese zeitliche und räumliche Trennung reduziert Wasserverluste, weil die Spaltöffnung während den heißesten Stunden geschlossen werden können, und erlaubt den CAM-Pflanzen ähnlich den C_4-Pflanzen, weniger Rubisco in den Blättern bereitzustellen, um den vorfixierten Kohlenstoff in Zucker umzuwandeln.

1.3.3 Akklimation an die steigende atmosphärische CO_2-Konzentration

Sogenannte Lichtsammelkomplexproteine, die in die Thylakoidmembran der Chloroplasten eingebettet sind, ernten die auf das Blatt auftreffende photosynthetisch aktive Strahlung (PAR). Diese Energie wird in Form von Reduktionspotentialen gespeichert und für die Enzymaktivierungen im Calvinzyklus bereitgestellt, um aus CO_2 und Wasser einfache Zucker zu assimilieren (Reece et al., 2010). Das Schlüsselenzym für die CO_2-Fixierung im Calvinzyklus ist Rubisco. Aufgrund der geringen Bindungsspezifität des Rubiscoenzyms können neben CO_2 auch O_2 und SO_2 an dessen reaktives Zentrum binden. Durch diese Eigenschaft ist Rubiso das Schlüsselenzym zweier unabhängiger Stoffwechselwege, der Photosynthese (Bindung von CO_2) und der Photorespiration (Bindung von O_2). Diese Konkurrenzsituation führt bei Pflanzen des C_3-Photosynthesetyps dazu, dass das Verhältnis von CO_2 zu O_2 im Mesophyll des Blattes einen direkten Einfluss auf das Verhältnis von Photosyntheserate zu Photorespirationsrate und somit dem Netto-Kohlenstoffgewinn der Pflanze hat. Laut Schlitter und Wildner (2001) steigt die Effizienz von Rubisco mit steigender

CO_2-Konzentration. Schlitter und Wildner (2001) beschreiben Rubisco als eines der langsamsten aller bekannten Enzyme, das bis zu drei CO_2 pro Sekunde zu assimilieren vermag. Unter sehr hohen atmosphärischen CO_2-Konzentrationen, wie sie zu Zeiten der Entwicklung des Enzyms in der Erdatmosphäre vorherrschten, mag die relative Langsamkeit des Enzyms ausreichend gewesen sein, da sehr wenig O_2 vorhanden war, um mit CO_2 um den Platz am reaktiven Zentrum von Rubisco zu konkurrieren. Den erdgeschichtlich sinkenden atmosphärischen CO_2-Konzentrationen begegneten Pflanzen mit einer quantitativen Erhöhung des Rubiscoenzyms (Schlitter und Wildner 2001), weshalb Rubisco in den photosynthetisch aktiven Organen bis zu 50% der löslichen Proteine ausmacht (C_3-Metabolismus) oder alternativen Stoffwechselwegen (C_4; siehe *Kapitel* 1.3.2). Diese Befunde stehen im Einklang mit den Beobachtungen von Seneweera et al. (2011), dass Blattstickstoff-, Rubisco-, lösliche Protein- und Chlorophyllkonzentrationen durch atmosphärische CO_2-Anreicherung signifikant absinken. Allerdings könnte die alternative Bindungsaffinität des Rubiscoenzyms mit O_2 und CO_2 eine Anpassung des C_3-Metabolismus darstellen, um bei hoher Lichteinstrahlung und gleichzeitig niedrigen atmosphärischen CO_2-Konzentrationen exzessiv absorbierte Lichtenergie, die die Kohlenstoffassimilation mittels Rubsico übersteigt abzuführen, bevor es zu Zellschädigungen kommen kann (Voet et al., 2010, Heldt und Heldt, 2003). Rachmilevitch et al. (2004) fanden bei Ackerschmalwand (*Arabidopsis thaliana* (L.) Heynh.) und Weizen (*Triticum aestivum* L.) Anzeichen, dass die Wurzelaufnahme von Nitrat vom Rubiscogehalt in den grünen Blättern reguliert wird. Darüber hinaus zeigen Bloom et al. (2010), dass steigende CO_2-Konzentrationen keinen oder einen negativen Effekt auf das Wachstum von C_3-Pflanzen hatte, wenn die Stickstoffquelle Nitrat war. Somit könnte dieser CO_2-Effekt auf die Nitratassimilation oberirdischer Pflanzenteile die zukünftige Verbreitung von C_3-Pflanzen beeinflussen (Bloom et al., 2010, 2012).

Für C_3-Pflanzen bedeutet die anthropogen bedingte Anreicherung der Atmosphäre mit CO_2 eine Leistungssteigerung des Rubiscoenzyms und bietet somit den Pflanzen die Option, die Enzymkonzentration in den Blättern zu reduzieren, um so Respirationskosten zu reduzieren. Eine Anreicherung der Atmosphäre mit CO_2 sollte somit zu einer Steigerung der Assimilationsraten führen und somit zu quantitativ mehr pflanzlicher Biomasse. Dies wurde vielfach in Versuchen nachgewiesen, in welchen eine Erhöhung der atmosphärischen CO_2-Konzentration die Blattassimilationsraten von C_3-Pflanzen unmittelbar erhöhten und so die Biomassenproduktion und die Erträge steigerten (Högy et al., 2010, 2009, Kimball et al., 2002, Ewert et al., 2002,

Amthor, 2001, Aben et al., 1999, Fangmeier et al., 1999, Nakano et al., 1997, Drake et al., 1997 und Wullschleger et al., 1992). Da die reproduktiven Organe vorwiegend aus den remobilisierbaren Ressourcen der vegetativen Organe gefüllt werden, sind auch hier als Konsequenz weitere $\frac{Kohlenstoff}{Sticklstoff}$-Verhältnisse zu beobachten (Fangmeier et al., 1999). Eine Reduktion der photosynthetischen Kapazität in den oberen Sonnenblättern wurde in C_3-Pflanzen unter erhöhten CO_2-Bedingungen häufig beobachtet (Lee et al., 2001, Rogers und Humphries, 2000, Drake et al., 1997 und Nakano et al., 1997).

Länger andauernde Exposition der Pflanzen in einer Umwelt mit erhöhter atmosphärischer CO_2-Konzentration führt zu einer Akklimation der Pflanze (Gutierrez et al., 2009, Ainsworth et al., 2003, Sage et al., 1989), die häufig eine Reduktion der Blattstickstoff- und Blattrubiscogehalte beinhaltet (Seneweera et al., 2011, Bloom et al., 2002, Drake et al., 1997, Nakano et al., 1997, Bowes, 1991). Bereits Webber et al. (1994), Stitt und Krapp (1999) und Conroy und Hocking (1993) zeigten, dass die Reduktion der Blattstickstoffgehalte Folge einer Optimierung des Photosyntheseapparates im Zuge der Akklimation an erhöhte CO_2-Konzentrationen ist. Die vertikale Verteilung der Stickstoffkomponenten des Photosytheseapparates im Bestand und dessen Akklimation an eine erhöhte atmosphärische CO_2-Konzentration wurde bisher allerdings nur in wenigen Studien untersucht (Del Pozo et al., 2007, Osborne et al., 1998, Adam et al., 2000, Bertheloot et al., 2012). In Ackerbohnen ($Vicia\ faba$ L.) zeigen die oberen Sonnenblätter im Bestand eine erhöhte photosynthetische Kapazität gegenüber tiefer im Bestand lokalisierten Blättern (Del Pozo und Dennett, 1999). Rubisco- und Stickstoffgehalte korrelieren positiv und sind in Blättern einer Bestandestiefe niedriger unter erhöhten atmosphärischen CO_2-Konzentrationen als in Kontrollpflanzen (Del Pozo et al., 2007, Osborne et al., 1998). Die Akklimation hängt dabei von der Stickstoffverfügbarkeit und dem Entwicklungsstadium der Pflanze ab (Adam et al., 2000). Über die erhöhte Biomassenproduktion hinaus wurde mehrfach von einem Rückgang der Ertragsqualität berichtet, da die niedrigeren Protein- und Aminosäurekonzentrationen die Back- und Braueigenschaften sowie den Nährwert beeinflussen (Högy et al., 2009, Stafford, 2007).

Der Grad der Akklimation an eine steigende atmosphärische CO_2-Konzentration kann auf Grundlage von A/C_i Kurven verstanden werden und hängt von den Umweltfaktoren ab, die die Photosyntheseleistung beeinflussen (Ainsworth and Rogers, 2007). Nimmt die photosynthetische Kohlenstofffixierung bei erhöhter atmosphärischer CO_2-Konzentration zu, so steigt der Bedarf an Stickstoff für das Biomassewachstum. Eine limitierte Stickstoffverfügbarkeit setzt so die Senkenkapazität für

Stickstoff herab (Rogers et al., 1998), reduziert die Stickstoffaufnahme und führt daher zu einer Akklimation des Photosyntheseapparates und weiteren $\frac{Kohlenstoff}{Stickstoff}$-Verhältnissen in den Pflanzenorganen (Miglietta et al., 1996). Stickstofflimitierung kann durch Topfeffekte induziert sein (Sage, 1994), da kleine Töpfe häufig artifizielles Wurzelwachstum verursachen oder das Wurzelwachstum und damit die Nährstoffaufnahme limitieren (Poorter et al., 2012, Thomas and Strain, 1991). Verpflanzen von CO_2-akklimatisierten *Gossypium hirsutum* L. Pflanzen in größere Töpfe zeigte, dass eine Umkehr des Akklimationsprozesses möglich ist, was darauf hinweist, dass die Rubiscoaktivität über die atmosphärische CO_2-Konzentration hinaus vom Gleichgewicht zwischen Kohlenstoff- und Stickstoffquellen und -senken abhängt (Thomas and Strain, 1991). Auch unter Freilandbedingungen konnte eine Akklimation von Sommerweizen bei erhöhter atmosphärischer CO_2-Konzentration beobachtet werden (Wall et al., 2000), wobei die Akklimation unter Bedingungen mit niedriger Stickstoffverfügbarkeit tendentiell stärker ausgeprägt ist als bei hoher (Ainsworth and Long, 2005).

Höhere Photosyntheseraten bei erhöhter atmosphärischer CO_2-Konzentration führen zu einer Konkurrenz bezüglich der Verwendung des aufgenommenen Stickstoffs für den Aufbau struktureller Biomasse und für die Optimierung des Photosyntheseapparates (Thornley, 2004, 2002, 1998). Basierend auf der Annahme, dass für den Aufbau struktureller Biomasse eine definierte Menge Stickstoff strukturell gebunden wird (Yin and van Laar, 2005, Thornley, 1998, 2004), und verfügbarer Stickstoff erst für die Bildung struktureller und dann photosynthetischer Komponenten verwendet wird (Jamieson and Semenov, 2000), bleibt bei limitierter Stickstoffaufnahme weniger Stickstoff für die Optimierung des Photosyntheseapparates übrig. Die Akklimation der N_P-Verteilung führt daher zu einer geringeren Photosyntheserate. Auch bei nicht limitierten Bedingungen resultiert ein ausgeprägterer Höhengradient der $\frac{Kohlenstoff}{Sticklstoff}$-Verhältntisse von den oberen zu den tieferen Blättern im Bestand (Biernath et al., 2013).

Aufgrund der Beobachtung weiterer $\frac{Kohlenstoff}{Sticklstoff}$-Verhältnisse in vegetativen (verfrühte Seneszenz) und generativen Organen bei erhöhten atmosphärischen CO_2-Konzentrationen leiteten Gifford et al. (2000) die "down-regulation of photosynthesis"-Hypothese (Taub und Wang, 2008; Drosselung der Photosynthese-Hypothese) ab. Als Teil dieser Hypothese schlugen Fangmeier et al. (2000, 1999) vor, dass niedrigere Kornproteingehalte eine Konsequenz niedrigerer Blattproteingehalte sind. Da photosynthetische Enzyme einen großen Teil des Gesamtstickstoffgehaltes eines Blattes einer C_3-Pflanze ausmachen und ein wichtiger Speicher für die post-anthetische Translokation von Nährstoffen für die Kornfüllung sind, ist die Reduktion eine Folge niedrigerer Rubiscokonzentrationen (Ainsworth and Long, 2005, Evans and Seemann, 1989). Demgegenüber stehen nicht weniger als zehn Hypothesen, die Anspruch erheben, die in Experimenten beobachteten weiteren $\frac{Kohlenstoff}{Sticklstoff}$-Verhältnisse

in oberirdischer Pflanzenbiomasse zu erklären (Review von Taub und Wang, 2008). Dies zeigt, dass die Mechanismen des CO_2-Effekts auf das Pflanzenwachstum bisher nicht vollständig verstanden sind. Ursache dafür sind art-, sorten- und umweltspezifische Unterschiede, deren Interaktionen teils sehr komplex sind. Im Rahmen von *Kapitel* 3 wurde die "down-regulation of photosynthesis"-Hypothese anhand eines mechanistischen Modells, das den Stickstoffumsatz in photosynthetisch aktiven Blättern in Abhängigkeit vom Lichteinfall und der für die Synthese zur Verfügung stehenden Aminosäuren, analysiert.

Neben der Reduktion der Stickstoffgehalte in photosynthetisch aktiven Organen und Speicherorganen wurde auch die Reduktion weiterer Elemente in der Pflanzenbiomasse beobachtet. So zeigen Blank et al. (2011) und Baxter et al. (1997) in zwei Grasarten (*Bromus tectorum* L. und *Poa alpina* L.) eine Reduktion der Phosphor- und Magnesiumkonzentrationen in den Blättern unter erhöhter atmosphärischer CO_2-Konzentration, während die Kaliumkonzentration nur in *Bromus* sank. Diese Ergebnisse lassen auf eine sinkende Grünfutterqualität mit steigender atmosphärischer CO_2-Konzentration schließen. Manderscheid et al. (1995) zeigen, dass erhöhte atmosphärische CO_2-Konzentrationen gewöhnlich die Mineralstoffkonzentrationen in Weizenbiomasse reduzierte. Dieser Effekt war ab dem Schossen messbar und vergrößerte sich bis zur Vollreife in vegetativer und generativer Biomasse. Fangmeier et al. (1999) fanden in Weizen in Open-Top-Kammern eine Reduktion von Kalium, Calcium, Schwefel, Zink und Mangan in den Blättern, aber nur von Calcium, Schwefel und Eisen im Korn. Högy et al. (2009) beobachten einen CO_2-Effekt, der im Weizenkorn zu niedrigeren Magnesium-, Eisen-, Cadmium- und Siliziumkonzentrationen führt, während die Kalium, Molybdän und Bleigehalte anstiegen. Diese Ergebnisse bestätigen Fernando et al. (2012) für Eisen und Calcium, allerdings waren auch die Gehalte von Schwefel und Zink signifikant niedriger. Bei Erbs et al. (2010) sind im Weizenkorn nur niedrigere Schwefelkonzentrationen signifikant. Demgegenüber zeigen Lieffering et al. (2004), dass im Reiskorn bei ausreichendem Nährstoffangebot außer Stickstoff keine anderen Elemente durch erhöhtes CO_2 reduziert wurden. Allerdings weisen die Autoren darauf hin, dass die Verfügbarkeit von Nährstoffen in ihrem Versuchsaufbau höher war als dies üblicherweise in Agrarökosystemen der Fall sein dürfte. Damit scheint der Nährwert von Kulturpflanzen mit steigender CO_2-Konzentration insgesamt zu sinken. Die Vermutung liegt nahe, dass der CO_2-Effekt auf Nährstoffkonzentrationen (außer Stickstoff) in pflanzlicher Biomasse stärker wie im Falle von Stickstoff von unterschiedlichen Umweltbedingungen abhängig ist. Die

wiederholten Berichte einer Reduktion von Schwefel, Phosphor, Eisen und Magnesium legen nahe, dass insbesondere die Aufnahme von Nährstoffen, die vorwiegend für den Aufbau und die Funktion des photosynthetischen Apparates notwendig sind (Heldt und Piechulla, 2011, Hell, 2006, Richter, 1998 und Heldt et al., 1986), ähnlich dem Stickstoff, bei erhöhter CO_2-Konzentration reduziert werden. Allerdings mögen Sorteneigenschaften, noch stärker als im Falle von Stickstoff, einen großen Einfluss auf die Interaktionen der Nährstoffassimilation mit den Umweltbedingungen haben. Deshalb sind weitere Versuche notwendig, um die Mechanismen der Nährstoffassimilation und deren Partitionierung auf unterschiedliche Pflanzenorgane identifizieren und beschreiben zu können.

Im Fokus der vorliegenden Arbeit standen Pflanzen des C_3-Photosynthesetyps und deren Akklimation an eine erhöhte atmosphärische CO_2-Konzentration. Eine Anwendung des im Rahmen dieser Arbeit entwickelten Modells auf den Umsatz photosynthetisch aktiven Stickstoffs in C_4-Pflanzen wurde bisher nicht durchgeführt. In der Literatur findet man bezüglich der Akklimation des Stickstoffgehalts in Blättern von C_4-Gräsern unter erhöhter CO_2-Konzentration wenig eindeutige Ergebnisse. Wand et al. (1999) finden in mehreren Grasarten eine Reduktion des Blattstickstoffgehalts um durchschnittlich 6%. Le Cain und Morgan (1998) finden eine weniger eindeutige Reduktion des Blattstickstoffgehalts in verschiedenen Grasarten mit unterschiedlichen Decarboxylierungsenzymgruppen von bis zu 10% (Nicotinamid Adenin Dinucleotid Phosphat-Malic Decarboxylierungsenzym) oder 0% (Nicotinamid Adenin Dinucleotid Malic Decarboxylierungsenzym). In Mais, der in $SPAR$-Kammern ("Soil Plant Atmosphere Research-Kammern": Pflanzenwachstumskammern unter Freilandbedingungen mit natürlichem Sonnenlicht) angebaut wurde fanden Kim et al. (2006, 2007) eine Reduktion der Blattstickstoffgehalte um 8%, weitere $\frac{Kohlenstoff}{Stickstoff}$-Verhältnisse in der Pflanze waren allerdings nicht signifikant (Kim et al., 2007 und Sardans et al., 2012). Lara and Andreo (2011) beschreiben, dass die photosynthetisch aktiven Stickstoffgehalte der Blätter, bezogen auf die Trockenmassen, sich zwischen C_3- und C_4-Pflanzen nicht unterscheiden. Allerdings sind bei C_4-Pflanzen die N_P-Gehalte bezogen auf die Blattfläche niedriger und die Funktionalität des photosynthetisch aktiven Stickstoffs ist unterschiedlich, da C_3-Pflanzen anteilig mehr N_P in Rubisco und weniger in Thyllakoide und sonstige lösliche Proteine investieren als C_4-Pflanzen. Die von Kim et al. (2006, 2007) beschriebene Reduktion der Blattstickstoffgehalte unter erhöhten CO_2-Bedingungen in einigen Versuchen mit C_4-Pflanzen deutet darauf hin, dass das im Rahmen dieser Arbeit entwickelte Mo-

dell auch für die Simulation der Akklimation von Pflanzen des C_4-Typs verwendet werden könnte.

1.4 Modelle und deren Beitrag zum Prozessverständnis

Aufgrund der zu erwartenden Charakteristika des Klimawandels mit einer Zunahme der Häufigkeit von Extremereignissen besteht zunehmender Bedarf, die dynamische Reaktion der Agrarökosysteme auf diese Veränderungen besser zu verstehen und beschreiben zu können. Dies ist notwendig, um die Landwirtbewirtschaftungssysteme besser an die Veränderungen anpassen zu können und Handlungsoptionen für die Landwirte entwickeln zu können.

Daher besteht Handlungsbedarf, Agrarökosysteme und die komplexen Wechselwirkungen zwischen Pflanze, Boden, Klima und Bewirtschaftung besser zu verstehen, um Konsequenzen menschlichen Handelns besonders hinsichtlich des Klimawandels für a) die Ökosysteme und b) die Menge und Qualität der Ernteprodukte abschätzen zu können. Mechanistisch orientierte Agrarökosystemmodelle können hierfür einen entscheidenden Beitrag leisten, da je nach Komplexitätsgrad der Modelle und je nach Fragestellung mit ihrer Hilfe i) das Prozessverständnis gefördert, ii) eine aus Feldmessungen abgeleitete Hypothese geprüft, iii) der derzeitige Wissensstand integriert und iv) die Interaktion der Stoffkreisläufe in komplexen Systemen berechnet werden kann.

1.4.1 Agrarökosystem- und Pflanzenwachstumsmodelle

Landwirtschaftliche und gartenbauliche Zusammenhänge zu verstehen und Erträge zu optimieren, ist seit der Erfindung des Ackerbaus vor ca. 12.000 Jahren ein wichtiges Interesse des Menschen. Ungünstiges Wetter und daraus resultierende Missernten hatten verheerende Wirkung auf den Gesundheitszustand der Bevölkerung. Die Landwirte nutzten einfache Regeln, welche die Zusammenhänge zwischen dem Wetter und den zu erwartenden Kulturpflanzenerträgen verdeutlichen und teils auch Prognosen bezüglich der zu erwartenden Ertragsqualität abgeben.

“Im Mai ein warmer Regen bedeutet Früchtesegen.” (Binder, 2003)

“Gibt’s im Juni Donnerwetter, wird auch das Getreide fetter.” (Binder, 2003)

Streng genommen handelt es sich bei den hier aufgeführten Regeln um einfache Modelle, die Landwirte durch aufmerksame Beobachtungen ihrer Umwelt ableiteten und über Generationen an die Nachkommen weitergaben. Diese empirischen Modelle

leiten Zusammenhänge zwischen beobachteten Wetter- oder Naturphänomenen und den zu erwartenden Erträgen bzw. deren Qualität her. Aus heutiger Sicht lassen sich diese empirischen Zusammenhänge oft physikalisch erklären. So bedeutet ein warmer Mairegen, dass die Saat gut aufläuft, und weder vertrocknet noch erfriert. Gewitter führen zu Nitrateintrag in die Böden, da Blitze ausreichend viel Energie freisetzen, wodurch der relativ reaktionsträge elementare Luftstickstoff mit Sauerstoff zu NO reagiert (Schumann und Huntrieser, 2007). Die NO Produktion durch Blitze beschreibt der Zel'dovich Mechanismus derart, dass während der anfänglich sehr heißen Blitzphase N_2 und O_2 dissoziieren und folglich NO gebildet wird (Goldenbaum und Dickerson, 1993, Zeldovich und Raizer,1967). Troposphärische NO reagieren dann mit OH weiter zu HNO_3. HNO_3 wird durch Gewitter mit Starkniederschlägen direkt nach der Entstehung aus der Atmosphäre ausgewaschen und als sogenannte "nasse Deposition" in terrestrische und aquatische Ökosysteme eingetragen (van Noije et al., 2006). Dort können Mikroorganismen und Pflanzen den zusätzlichen Stickstoffeintrag bei Bedarf assimilieren. Eine Düngergabe im Juni fällt in weiten Teilen Europas bei Sommer- und Wintergetreiden in die Korninitialisierungs- und Kornfüllungsphase, wodurch ein positiver Effekt auf Erträge und deren Qualität zu erwarten ist (Baruth, 2012, Sonnleitner, 2011, König, 2010). Diese Depositionen waren besonders zu Zeiten vorindustrieller Landwirtschaft ohne die Möglichkeit, schnell wirksame Mineraldünger zu applizieren, ein signifikanter Nährstoffeintrag in Agrarökosysteme.

Um die Systeme zu verstehen und Prognosen zu stellen ist eine Modellvorstellung von dem bewirtschafteten Agrarökosystem notwendig und von den Prozessen, die die Erträge beeinflussen. Um Hypothesen für die Interaktionen von Klimaveränderungen und Umwelt auf landwirtschäftliche Erträge und die Ertragsqualität abzuleiten, werden weltweit Versuche an unterschiedlichen Standorten mit unterschiedlichen Pflanzenarten und -sorten in unterschiedlichen Produktionssystemen durchgeführt. Aufgrund der Vielfalt und der Komplexität der Systeme ist es schwer, die unterschiedlichen Versuchsergebnisse eindeutig zu erklären und eindeutige Rückschlüsse auf die Interaktionen zwischen Pflanzenphysiologie und Umwelt zu ziehen. Um die komplexen Interaktionen zwischen Boden, Pflanze und Atmosphäre besser zu verstehen, werden heute bevorzugt mathematische Agrarökosystemcomputermodelle verwendet, die das Potential haben, die dynamischen Zusammenhänge darzustellen.

In der Modellierung homogener Kulturpflanzenbestände werden eine Vielzahl von Modellen verwendet, deren Komplexitätsgrad sich in Bezug auf die Abbildung von

Einzelprozessen teils stark unterscheiden (Zhu et al., 2012, Biernath et al., 2011, Wang, 1997). Kriterien für diese Unterschiede sind der Nutzen des Modells, die Skala der Anwendung, der Stand der Wissenschaft bei der Modellentwicklung sowie der potentielle Nutzer. Modelle, die man dazu verwendet, wissenschaftliche Hypothesen zu testen, sind im Allgemeinen komplexer und physikalischer als jene, die betriebswirtschaftlich in der Landwirtschaft eingesetzt werden, beispielsweise für die Abschätzung von Bewässerungs- und Düngerapplikationsmengen (Grunwald, 1997).

Die vorliegende Arbeit zeigt Möglichkeiten und Grenzen von Pflanzenwachstumsmodellen, Erträge und deren Qualität unter verschiedenen Umweltbedingungen mit Berücksichtigung des Einflusses ansteigender atmosphärischer CO_2-Konzentration zu prognostizieren. Die Ergebnisse in *Abschnitt* 1 dieser Arbeit zeigten, dass mechanistische Pflanzenwachstumsmodelle die Dynamiken umweltfaktorieller Interaktionen meist besser treffen und so entscheidend dazu beitragen können, das Prozessverständnis zu verbessern. Andererseits sind einfachere, mehr empirische Modelle aufgrund ihrer Robustheit von Vorteil, wenn nur wenige Messwerte oder Sortenkenntnisse vorliegen, um das Modell zu parametrisieren. Dies ist bei Simulationen auf regionaler und globaler Skala häufig der Fall. In *Abschnitt* 1 zeigte sich ferner, dass besonders eine adäquate Lichtverteilung und Lichtnutzung im Bestand einen großen Einfluss auf die Biomassenproduktion und die Erträge haben. Dies liegt vor allem daran, dass das Lichtregime im Bestand Kerngrößen wie die Transpiration und die Blatttemperatur steuert und somit einen direkten Einfluss auf die Wasser- und Nährstoffaufnahme aus dem Boden und die photosynthetische Kohlenstofffixierung hat. Auf Grundlage der Ergebnisse in *Abschnitt* 1 wurde in *Abschnitt* 2 das Photosynthesemodell des Pflanzenwachstumsmodells GECROS für die Entwicklung des neuen Akklimationsmodells herangezogen und erweitert. Im GECROS-Photosynthesemodell nimmt der Lichteinfall auf die Blätter, in Anlehnung an das Lambert-Beer Gesetz für turbide Medien, exponentiell mit der Bestandestiefe unter Berücksichtigung der direkten, diffusen und gestreuten Strahlung ab. Ähnlich der Lichtverteilung nimmt der Gehalt photosynthetisch aktiven Stickstoffs exponentiell mit der Bestandstiefe ab. Die Photosyntheseleistung des Bestandes wird durch einen sogenannten "Zwei-Blatt-Ansatz", der Sonnen- und Schattenblätter berücksichtigt, mit dem Farquhar-Photosynthesemodell (Farquhar et al., 1980) berechnet. Die Stickstoffaufnahme für Wachstum, Photosynthese und Kornfüllung wird i) aktivitätsgetrieben berechnet, um die Photosynthese zu optimieren, ii) bedarfsgetrieben, um Zielstickstoffkonzentrationen in den Organen zu decken, und iii) durch eine ma-

ximale Stickstoffaufnahmerate gedeckelt.

1.4.2 Photosynthesemodelle

Die Assimilation von Kohlenstoff über das Blatt ist abhängig von der aufgenommenen Strahlungsenergie und lässt sich grundsätzlich in zwei Hauptprozesse einteilen: Die Lichtaufnahme im Bestand und die Photosynthese.

Der Komplexitätsgrad der Beschreibung dieser Einzelprozesse variiert in Pflanzenwachstumsmodellen. Während einfache Lichtmodelle nur die Abundanz direkten Lichts im Bestand berücksichtigen nimmt der Komplexitätsgrad mit der Berücksichtigung des diffusen (Ablenkung des Lichts durch die Atmosphäre) und gestreuten (Streuung im Bestand) Lichts zu (Bittner et al., 2012). Die Lichtabsorption wird in einfachen Photosynthesemodellen mit Hilfe eines Umrechnungsfaktors, der sogenannten Lichtnutzungseffizienz, berechnet, wodurch die Darstellung der Biochemie der Photosynthese umgangen wird. Die genotypspezifische Lichtnutzungseffizienz ist ein empirischer Wert, der mit steigender atmosphärischer CO_2-Konzentration erhöht wird (Ritchie et al., 1987, Priesack, 2006).

Das C_3-Blattphotosynthesemodell von Farquhar et al. (1980) ist wesentlich um den Effekt von Umweltveränderungen auf die Blattphotosyntheseraten zu untersuchen. Dieses Modell ist die Grundlage um von der Blattphotosynthese auf den Bestand zu skalieren (De Pury and Farquhar, 1997, Wang and Jarvis, 1990, Amthor, 1995, Lloyd and Farquhar, 1996, Wittig et al., 2005 und Laisk and Edwards, 2009). Mit Hilfe dieses Modells können aus Gaswechselraten, die am lebenden Blatt gemessen werden, Blattphotosyntheseraten und deren Akklimation an höhere atmosphärische CO_2-Konzentrationen abgeleitet werden. Der Effekt eines Anstiegs der atmosphärischen CO_2-Konzentration wird als Zusammenhang zwischen der intrazellulären CO_2-Konzentration (C_i) und der Photosyntheserate (A) dargestellt, einer sogenannten A/C_i-Kurve (Sage et al., 1989, Griffin and Seemann, 1996, Wullschleger, 1993 und Bunce, 2000). Darauf basierend wurden für lichtgesättigte Bedingungen eine Reihe mechanistischer Photosynthesemodelle entwickelt die mehr oder weniger komplex die verschiedenen Phasen des Calvinzyklus berücksichtigen (Abbildung 1.2). Dabei werden verschiedene Kapazitäten der Photosynthese unterschieden, die die Kohlenstoffassimilationsrate limitieren (Farquhar et al., 1980, Farquhar und von Caemmerer, 1982, Sharkey, 1985, 1989 und Sage, 1990):

1. Die Kapazität des Rubiscoenzyms, die CO_2-Fixierung zu katalysieren.
2. Die Kapazität der Lichtabsorption und des Elektronentransports.
3. Die Kapazität der Assimilatsynthese, Regeneration anorganischen Phosphors (P_i) für die Photophosphorylierung und Regeneration von Rubiscobiphosphat.

Wang und Engel (2000) übernahmen für ihr Modell die sogenannte Blackmanfunktion (Blackman, 1905), die sich in Abhängigkeit von der CO_2-Konzentration im Zellinneren aus zwei Kurven zusammensetzt: Ein zunächst linearer Anstieg der Photosyntheserate (maximale Carboxylierungsrate = Rubiscokapazität), geht unter höheren CO_2-Konzentrationen mit dem Erreichen des elektronentransportlimitierten Bereichs (P_i-Regeneration) in einen konstanten Wert über (Abbildung 1.2A).

Das Modell von Farquhar et al. (1980) berücksichtigt die Biochemie des Blattes inklusive der CO_2-Diffusion ins Blattinnere, und der Abundanz und Aktivität photosynthetisch aktiven Stickstoffs. Die tatsächlichen Assimilationsraten sind das Minimum zweier sich überlagernder, nichtlinearer Prozesse (Rubiscokapazität und Elektronentransportlimitierung). Dieses Modell wird heute vorwiegend in Pflanzenwachstumsmodellen verwendet, die dazu dienen, Mechanismen dynamischen Pflanzenwachstums unter variablen Umweltbedingungen zu simulieren (Abbildung 1.2C).

Sage (1990, 1994) definiert die Reaktionskurve der Photosynthese auf die CO_2-Konzentration als das Minimum dreier Prozesse. Bei ausreichendem Lichtangebot gilt, dass in Blättern terrestrischer C_3-Pflanzen die Photosynthese unter niedrigen CO_2-Konzentrationen von der Rubiscokapazität limitiert wird. Unter mittleren CO_2-Konzentrationen ist sie elektronentransportlimitiert, und unter hohen zellinternen CO_2-Konzentrationen wirkt die Geschwindigkeit der P_i-Regeneration limitierend (Farquhar et al., 1980, Harley und Sharkey, 1991, Sharkey, 1985, Sage, 1994; Abbildung 1.2D).

Eine mathematisch einfachere, robuste Methode ist die Beschreibung der CO_2-Assimilation mit Hilfe einer hyperbolischen Funktion ("non-rectangular hyperbola") der absorbierten photosynthetisch aktiven Strahlung (Goudriaan und van Laar, 1994, Thornley und France, 2007, Bertheloot et al., 2011). Diese empirische Funktion approximiert die drei limitierenden Kapazitäten des Calvinzyklus als Hyperbel (Abbildung 1.2B). Jenseits des CO_2-Kompensationspunktes steigt die Photosyntheseleistung mit steigender CO_2-Konzentration zunächst an. Bei hoher zellinterner CO_2-

Konzentration flacht die Kurve ab und nähert sich einer horizontalen Sättigungsphotosyntheseleistung. Der CO_2-Kompensationspunkt ist die CO_2-Konzentration, bei der die Produktion an Assimilaten exakt dem Verbrauch durch die Atmung entspricht: $Netto\text{-}CO_2\text{-}Assimilationsrate = 0$.

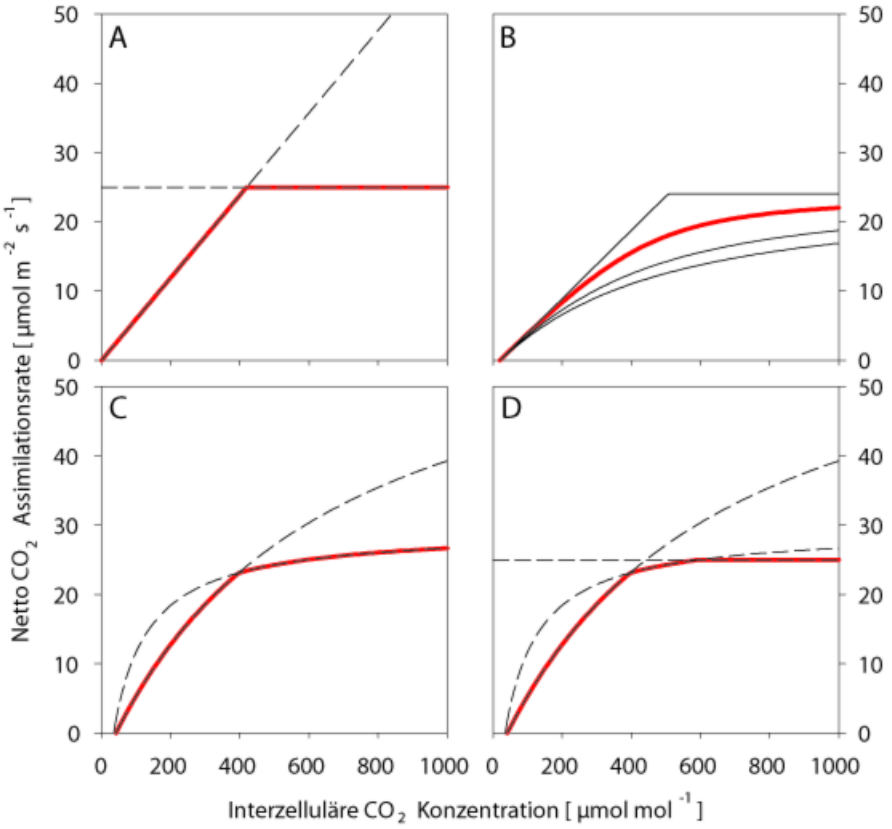

Abbildung 1.2: Modellierung der netto-Assimilationsraten in Abhängigkeit der zellinternen CO_2-Konzentration (C_i). **A**: Blackman Modell (Blackman, 1905, Wang, 1997): $A = MIN(A_{max},\ m \times C_i)$; **B**: "(non-)rectangular Hyperbola" (Thornley, 1998, Tubiello et al., 2007): $A = \frac{(\alpha \times C_i + A_{max}) - \sqrt{(\alpha \times C_i)^2 - 4\xi\alpha \times C_i \times A_{max}}}{2\xi}$; **C**: Farquhar Modell (Farquhar et al., 1980, Yin et al., 2004): $A = MIN(A_c,\ A_j)$ mit $A_c = \frac{V_{c,max} \times (C_i - \Gamma)}{C_i + K_m} - R_d$ und $A_j = \frac{J_{max} \times (C_i - \Gamma)}{4 \times (C_i + 2\Gamma)} - R_d$; **D**: Sage Modell Sage (1994, 1990): $A = MIN(A_c,\ A_j,\ A_{max})$. Durchgezogene, fette Linien in **A**, **C** und **D** stellen die Summe der Minimumfunktionen ($MIN(Funktion\,x,\ Funktion\,y,\ Funktion\,z)$) dar und in **B** für die Quantum Effizienz $\xi = 0,9$. In **B** variiert ξ von der obersten zur untersten Kurve mit $\xi = 1,0;\ 0,9;\ 0,6$ und $0,3$. Die verwendeten Parameterwerte sind $m = 0,06$; $A_{max} = 25$ µ$mol\ m^{-2}\ s^{-1}$; $\alpha = 0,0494$ µ$mol\ CO_2\ (mol\ PAR)^{-1}$; $\Gamma = 31,68$ µ$mol\ mol^{-1}$; $V_{c,max25} = 80\ J\ mol^{-1}$; $J_{max,25} = 140\ J\ mol^{-1}$; $K_m = 62,7$ µ$mol\ mol^{-1}$; $R_d = 0,99$ µ$mol\ m^{-2}\ s^{-1}$.

1.5 Datengrundlage

Die Datengrundlage dieser Arbeit basiert auf Open-Top-Kammerexperimenten des "IMPETUS" Projekts in Giessen aus den Jahren 1998 und 1999 (Schütz und Fangmeier, 2001), sowie auf einem Mini-FACE (Free Air Carbon Enrichment) Versuch in Stuttgart-Hohenheim des Jahres 2008 (Högy et al., 2012).

1.5.1 Open-Top-Kammerexperiment Gießen

Der detaillierte Aufbau der Kammern ist in Fangmeier et al. (1992) beschrieben und ähnelt der Konstruktion von Heagle et al. (1973) allerdings erweitert um ein Dach, um Niederschlag durch Regen zu unterbinden. Eine Kammer ist ca. 3 m hoch und hat einen Durchmesser von 3 m. Die Außenhaut der Kammern besteht aus 0,2 mm dicker Polyethylenfolie. Diese Folie ist für Strahlung im photosynthetisch aktiven Bereich transmissiv. In den Kammern wurde Sommerweizen (*Triticum aestivum* L. cv. 'Minaret') bei einer Pflanzdichte 350 Pflanzen m^{-2} angebaut. Die Behandlungsvarianten enthielten i) zwei verschiedene atmosphärische CO_2-Konzentrationen, ii) zwei verschiedene Bodentypen (Cambisol und Tschernosem) und iii) verschiedene Wasserverfügbarkeiten (Wasser limitierend bzw. nicht limitierend für das Pflanzenwachstum). Während der Weizen 1998 in Töpfen mit einer Bodenoberfläche von 0,27 m^2 und einer Tiefe von 0,4 m kultiviert wurde, betrug die "Feldgröße" im Jahr 1999 1,765 m^2 bei einer Tiefe von 0,5 m (Schütz, 2002). Es wurde der Effekt von zwei atmosphärischen CO_2-Stufen (ambient: 380 bzw. 383 ppm; angereichert: 634 bzw. 672 ppm), zwei Bodentypen (Chernozem vs. Cambisol (FAO, 2006) bzw. Schwarzerde vs. Braunerde (AG BODEN, 2005)) und zwei Bewässerungsstufen (begrenzte und unbegrenzte Wasserverfügbarkeit) auf das Wachstum von Sommerweizen untersucht. Versuch und Ergebnisse sind in (Schütz and Fangmeier, 2001, Schütz, 2002) beschrieben.

1.5.2 Mini-FACE Hohenheim

Die Mini-FACE Anlage in Hohenheim umfasst 15 Mini-FACE Einheiten mit je 2 m Durchmesser und dient der Untersuchung des Einflusses steigender atmosphärischer CO_2-Konzentrationen auf das Pflanzenwachstum und die biochemische Zusammensetzung pflanzlicher Gewebe. Im Vordergrund stehen dabei landwirtschaftliche Kulturpflanzen, da mögliche Veränderungen der Biomasse und deren Qualität sich di-

rekt auf die Verarbeitung der Agrarprodukte (z.B. die Back- oder Braueigenschaften) und deshalb die menschliche Ernährung auswirkt (Stafford, 2007). Der Boden der Versuchsanlage ist eine schwach pseudovergleyte Parabraunerde aus gebanktem Muschelkalk mit Lößauflage. Im Jahre 2008 wurde auf dieser Anlage in zwei Hauptbehandlungsvarianten zu je fünf Einheiten mit unterschiedlichen atmosphärischen CO_2-Konzentrationen Sommerweizen (*Triticum aestivum* L. cv. 'Triso') bei einer Saatdichte von 360 Pflanzen m^{-2} angebaut. Die ambiente CO_2-Konzentration betrug dabei 418±19 ppm und die erhöhte betrug 569±156 ppm. Zusätzlich wurden unter ambienten Bedingungen auf den übrigen fünf Mini-FACE Einheiten der Effekt der FACE-Ringkonstruktion ermittelt. Versuch und Teile der Ergebnisse sind in Högy et al. (2012) beschrieben.

1.6 Forschungsansatz und Kapitelübersicht

Die vorliegende Arbeit entstand im Rahmen eines Teilprojekts des DFG-finanzierten Projektes PAK 346 “Struktur und Funktionen von Agrarlandschaften unter dem Einfluss des globalen Klimawandels - Prozessverständnis und Prognosen auf der regionalen Skala”. Ziel dieses Projektes war es, Prognosen für die Entwicklung von Struktur und Funktion von Agrarlandschaften bis zum Jahr 2030 unter Berücksichtigung des Klimawandels und verschiedener sozioökonomischer Szenarien abzuleiten. Dies sollte mit Hilfe eines neuen integrierten Landsystemmodells bewerkstelligt werden, das regionale Klimamodelle mit Landoberflächenmodellen (Boden- und Pflanzenwachstumsmodelle) sowie Multi-Agent-Systemen vereint (DFG-PAK346, 2012). Ziel der vorliegenden Arbeit war es dabei, existierende Pflanzenwachstumsmodelle hinsichtlich der Akklimation des Pflanzenwachstums an die fortschreitende CO_2-Anreicherung der Atmosphäre zu evaluieren und zu erweitern.

In *Kapitel* 2 wurden im Rahmen eines Modellvergleichs die Pflanzenwachstumsmodelle für Kulturpflanzenbestände CERES-Wheat 2.0 (Ritchie und Godwin, 1987, Ritchie et al., 1987), SUCROS2 (Goudriaan und van Laar, 1994, Groot, 1987, Spitters et al., 1989, van Keulen et al., 1992, van Keulen and van Laar, 1982), GECROS (Yin and van Laar,2005) und SPASS (Wang, 1997, Wang und Engel, 2000) im Modellsystem Expert-N (Priesack et al., 2006, Priesack, 2006, Priesack und Bauer, 2003) eingebettet. Während sich die Komplexitätsgrade der Pflanzenwachstumsmodelle unterscheiden, bleibt die Modellumwelt, d.h. die Teilmodelle zur Beschreibung des Bodens, der Transformationen und Flüsse von Kohlenstoff und Stickstoff, der Bodenwasserdynamik, des Energietransfers und der Kulturmaßnahmen identisch. Auf diese Weise konnte die Eignung der Pflanzenwachstumsmodelle, das Bestandeswachstum unter variablen Umweltbedingungen abzubilden, analysiert werden. Unterschiede in den Simulationsergebnissen ließen sich somit eindeutig auf das jeweilige Pflanzenwachstumsmodell oder einzelne Submodelle zurückführen, ohne dass sie durch mögliche Unterschiede der Teilmodelle, die die Umweltbedingungen darstellen, verzerrt wurden. Die vier Pflanzenwachstumsmodelle wurden anhand eines Open-Top-Kammer Datensatzes hinsichtlich ihrer Funktionalität, Sommerweizenwachstum unter unterschiedlichen Umweltbedingungen zu simulieren, analysiert (*Kapitel* 1.3.1).

Im ersten Forschungsabschnitt zeigte sich die Stärke mehr mechanistischer Modelle, die Akklimation des Bestandes an die Dynamiken atmosphärischer CO_2-

Konzentration und pflanzenverfügbarem Bodenwasser zu simulieren. Es zeigte sich die Notwendigkeit, die Bestandeslichtverteilung adäquat zu modellieren, wenn Schlüsselgrößen wie die Wasser- und Nährstoffaufnahme aus dem Boden, die Biomassenproduktion, die Transpiration und die Partitionierung von Assimilaten auf verschiedene Organe simuliert werden sollen. Insbesondere die Lichtverteilung und Nutzung im Bestand wurden als Schwachstellen der weniger mechanistischen Bestandesmodelle (SUCROS und CERES) identifiziert, wodurch sich folglich die Interaktionen von Boden, Wasserverfügbarkeit und CO_2-Konzentration auf die Dynamik des Weizenwachstums schlechter abbilden ließen als mit GECROS oder SPASS. Darüber hinaus zeigte sich allerdings auch, dass der geringere Parameterisierungsaufwand und eine größere Robustheit gegenüber Umweltbedingungen durchaus positive Simulationsergebnisse liefern können (SUCROS). Dies ist von Vorteil, wenn wenig sortenspezifische

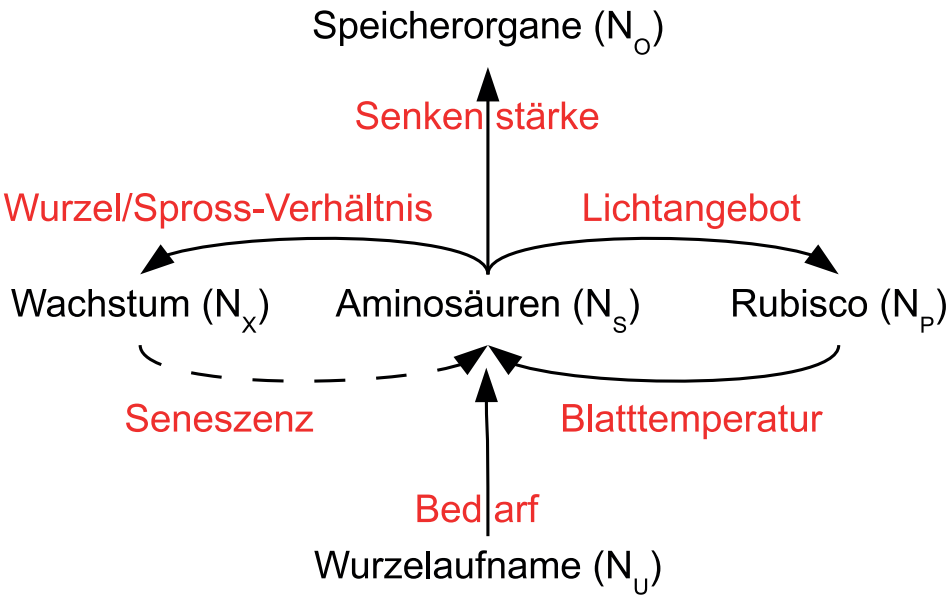

Abbildung 1.3: Schema der Stickstoffpartitionierung in der Pflanze. Zielkonflikt zwischen der Verwendung der in der Pflanze mobilen Stickstoffspezies (vorwiegend Aminosäuren, N_S) entweder für die Synthese photosynthetisch aktiven Stickstoffs (N_P), oder für das Wachstum der Pflanze (N_X). Rote Schrift kennzeichnet die Faktoren bzw. Prozesse die an der Steuerung der jeweiligen durch Pfeile dargestellten Prozessen der Stickstoffpartitionierung beteiligt sind. N_O indiziert die Einlagerung von Stickstoff in Speicherorgane und N_U ist die Wurzelaufnahme von Stickstoff. Dieses Modell basiert auf einem theoretischen Vorschlag von Thornley (1998, 2004) zur Akklimation der Pflanze an atmosphärische CO_2-Anreicherung.

Informationen für die Modellparametrisierung zur Verfügung stehen, bringt jedoch umgekehrt wenig Nutzen, um das Prozessverständnis zwischen Pflanzenwachstum und Umweltbedingungen, insbesondere hinsichtlich einer CO_2-Anreicherung der Atmosphäre, zu erweitern.

In *Kapitel* 3 wird ein neues Photosynthesemodell, das ein Stickstoffumsatzmodell verwendet, beschrieben. Dieses neue Modell beschreibt die Akklimation der Pflanze an veränderte Umweltbedingungen, insbesondere eine erhöhte atmosphärische CO_2-Konzentration. Es ersetzt das Photosynthesemodell im Pflanzenwachstumsmodell GECROS. GECROS hatte sich bereits im in *Kapitel* 2 beschriebenen Modellvergleich (Biernath et al., 2011) bezüglich der Abbildung von Interaktionen verschiedener Umweltfaktoren auf das Weizenwachstum in Open-Top-Kammern als geeignet herausgestellt, Pflanzenwachstumsdynamiken abzubilden.

GECROS verwendet für die Berechnung der Bestandesphotosynthese einen sogenannten "Two-Leaf" Ansatz, bei dem die Photosyntheseleistung getrennt für Blätter, die aktuell direktes Sonnenlicht empfangen und Blätter, die aktuell ausschließlich gestreutes Licht empfangen, berechnet wird. Die Lichtverteilung im Bestand wird nach dem Lambert-Beer Gesetz berechnet, das eine exponentielle Abnahme des Lichts mit dem kumulativen LAI annimmt.

In dem im Rahmen dieser Arbeit entwickelten Modell wurde die im GECROS Modell verwendete analytische Lösung für die Bestandesphotoynthese derart modifiziert, dass die empfangene Lichtmenge und die N_p-Abundanz der sonnenbeschienenen und beschatteten Blätter einzelner Bestandesschichten bestimmt werden. Die statische exponentiell abnehmende N_P-Verteilung mit der Bestandstiefe des unmodifizierten GECROS-Modells ist im neuen Modell die Zielgröße für den im Blatt bzw. in der Blattschicht angestrebten N_P-Gehalt, den die Pflanze zu erreichen versucht, um die Photosyntheseleistung zu optimieren. Die Synthese und der Abbau von N_P werden durch ein dynamisches Umsatzmodell (Thornley, 1998, 2004) beschrieben, das auf der Annahme basiert, dass Proteine ständigen Auf- und Abbauprozessen unterliegen (Abbildung 1.3). Dabei ist der N_P-Abbau ein direkt proportional von der N_P-Menge abhängiger Prozess, der möglicherweise von der Blatttemperatur beeinflusst wird. Der N_P-Aufbau ist von der Menge an photosynthetisch aktiver Strahlung (PAR) abhängig, die in einer bestimmten Tiefe des Bestandes auf den Blattflächen grüner Blätter auftrifft. Er hängt außerdem von der Blattbiomasse in einer Blattschicht und den in dieser Blattschicht zur Synthese von N_P verfügbaren Aminosäuren ab. Dabei

wird der aktuelle N_P-Gehalt einer Blattschicht mit dem potentiellen ($\equiv$ optimalen) Gehalt verglichen, der sich aus der exponentiellen Verteilung über die Bestandestiefe ableitet. Ist der aktuelle Gehalt kleiner als der potentielle N_P-Gehalt, so wird aus dem Pool der verfügbaren Aminosäuren für die N_P-Synthese neues N_P synthetisiert. Ist der aktuelle Gehalt größer oder gleich dem potentiellen Gehalt oder stehen keine verfügbaren Aminosäuren zur Verfügung, wird in der Blattschicht kein neues N_P synthetisiert. Überschüssiges N_P steht zur Synthese in der nächst tieferen Blattschicht zur Verfügung und wird für das Wachstum der Pflanze bereitgestellt. In dieser Modellversion beeinflussen das Entwicklungsstadium und die Seneszenz den potentiellen N_P-Gehalt der Blätter; ein möglicher Effekt des N_P-Abbaus auf das Entwicklungsstadium und die Seneszenz werden allerdings nicht berücksichtigt.

Simulationen mit der dynamischen Modellerweiterung des GECROS-Modells im Rahmen dieser Arbeit erlauben die Abbildung der durch CO_2-Anreicherung induzierten "beschleunigten Seneszenz" der unteren Blattschichten in einem Weizenbestand relativ zu den Simulationsergebnissen des unmodifizierten GECROS Modells, das eine exponentielle Abnahme der N_P-Gehalte in den Blättern über die Bestandestiefe annimmt (Abbildung 1.4). Derartige beschleunigte Seneszenz unter erhöhten CO_2-Bedingungen, die zu einer Reduktion der Photosyntheseleistung führt, wurde von Zhu et al. (2009), Fangmeier et al. (2000), Ludewig und Sonnewald (2000) und Peet et al. (1986) in Blättern von Weizen (*Triticum aestivum* L.), Gerste (*Hordeum vulgare* L.), Tabak (*Nicotiana tabacum* L.) und Gurke (*Cucumis sativus* L.) beobachtet. Verstärkt abnehmende Blattstickstoff-, Rubisco-, lösliche Protein- und Chlorophyllgehalte in den Blättern mit der Bestandstiefe unter erhöhter atmosphärischer CO_2-Konzentration fanden Seneweera et al. (2011) für Reis (*Oryza sativa* L.). Auch die Simulationen für Weizenwachstum mit dem im Rahmen dieser Arbeit entwickelten Stickstoffumsatzmodell zeigen diese vom exponentiellen Profil abweichende Tiefenverteilung der N_P-Gehalte (Abbildung 1.4). Dabei sind die N_P-Gehalte der oberen Blattschichten unter erhöhter CO_2-Konzentration höher und in den unteren Blattschichten niedriger als in Simulationen mit dem unmodifizierten GECROS Modell. Dieser Effekt verstärkt sich nach der Anthese ($\rightarrow$ beschleunigte Seneszenz) und basiert auf weiteren $\frac{Kohlenstoff}{Stickstoff}$-Verhältnissen in der Pflanzenbiomasse.

Das neue Modell zeigt, dass die effizientere Nutzung des assimilierten Stickstoffs unter CO_2-angereicherten Bedingungen die Ausbildung geringerer Wurzelbiomassen erlaubt, da relativ weniger Nährstoffe aufgenommen werden müssen, um mehr oberirdische Biomasse zu produzieren. Dieses Ergebnis basiert auf der Modellannahme,

dass das $\frac{Spross}{Wurzel}$-Biomasseverhältnis dem $\frac{Kohlenstoff}{Stickstoff}$-Verhältnis in der Gesamtpflanze entspricht (Priesack und Gayler, 2009: Gleichung 35). Die vom Modell prognostizierte Verschiebung des $\frac{Spross}{Wurzel}$-Biomasseverhältnisses zugunsten des Sprosses bei atmosphärischer CO_2-Anreicherung würde somit zu geringeren Kohlenstoffeinträgen in die Böden führen. Bei Modellen ohne dynamisches Photosyntheseakklimationsmodell für das Kulturpflanzenwachstum unter der prognostizierten Erhöhung der atmosphärischen CO_2-Konzentrationen der kommenden Jahrzehnte (IPCC, 2012) würde dagegen ein höherer Eintrag progonstiziert.

In *Kapitel* 4 wird die Lichtverteilung in einem geschlossenen Bestand junger Buchen untersucht. Der Bestand wird dabei in einen Voxelraum, der n^3 Würfel (Voxel) enthält, eingeteilt. Jedem Voxel werden Parameterwerte für die Transmissivität, die Absorption und die Reflektion des einfallenden Lichts zugeteilt. Diese Werte unterscheiden sich je nach Voxelkategorie. Je nach Lage des Voxels enthält das Voxel somit die Information Luft, Blatt oder Stängel. Während ein Luftvoxel keine Strahlung absorbiert oder reflektiert und keine Strahlung auslöscht, absorbiert ein Stängelvoxel einen Großteil der Strahlung und reflektiert einen Teil. Ein Blattvoxel absorbiert bzw. filtert einen Teil der Strahlung, lässt einen Anteil passieren (Transmission) oder reflektiert einen Teil des Lichts (gestreutes Licht).

Dafür wurde ein Bestand junger Buchen mit einem Laserscanner eingescannt und in einen 3D Voxelraum eingeteilt. Der Bestand wurde mit 9 Lampen (Osram HQI-TS 400 W/D, Osram GmbH, München, Deutschland) beleuchtet, deren Strahlungsmenge und Strahlungswinkel bekannt waren. Die an einer Vielzahl von Orten im Bestand ankommende Strahlung wurde in verschiedenen Tiefen gemessen. Im Modell sind die Endpunkte eines jeden Lichtstrahls die Mitte des nächsten durchdrungenen Voxels. Bei m Voxeln ergeben sich $9 \cdot m$ Strahlen. Je nachdem, welche Art von Voxel der Strahl durchschnitt, wurde er abgeschwächt und oder abgelenkt. Die im Bestand gemessenen und die simulierten Lichtwerte am Boden des Bestandes wurden abschließend miteinander verglichen und ausgewertet.

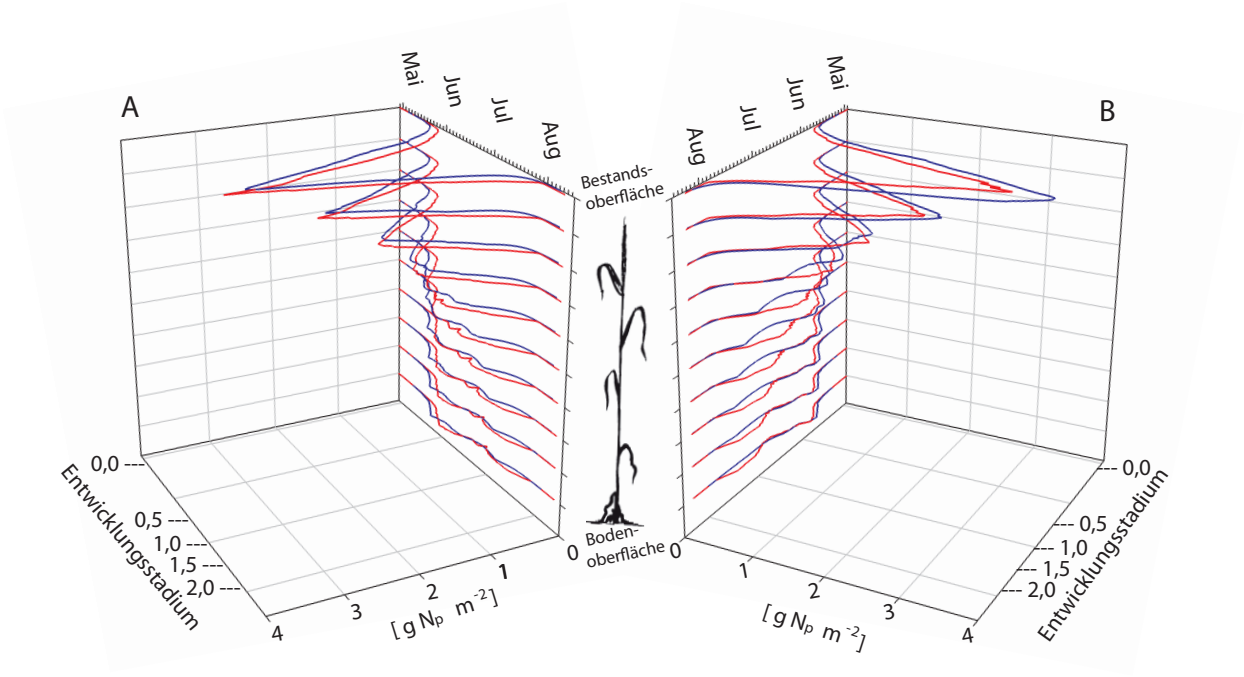

Abbildung 1.4: Dynamik der simulierten photosynthetisch aktiven Stickstoff (N_p) Gehalte in verschiedenen Bestandestiefen ($n = 10$ Schichten) eines Sommerweizenbestandes in Open-Top-Kammern in Gießen. A: ambiente atmosphärische CO_2-Konzentration (384 ppm); B: erhöhte atmosphärische CO_2-Konzentration (673 ppm). Rot: Expert-N-GECROS (XN-G); Blau: Expert-N-GECROS mit dynamischer, Licht gesteuerter N_p-Synthese (XN-GN). Reduzierte N_p-Gehalte gegenüber Simulationen mit XN-G in den oberen Bestandesschichten in A; Erhöhte N_p-Gehalte gegenüber den Simulationen mit XN-G in B. In B: Erhöhte CO_2-Konzentration führt zu beschleunigter Seneszenz (niedrigere N_p-Gehalte) in den tieferen Blattschichten nach der Anthese (Entwicklungsstadium 1,0 nach Penning de Vries et al., 1989).

1.7 Forschungsausblick

Eine direkte Messung der N_P-Gehaltstiefenverteilung in Beständen wäre wünschenswert, um die Funktionalität des Modells direkt zu evaluieren. Dies ist deshalb schwierig, weil in einem geschlossenen Bestand die Blätter gewöhnlich nicht horizontal angeordnet sind. Je nach dem Blattstellungswinkel und der Blattlänge kann somit ein und dasselbe Blatt Element mehrerer Bestandesschichten sein. Eine dreidimensionale Erfassung des Bestandes und die direkte Messung der Blattstickstoffgehalte mittels Remotesensing-Methoden könnte einen Weg bereiten, das neue Stickstoffumsatzmodell im Bestand zu evaluieren. Berücksichtigt werden muss dabei, dass sich die Korrelation von Blattstickstoff-, Chorophyll- und Rubiscogehalten häufig art- und sortenspezifisch unterscheiden (Seneweera et al., 2011). Entscheidend ist in jedem Fall, dass der Bestand während der Messung nicht gestört wird, da jede Störung zu einer Akklimation des Blattes an neue Umweltbedingungen (insbesondere an veränderte Lichtverhältnisse) führen würde. Die Ermittlung von Rubiscoumsatzraten in Abhängigkeit von der Blatttemperatur könnte entscheidend dazu beitragen das Modell genotypspezifisch zu parametrisieren.

Ähnlich der Akklimation, dem Zielkonflikt für die Partitionierung von Stickstoff in der Pflanze, ist ein derartiger Mechanismus auch für weitere Nährelemente zu erwarten. Eine Erweiterung des im Rahmen dieser Arbeit entwickelten Pflanzenwachstumsmodells hinsichtlich der Aufnahme und des Umsatzes weiterer Nährelemente unter Berücksichtigung der Akklimation an eine steigende atmosphärische CO_2-Konzentration scheint daher sinnvoll. In einem ersten Ansatz wäre die Akklimation an jene Nährelemente zu modellieren, die in Experimenten stärker einheitliche CO_2-Antworten bezüglich der Nährelementgehalte in Blättern und Ertrag von Kulturpflanzen offenbarten (z.B. Schwefel, Eisen, Phosphor und Magnesium; Fernando et al., 2012, Erbs et al., 2010, Högy et al., 2009 und Fangmeier et al., 1999). Diese sind die Nährelemente, die vorwiegend für die Optimierung des photosynthetischen Apparates relevant sind. In einer ersten Modellapproximation könnten die Umsätze proportional an den pflanzeninternen Stickstoffumsatz angelehnt werden.

Bisher werden Lichtverteilungen in Beständen meist nach dem Lambert-Beer Gesetz exponentiell abnehmend beschrieben (Monsi and Saeki, 2005). Unter der Annahme, dass die photosynthetische Kapazität linear mit dem Blattstickstoffgehalt zusammenhängen, wird nach Charles-Edwards et al. (1987) häufig auch die Extinktion des Blattstickstoffgehalts als proportional zur Lichtauslöschung im Bestand beschrieben

(z.B. in GECROS). Im Bestand beeinflussen sich Licht- und N_P-Verteilungen interaktiv. Daher erscheint es sinnvoll, deren Verteilungen durch ein Verfahren abzubilden, das diese Abhängigkeit dynamisch abzubilden vermag. Eine relative Häufung der N_P-Konzentration in einer Blattschicht würde eine verstärkte Lichtextinktion bedingen, während eine geringere N_P-Konzentration mehr Licht tiefer in den Bestand eindringen ließe, wodurch die N_P-Produktion in tieferen Blattschichten angeregt würde. Befindet sich die Pflanze im Equilibrium wäre zu erwarten, dass sich sowohl die Licht- als auch die N_P-Verteilungen der exponentiellen Verteilung annähern würden. Aufgrund des Wachstums und gewöhnlich dynamisch limitierter Nährstoffverfügbarkeit und variablem Nährstoffbedarf dürfte ein solcher Equilibriumzustand der Pflanze in Agrarökosystemen selten vorkommen. Somit würden sich auch für die Lichtverteilungen dynamisch von der exponentiellen Verteilung abweichende Verteilungsmuster ergeben, ähnlich den durch steigende CO_2-Konzentrationen induzierten resultierenden N_P-Verteilungen in *Kaptiel* 3 dieser Arbeit.

Literaturverzeichnis

Aben, S., S. Seneweera, O. Ghannoum, and J. Conroy: 1999, 'Nitrogen requirements for maximum growth and photosynthesis of rice, *Oryza sativa* L.-cv. Jarrah grown at 36 and 70 Pa CO_2'. *Australian Journal of Plant Physiology* **26**, 759–766.

Adam, N., G. Wall, B. Kimball, J. P. Pinter, R. LaMorte, D. Hunsaker, F. Adamsen, T. Thompson, A. Matthias, L. S.W., and A. Webber: 2000, 'Acclimation response of spring wheat in a free-air CO_2 enrichment (FACE) atmosphere with variable soil nitrogen regimes. 1. Leaf position and phenology determine acclimation response'. *Photosynthesis Research* **66**, 65–77.

AG BODEN: 2005, *Bodenkundliche Kartieranleitung*. Hannover, Germany: Schweizerbart'Sche Verlagsbuchhandlung, 5. Edition. Ad-hoc-Arbeitsgruppe Boden; Vorsitz: Wolf Eckelmann.

AGP III: 2009, 'An update of the Angiosperm Phylogeny Group classification for the orders and families of flowering plants: APG III'. *Botanical Journal of Linnean Society* **161**, 105–121.

Ainsworth, E., P. Davey, G. Hymus, C. Osborne, A. Rogers, H. Blum, J. Nosberger, and S. Long: 2003, 'Is stimulation of leaf photosynthesis by elevated carbon dioxide concentration maintained in the long term? A test with *Lolium perenne* grown for 10 years at two nitrogen fertilization levels under Free Air CO_2 enrichment (FACE)'. *Plant Cell and Environment* **26**, 759–766.

Ainsworth, E. and S. Long: 2005, 'What have we learned from 15 years of free-air CO_2 enrichment (FACE)? A meta-analytic review of the responses of photosynthesis, canopy properties and plant production to rising CO_2'. *New Phytologist* **165**, 351–372.

Ainsworth, E. and A. Rogers: 2007, 'The response of photosynthesis and stomatal conductance to rising [CO_2]: mechanisms and environmental interactions'. *Plant, Cell and Environment* **30**, 258–270.

Amthor, J.: 1995, 'Terrestrial higher-plant response to increasing atmospheric [CO_2] in relation to the global carbon cycle.'. *Global Change Biology* **1**, 243–274.

Amthor, J.: 2001, 'Effects of atmospheric CO_2 concentration on wheat yield; review on results from experiments using various approaches to control CO_2 concentration'. *Field Crops Research* **73**, 1–34.

Amthor, J. and D. Baldocchi: 2001, 'Terrestrial Higher Plant Respiration and Net Primary Production'. In: *Terrestrial Global Productivity*. pp. 33–59, Academic Press.

Anonym: 2012, 'Agrargeschichte'. Online, 2012/06/22. URL http://www.wissenschaft-online.de/abo/lexikon/geogr/164.

Barker, T., I. Bashmakov, L. Bernstein, J. Bogner, P. Bosch, R. Dave, O. Davidson, B. Fisher, S. Gupta, K. Halsnæs, G. Heij, S. Kahn Ribeiro, S. Kobayashi, M. Levine, D. Martino, O. Masera, B. Metz, L. Meyer, G.-J. Nabuurs, A. Najam, N. Nakicenovic, H.-H. Rogner, J. Roy, J. Sathaye, R. Schock, P. Shukla, R. Sims, P. Smith, D. Tirpak, D. Urge-Vorsatz, and D. Zhou: 2007, 'Mitigation. Contribution of Working Group III to the Fourth Assessment Report of the Intergovernmental Panel on Climate Change'. In: B. Metz, O. Davidson, P. Bosch, R. Dave, and L. Meyer (eds.): *Climate Change 2007*. Cambridge University Press, Cambridge, United Kingdom and New York, NY, USA.

Barnola, J.-M., D. Raynaud, Y. Korotkevich, and C. Lorius: 2011, 'Vostok Ice Core Provides 160,000-Year Record of Atmospheric CO_2'. In: D. Archer and R. Pierrehumbert (eds.): *The Warming Papers*, Heft 329. pp. 408–414, Blackwell Publishing Ltd.

Baruth, B.: 2012, 'Crop Monitoring in Europe'. *MARS Bulletin* **20, draft version**, 1–38.

Baxter, R., T. Ashenden, and J. Farrar: 1997, 'Effect of elevated CO_2 and nutrient status on growth, dry matter and nutrient content of *Poa alpina* var. Vivipara L'. *Journal of Experimental Botany* **48**, 1477–1486.

Beck, E.-G.: 2007, '180 years of atmospheric CO_2 gas analysis by chemical methods'. *Energy & Environment* **18**, 259–282.

Beerling, D.: 2005, 'Leaf evolution: gases, genes and geochemistry'. *Annals of Botany* **96**, 345–352.

Berg, B., H. Schenke, J. Eisele, E. Leisen, and A. Paffrath: 2003, 'Getreideanbau'. In: *Dokumentation 10 Jahre „Leitbetriebe Ökologischer Landbau NRW"- 10 Jahre Netzwerk Ökologischer Landbau in NRW: Wissenschaft - Beratung - Praxis*, Heft 105. pp. 45–63, Schriftenreihe des Lehr- und Forschungsschwerpunktes Ümweltverträgliche und Standortgerechte Landwirtschaft", Landwirtschaftliche Fakultät der Rheinischen Friedrich-Wilhelms-Universität Bonn. URL http://www.oekolandbau.nrw.de/pdf/leitbetriebe/dokumentation_10_jahre/getreidebau.pdf.

Bertheloot, J., B. Andrieu, and P. Martre: 2012, 'Light-nitrogen relationships within reproductive wheat canopy are modulated by plant modular organization'. *European Journal of Agronomy* **42**, 11–21.

Bertheloot, J., P. Cournède, and B. Andrieu: 2011, 'NEMA, a functional-structural model of nitrogen economy within wheat culms after flowering. I. Model description'. *Annals of Botany* **108**, 1085–1096.

Biernath, C., S. Bittner, C. Klein, S. Gayler, R. Hentschel, P. Hoffman, P. Högy, A. Fangmeier, and E. Priesack: 2013, 'Modeling acclimation of leaf photosynthesis to atmospheric CO_2 enrichment'. *European Journal of Agronomy* **48**, 74–87.

Biernath, C., S. Gayler, S. Bittner, C. Klein, P. Högy, A. Fangmeier, and E. Priesack: 2011, 'Evaluating the ability of four crop models to predict different environmental impacts on spring wheat grown in open-top chambers'. *European Journal of Agronomy* **35**, 71–82.

Binder, E.: 2003, *Bauern- und Wetterregeln*. Ulmer, Stuttgart, Germany, 2. Edition.

Bittner, S., S. Gayler, C. Biernath, J. Winkler, S. Seifert, H. Pretzsch, and E. Priesack: 2012, 'Evaluation of a ray-tracing canopy light model based on terrestrial laser scans'. *Canadian Journal of Remote Sensing* **38**, 619–628.

Blackman, F.: 1905, 'Optima and limiting factors'. *Annals of Botany* **19**, 281–295.

Blank, R., T. Morgan, L. Ziska, and R. White: 2011, 'Effect of Atmospheric CO_2 Levels on Nutrients in Cheatgrass Tissue'. *Natural Resources and Environmental Issues* **16**, 1–6.

Bloom, A., J. Asensio, L. Randall, S. Rachmilevitch, A. Cousins, and E. Carlisle: 2012, 'CO_2 enrichment inhibits shoot nitrate assimilation in C_3 but not C_4 plants and slows growth under nitrate in C_3 plants'. *Ecology* **93**, 355–367.

Bloom, A., M. Burger, J. Asensio, and A. Cousins: 2010, 'Carbon Dioxide Enrichment Inhibits Nitrate Assimilation in Wheat and Arabidopsis'. *Sience* **328**, 899–903.

Bloom, A., D. Smart, D. Nguyen, and P. Searles: 2002, 'Nitrogen assimilation and growth of wheat under elevated carbon dioxide'. *Proceedings of the National Academy of Sciences of the United States of America* **99**, 52–58.

Bowes, G.: 1991, 'Growth at elevated CO_2-photosynthetic responses mediated through Rubisco'. *Plant Cell and Environment* **14**, 795–806.

BpB: 2010, 'Bevölkerungsentwicklung'. Online, 2012/07/11. URL http://www.bpb.de/wissen/I6T8RL.

Bunce, J.: 2000, 'Acclimation of photosynthesis to temperature in eight cool and warm climate C_3 species: Temperature dependence of parameters of a biochemical photosynthesis model'. *Photosynthesis Research* **63**, 59–67.

Chai, T., M. Fadzillah, M. Kusnan, and M. Mahmood: 2005, 'Water stress-induced oxidative damage and antioxidant responses in micropropagated banana plantlets'. *Biologica Plantarum* **49**, 153–156.

Charles-Edwards, D., H. Stutzel, R. Ferraris, and D. Beech: 1987, 'An analysis of spatial variation in the nitrogen content of leaves from different horizons within a canopy'. *Annals of Botany* **60**, 421–426.

Collins, W., V. Ramaswamy, M. Schwarzkopf, Y. Sun, R. Portmann, Q. Fu, S. Casanova, J. Dufresne, D. Fillmore, P. Forster, V. Galin, L. Gohar, W. Ingram, D. Kratz, M. Lefebvre, J. Li, P. Marquet, V. Oinas, Y. Tsushima, T. Uchiyama, and W. Zhong: 2006, 'Radiative forcing by well-mixed greenhouse gases: Estimates from climate models in the Intergovernmental Panel on Climate Change (IPCC) Fourth Assessment Report (AR4)'. *Journal of Geophysical Research* **111**, 1–2.

Conroy, J. and P. Hocking: 1993, 'Nitrogen nutrition of C_3 plants at elevated atmospheric CO_2 concentrations'. *Physiologia Plantarum* **89**, 570–576.

Dana1981 and J. Abraham: 2011, 'IEA CO_2 Emissions Update 2010 - Bad News'. Online, 2012/06/14. URL http://www.skepticalscience.com/iea-co2-emissions-update-2010.html.

De Pury, D. and G. Farquhar: 1997, 'Simple scaling of photosynthesis from leaves to canopies without the errors of big-leaf models'. *Plant Cell and Environment* **20**, 537–557.

Del Pozo, A. and M. Dennett: 1999, 'Analysis of the distribution of irradiance, leaf nitrogen and photosynthesis within the canopy of *Vicia faba* L. at two contrasting densities'. *Australian Journal of Agricultural Research* **50**, 183–189.

Del Pozo, A., M. Perez, D. Gutierrez, A. Alonso, R. Morcuende, and R. Martinez-Carrasco: 2007, 'Gas exchange acclimation to elevated CO_2 in upper-sunlit and lower-shaded canopy leaves in relation to nitrogen acquisition and partitioning in wheat grown in field chambers'. *Environmental and Experimental Botany* **59**, 371–380.

DFG-PAK346: 2012, 'Struktur und Funktionen von Agrarlandschaften unter dem Einfluss des globalen Klimawandels - Prozessverständnis und Prognosen auf der regionalen Skala'. Online, 2012/09/13. URL https://lsc.uni-hohenheim.de/klimawandel0.

Drake, B., M. GonzalezMeler, and S. Long: 1997, 'More efficient plants: a consequence of rising CO_2?'. *Plant Molecular Biology* **48**, 609–639.

Dudley, R.: 1998, 'Atmospheric oxygen, giant Paleozoic insects and the evolution of aerial locomotor performance'. *Journal of Experimental Botany* **201**, 1043–1050.

Erbs, M., R. Manderscheid, G. Jansen, S. Seddig, A. Pacholski, and H.-J. Weigel: 2010, 'Effects of free-air CO_2 enrichment and nitrogen supply on grain quality parameters and elemental composition of wheat and barley grown in a crop rotation'. *Agriculture Ecosystem & Environment* **136**, 59–68.

Etheridge, D., L. Steele, R. Langenfelds, R. Francey, J.-M. Barnola, and V. Morgan: 1998, 'Historical CO_2 record from the Law Dome DE08, DE08-2, and DSS ice cores'. online, 2012/09/13. URL ftp://ftp.ncdc.noaa.gov/pub/data/paleo/icecore/antarctica/law/law_co2.txt.

Evans, J. and J. Seemann: 1989, 'The allocation of protein nitrogen in the photosynthetic apparatus: costs, consequences, and control'. In: W. Briggs (ed.): *Photosynthesis*. pp. 183–205, Alan R. Liss, New York.

Ewert, F., D. Rodriguez, P. Jamieson, M. Semenov, R. Mitchell, J. Goudriaan, J. Porter, B. Kimball, P. Pinter Jr, R. Manderscheid, H. Weigel, A. Fangmeier, E. Fereres, and F. Villalobos: 2002, 'Effects of elevated CO_2 and drought on wheat: testing crop simulation models for different experimental and climatic conditions'. *Agriculture Ecosystem & Environment* **93**, 249–266.

Fangmeier, A., B. Chrost, P. Högy, and K. Krupinska: 2000, 'CO_2 enrichtnent enhances flag leaf senescence in barley due to greater grain nitrogen sink capacity'. *Environmental and Experimental Botany* **44**, 151–164.

Fangmeier, A., L. De Temmerman, L. Mortensen, K. Kemp, B. J., R. Mitchell, M. Van Oijen, and H.-J. Weigel: 1999, 'Effects on nutrients and on grain quality in spring wheat crops grown under elevated CO_2 concentrations and stress conditions in the European, multiple-site experiment 'ESPACE-wheat". *European Journal of Agronomy* **10**, 215–229.

Fangmeier, A., W. Stein, and Jäger, H.-J.: 1992, 'Advantages of an open-top chamber plant exposure system to assess the impact of atmospheric trace gases on vegetation'. *Angewandte Botanik* **66**, 97–105.

FAO: 2006, 'World reference base for soil resources 2006 - A framework for international classification correlation and communication'. *World Soil Resources Reports* **103**, 145. Online, 2012/09/13. URL ftp://ftp.fao.org/agl/agll/docs/wsrr103e.pdf.

FAOSTAT: 2012, 'Production Crops: World - Cereals, Total from 1961 to 2010'. Online, 2012/09/12. URL http://faostat3.fao.org/home/index.html.

Farquhar, G. and S. von Caemmerer: 1982, 'Modelling of photosynthetic responses to environmental conditions'. In: O. Lange, P. Nobel, C. Osmond, and H. Ziegler (eds.): *Encyclopedia of Plant Physiology (New Series)*, Heft 12B of *Physiological Plant Ecology II*. pp. 549–587, Springer-Verlag, Germany.

Farquhar, G., S. von Caemmerer, and J. Berry: 1980, 'A biochemical model of photosynthetic CO_2 assimilation in leaves of C_3 species'. *Planta* **149**, 78–90.

Fernando, N., J. Panozzo, M. Tausz, R. Norton, G. Fitzgerald, and S. Seneweera: 2012, 'Rising atmospheric CO_2 concentration affects mineral nutrient and protein concentration of wheat grain'. *Food Chemistry* **133**, 1307–1311.

Firor, J.: 1993, *Herausforderung Weltklima - Ozonloch, globale Erwärmung und saurer Regen*. Spektrum Akademischer Verlag, Heidelberg, Berlin, Oxford.

Gifford, R., D. Barret, and J. Lutze: 2000, 'The effects of elevated [CO_2] on the C:N and C:P ratios of plant tissues'. *Plant and Soil* **224**, 1–14.

Goldenbaum, G. and R. Dickerson: 1993, 'Nitric oxide production by lightning discharges'. *Journal of Geophysical Research* **98**, 18333–18338.

Goudriaan, J. and H. van Laar: 1994, *Modelling Potential Crop Growth Processes*. Kluwer Academic Publishers, Dordrecht, the Netherlands.

Griffin, K. and J. Seemann: 1996, 'Plants, CO_2 and photosynthesis in the 21^{st} century.'. *Chemistry & Biology* **3**, 245–254.

Grolle, J.: 2010, 'Der Spiegel - Konkurrenz für Gott'. Online, 2012/09/13. URL http://www.spiegel.de/spiegel/print/d-68525307.html.

Groot, J.: 1987, *Simulation of Nitrogen Balance in a System of Winter Wheat and Soil*. Simulation Report CARBO-TT No. 13. Centre for Agrobiological Research (CABO) and Department of Theoretical Production Ecology, Agricultural University Wageningen, the Netherlands.

Grunwald, S.: 1997, 'GIS-gestützte Modellierung des Landschaftswasser- und Stoffhaushaltes mit dem Modell AGNPS'. *Schriftenreihe zur Bodenkunde, Landeskultur und Landschaftsökologie* **14**, 170 p. Disssertationsschrift, Gießen, Germany.

Gutierrez, D., E. Gutierrez, P. Perez, R. Morcuende, A. Verdejo, and R. Martinez-Carrasco: 2009, 'Acclimation to future atmospheric CO_2 levels increases photochemical efficiency and mitigates photochemistry inhibition by warm temperatures in wheat under field chambers'. *Physiologia Plantarum* **137**, 86–100.

Harley, P. and T. Sharkey: 1991, 'An improved model of C_3 photosynthesis at high CO_2: reversed O_2 sensitivity explained by lack of glycerate reentry into the chloroplast'. *Photosynthesis Research* **27**, 169–178.

Heß, D.: 1999, *Pflanzenphysiologie: Molekulare und biochemische Grundlagen von Stoffwechsel und Entwicklung der Pflanzen*. Eugen Ulmer Verlag Stuttgart, 10. Edition.

Heagle, A., D. Body, and W. Heck: 1973, 'An open-top field chamber to assess the impact of air pollution on plants'. *Journal of Environmental Quality* **2**, 365–368.

Heldt, H.-W., U. Flügge, and M. Stitt: 1986, 'Kohlenhydratstoffwechsel der pflanzlichen Photosynthese'. *Biologie in unserer Zeit* **4**, 97–105.

Heldt, H.-W. and F. Heldt: 2003, *Pflanzenbiochemie*. Spektrum Akademie Verlag, Germany, 3. Edition.

Heldt, H.-W. and B. Piechulla: 2011, *Plant Biochemistry*. Academic Press; Spektrum Akademischer Verlag, Heidelberg, 4. Edition.

Hell, R.: 2006, 'Was macht der Schwefel in der Zwiebel?'. *UniSpiegel, Universität Heidelberg* **3**. Online, 2012/09/13. URL http://www.uni-heidelberg.de/presse/ruca/ruca06-3/wasm.html.

Högy, P., M. Brunnbauer, P. Koehler, K. Schwadorf, J. Breuer, J. Franzaring, D. Zhunusbayeva, and A. Fangmeier: 2012, 'Grain quality characteristics of spring wheat (*Triticum aestivum*) as affected by free-air CO_2 enrichment'. *Environmental and Experimental Botany* **accepted for publication**.

Högy, P., M. Keck, K. Niehaus, J. Franzaring, and A. Fangmeier: 2010, 'Effects of atmospheric CO_2 enrichment on biomass, yield and low molecular weight metabolites in wheat grain'. *Journal of Cereal Science* **52**, 215–220.

Högy, P., H. Wieser, P. Köhler, K. Schwadorf, J. Breuer, J. Franzaring, R. Muntifering, and A. Fangmeier: 2009, 'Effects of elevated CO_2 on grain yield and quality of wheat: results from a three-year FACE experiment'. *Plant Biology* **11**, 60–69.

Hoffman, P., A. Kaufman, G. Halverson, and D. Schrag: 1998, 'A Neoproterozoic Snowball Earth'. *Science* **281**, 1342–1346.

Honda, M.: 2010, 'Phylogeny of Carnivorous Plants'. Online, 2012/07/11. URL http://www.honda-e.com/A03_Classification/PhylogeneticCladeTreeAPG2009.htm.

Ibetsberger, C.: 2004, 'Eiszeiten in der Erdgeschichte'. Online, 2012/06/22. URL http://www.raumfahrer.net/astronomie/planeterde/eiszeiten.shtml.

IPCC: 2012, 'Summary for Policymakers'. In: C. Field, V. Barros, T. Stocker, D. Qin, D. Dokken, K. Ebi, M. Mastrandrea, K. Mach, G.-K. Plattner, S. Allen, M. Tignor, and P. Midgley (eds.): *Managing the Risks of Extreme Events and Disasters to Advance Climate Change Adaption*. pp. 1–19, Cambridge University Press, Cambridge, UK, and New York, NY, USA.

Jacobs, B., J. Kingston, and L. Jacobs: 1999, 'The origin of grass-dominated ecosystems'. *Annals of the Missouri Botanical Garden* **86**, 590–643.

Jamieson, P. and M. Semenov: 2000, 'Modelling nitrogen uptake and redistribution in wheat'. *Field Crops Research* **68**, 21–29.

Jones, M.: 2011, 'C_4 species as energy crops'. In: A. Raghavendra and R. Rowan F. Sage (eds.): *C_4 Photosynthesis and Related CO_2 Concentrated Mechanisms (Advances in Photosynthesis and Respiration)*. pp. 379–397, Springer Netherlands.

Köcher-Schulz, B.: 2012, 'Eckpunkte der landwirtschaftlichen Entwicklung'. Online, 2012/06/22. URL http://www.bioinfo.at/jart/prj3/bioinfo/main.jart?

Kim, S.-H., D. Gitz, R. Sicher, J. Baker, D. Timlin, and V. Reddy: 2007, 'Temperature dependence of growth, development, and photosynthesis in maize under elevated CO_2'. *Environmental and Experimental Botany* **61**, 224–236.

Kim, S.-H., R. Sicher, H. Bae, D. Gitz, J. Baker, D. Timlin, and V. Reddy: 2006, 'Canopy photosynthesis, evapotranspiration, leaf nitrogen, and transcription profiles of maize in response to CO_2 enrichment'. *Global Change Biology* **12**, 588–600.

Kimball, B., K. Kobayashi, and M. Bindi: 2002, 'Responses of agricultural crops to free-air CO_2 enrichment'. *Advances in Agronomy* **77**, 293–368.

Kindell, H. and D. Pimentel: 1994, 'Constraints on the Expansion of Global Food Supply'. *Ambio* **23**. The Royal Swedish Academy of Sciences. Online, 2012/09/13. URL http://www.jayhanson.us/page36.htm.

König, W.: 2010, 'Ernteprognose 20.07.2010'. Online, 2012/08/08. URL http://www.braugerstengemeinschaft.de/index.php?StoryID=99.

Kondratyev, K. and N. Moskalenko: 1984, 'The role of carbondioxide and other minor gaseous components and aerosols in the radiation budget'. In: H. Houghton (ed.): *The Global Climate*. pp. 225–233, Cambridge University Press, Cambridge.

Kraus, H.: 2004, *Die Atmosphäre der Erde - Eine Einführung in die Meteorologie*. Springer Verlag, Berlin, Heidelberg, Germany, 3 Edition.

KSK 2020Plus: 2011, 'Klimaschutzkonzept 2020Plus'. online, 2012/06/24. URL http://www.energie-zentrum.com/pdf/klimaschutzkonzept_2020plus.pdf.

Laisk, A. and G. Edwards: 2009, 'Leaf C_4 Photosynthesis in silica: The CO_2 Concentrating Mechanism'. In: A. Laisk, L. Nedbal, and Gofindjee (eds.): *Photosynthesis in silico - Understanding Complexity from Molecules to Ecosystems*. pp. 323–349, Springer Dordrecht, The Netherlands.

Lara, M. and C. Andreo: 2011, *Abiotic Stress in Plants- Mechanisms and Adaptions*, Chapt. C_4 Plants Adaption to High Levels of CO_2 and to Drought Environments, p. 428. InTech.

Le Cain, D. and J. Morgan: 1998, 'Growth, gas exchange, leaf nitrogen and carbohydrate concentrations in NAD-ME and NADP-ME C_4 grasses grown in elevated CO_2'. *Physiologia Plantarum* **102**, 297–306.

Lee, T., M. Tjoelker, D. Ellsworth, and P. Reich: 2001, 'Leaf gas exchange responses of 13 prairie grassland species to elevated CO_2 and increased nitrogen supply'. *New Phytologist* **150**, 405–418.

Lieffering, M., H.-Y. Kim, K. Kobayashi, and M. Okada: 2004, 'The impact of elevated CO_2 on the elementalconcentrations of field-grownrice grains'. *Field Crops Research* **88**, 279–286.

Lloyd, J. and G. Farquhar: 1996, 'The CO_2 dependence of photosynthesis, plant growth responses to elevated CO_2: concentrations and their interaction with soil nutrient status. I. General principles and forest ecosystems.'. *Functional Ecology* **10**, 4–32.

Ludewig, F. and U. Sonnewald: 2000, 'High CO_2-mediateddown-regulation of photosynthetic gene transcripts is caused by accelerated leaf senescence rather than sugar accumulation'. *FEBS Letters* **479**, 19–24.

Manderscheid, R., J. Bender, H. Jager, and H. Weigel: 1995, 'Effects of season long CO_2 enrichment on cereals. II. Nutrient concentrations and grain quality'. *Agriculture Ecosystem & Environment* **54**, 175–185.

Manier, G.: 2004, 'Einführung in die Umweltmeteorologie'. Online, 2012/08/13. URL http://www.meteor.tu-darmstadt.de/umet/script/.

McElwain, J., F. Mayle, and D. Beerling: 2002, 'Stomatal evidence for a decline in atmospheric CO_2 concentration during the Younger Dryas stadial: a comparison with Antarctic ice core records'. *Journal of Quaternary Science* **17**, 21–29.

Miglietta, E., A. Giuntoli, and M. Bindi: 1996, 'The effect of free air carbon dioxide enrichment (FACE) and soil nitrogen availability on the photosynthetic capacity of wheat.'. *Photosynthesis Research* **47**, 281–290.

Monsi, M. and T. Saeki: 2005, 'On the Factor Light in Plant Communities and its Importance for Matter Production'. *Annals of Botany* **95**, 549–567.

Myhre, G., E. Highwood, K. Shine, and F. Stordal: 1998, 'New estimates of radiative forcing due to well mixed greenhouse gases'. *Geophysical Research Letters* **25**, 2715–2718.

Nakano, H., A. Makino, and T. Mae: 1997, 'The effect of elevated partial pressures of CO_2 on the relationship between photosynthetic capacity and N content in rice leaves'. *Plant Physiology* **115**, 191–198.

Narbonne, G.: 2008, 'The Gaskiers glaciation as a significant divide in Ediacaran history and stratigraphy'. In: *HPS-09 Stratigraphic correlation of Neoproterozoic strata*. International Geological Congress.

Osborne, C., J. LaRoche, J. Garcia, B. Kimball, G. Wall, P. Pinter, R. LaMorte, G. Hendrey, and S. Long: 1998, 'Does leaf position within a canopy affect acclimation of photosynthesis to elevated CO_2?'. *Plant Physiology* **177**, 1037–1045.

Peet, M., S. Huber, and D. Patterson: 1986, 'Acclimation to high CO_2 in Monoecious Cucumbers: II. carbon exchange rates, enzyme activities, and starch and nutrient concentrations'. *Plant Physiology* **80**, 63–67.

Penning de Vries, F., D. Jansen, H. ten Berge, and A. Bakema: 1989, *Simulation of ecophysiological processes of growth in several annual crops*, Heft 29 of *Simulation Monographs*. Pudoc Wageningen, The Netherlands.

Petit, R., J. Jouzel, D. Raynaud, N. Barkov, J.-M. Barnola, I. Basile, M. Bender, J. Chappellaz, M. Davis, G. Delaygue, M. Delmotte, V. Kotlyakov, M. Legrand, V. Lipenkov, C. Lorius, L. PÉpin, C. Ritz, E. Saltzman, and M. Stievenard: 1999, 'Climate and atmospheric history of the past 420,000 years from the Vostok ice core, Antarctica'. *Nature* **399**, 429–436.

Poorter, H., J. Bühler, D. van Dusschoten, J. Climent, and J. Postma: 2012, 'Pot size matters: a meta-analysis of the effects of rooting volume on plant growth'. *Functional Plant Biology* **39**, 839–850.

Priesack, E.: 2006, *Expert-N Dokumentation der Modellbibliothek. FAM-Bericht 60.* Hieronymus, München.

Priesack, E. and C. Bauer: 2003, *Expert-N Datenmanagement Version 3.0, FAM-Bericht 59.* Hieronymus, München.

Priesack, E. and S. Gayler: 2009, 'Agricultural crop models: Concepts of resource acquisition and assimilate partitioning'. In: U. Lüttge, W. Beyschlag, and J. Murata (eds.): *Progress in Botany 70.* pp. 195–222, Springer-Verlag, Berlin, Heidelberg,Germany.

Priesack, E., S. Gayler, and H. Hartmann: 2006, 'The impact of crop growth submodel choice on simulated water and nitrogen balances'. *Nutrient Cycling in Agroecosystems* **75**, 1–13.

Rachmilevitch, S., A. Cousins, and A. Bloom: 2004, 'Nitrate assimilation in plant shoots depends on photorespiration'. *Proceedings of the National Academy of Sciences of the United States of America* **101**, 11506–11510.

Ramaswamy, V., O. Boucher, J. Haigh, D. Hauglustaine, J. Haywood, G. Myhre, T. Nakajima, G. Shi, S. Solomon, R. Betts, R. Charlson, C. Chuang, J. Daniel, A.

Del Genio, R. van Dorland, J. Feichter, J. Fuglestvedt, P. d. F. Forster, S. Ghan, A. Jones, J. Kiehl, D. Koch, C. Land, J. Lean, U. Lohmann, K. Minschwaner, J. Penner, D. Roberts, H. Rodhe, G. Roelofs, L. Rotstayn, T. Schneider, U. Schumann, S. Schwartz, M. Schwarzkopf, K. Shine, S. Smith, D. Stevenson, F. Stordal, I. Tegen, Y. Zhang, F. Joos, and J. Srinivasan: 2011, 'Radiative forcing of climate change'. In: J. Houghton, Y. Ding, D. Griggs, M. Noguer, P. van der Linden, X. Dai, K. Maskell, and C. Johnson (eds.): *Climate Change 2001: The Scientific Basis. Contribution of Working Group I to the Third Assessment Report of the Intergovernmental Panel on Climate Change*. pp. 349–416, Cambridge University Press, Cambridge, United Kingdom and New York, NY, USA.

Reece, J., L. Urry, M. Cain, S. Wasserman, P. Minorsky, and J. R.B.: 2010, *Campbell Biology*. Pearson Benjamin Cummings, 9. Edition.

Revelle, R. and H. Suess: 1957, 'Carbon dioxide exchange between atmosphere and ocean and the question of an increase of atmospheric CO_2 during past decades'. *Tellus* **9**, 18–27.

Richter, G.: 1998, *Stoffwechselphysiologie der Pflanzen - Physiologie und Biochemie des Primär- und Sekundärstoffwechsels*. Georg Thieme Verlag, Stuttgart, Germany, 6. Edition.

Ritchie, J. and D. Godwin: 1987, 'CERES Wheat 2.0'. Online, 2011/05/10. URL http://nowlin.css.msu.edu/indexritchie.html.

Ritchie, J., D. Godwin, and S. Otter-Nacke: 1987, 'CERES-WHEAT. A simulation model of wheat growth and development'. *Unpublished model documentation.*

Rogers, A., B. Fischer, J. Bryant, M. Frehner, H. Blum, C. Raines, and S. Long: 1998, 'Acclimation of photosynthesis to elevated CO_2 under low-nitrogen nutrition is affected by the capacity for assimilate utilization. Perennial ryegrass under freeair CO_2 enrichment.'. *Plant Physiology* **118**, 683–689.

Rogers, A. and S. Humphries: 2000, 'A mechanistic evaluation of photosynthetic acclimation at elevated CO_2'. *Global Change Biology* **6**, 1005–1011.

Sage, R.: 1990, 'A model describing the regulation of ribulose-1,5-biphosphate carboxylase, electron transport, and triose phosphate use in response to light intensity and CO_2 in C_3 plants'. *Plant Physiology* **94**, 1728–1734.

Sage, R.: 1994, 'Acclimation of photosynthesis to increasing atmospheric CO_2: The gas exchange perspective'. *Photosynthesis Research* **39**, 351–368.

Sage, R.: 2004, 'The evolution of C_4 photosynthesis'. *New Phytologist* **161**, 341–370.

Sage, R., T. Sharkey, and J. Seemann: 1989, 'Acclimation of photosynthesis to elevated CO_2 in 5 C_3 species'. *Plant Physiology* **89**, 590–596.

Sardans, J., A. Rivas-Ubach, and J. Peñuelas: 2012, 'The C:N:P stoichiometry of organisms and ecosystems in a changing world: a review and perspectives.'. *Perspectives in Plant Ecology, Evolution and Systematics* **14**, 33–47.

Schlitter, J. and G. Wildner: 2001, 'Partnerwahl mit (r)evolutionärem Trick'. *RUBIN Wissenschaftsmagazin* pp. 12–17.

Schönwiese, C.: 1995, *Klimaänderungen*. Springer Verlag, Berlin, Heidelberg, New York.

Schopfer, P. and A. Brennicke: 2010, *Pflanzenphysiologie*. Spektrum Akademischer Verlag, Heidelberg, Germany, 7. Edition.

Schütz, M.: 2002, 'Untersuchungen zum Wachstum und Gaswechsel von Weizenbeständen unter globalen Klimaveränderungen unter besonderer Berücksichtigung von Veränderungen der atmosphärischen CO_2-Konzentrationen und des Bodenwasserhaushalts'. Ph.D. thesis, Justus-Liebig-Universität-Gießen.

Schütz, M. and A. Fangmeier: 2001, 'Growth and yield responses of spring wheat (*Triticum aestivum* L. cv Minaret) to elevated CO_2 and water limitation'. *Environmental Pollution* **114**, 187–194.

Schumann, U. and H. Huntrieser: 2007, 'The global lightning-induced nitrogen oxides source'. *Atmospheric Chemistry and Physics* **7**, 2623–2818.

Seneweera, S., A. Makino, N. Hirotsu, R. Norton, and Y. Suzuki: 2011, 'New insight into photosynthetic acclimation to elevated CO_2: The role of leaf nitrogen and ribulose-1,5-biphosphate carboxylase/oxygenase content in rice leaves'. *Environmental and Experimental Botany* **71**, 128–136.

Sharkey, T.: 1985, 'Photosynthesis in intact leaves of C_3 plants: physics, physiology and rate limitations'. *Botanical Review* **51**, 53–105.

Sharkey, T.: 1989, 'Evaluating the role of rubisco regulation in photosynthesis in C_3 plants'. *Philosophical Transactions of the Royal Society of London. Series B, Biological Sciences* **323**, 435–448.

Siegenthaler, U., T. Stocker, E. Monnin, D. Luthi, J. Schwander, B. Stauffer, D. Raynaud, J.-M. Barnola, H. Fischer, V. Masson-Delmotte, and J. Jouzel: 2005,

'Stable carbon cycle-climate relationship during the late pleistocene'. *Science* **310**, 1313–1317.

Smrcka, A. and S. Szarek: 1986, 'Phenotypical Temperature Adaptation of Protein Turnover in Desert Annuals'. *Plant Physiology* **80**, 206–210.

Sonnleitner, G.: 2011, 'Erwartung einer unterdurchschnittlichen Ernte bekräftigt sich'. Online, 2012/08/08. URL http://www.bauernverband.de/erwartung-unterdurchschnittlichen-ernte-bekraeftigt.

Spitters, C., H. van Keulen, and D. van Kraalingen: 1989, 'Simulation and Systems Management in Crop Protection'. *Simulation Monographs, Pudoc, Wageningen* **32**, 147–181.

Stafford, N.: 2007, 'The other greenhouse effect'. *Nature* **448**, 526–528.

Stitt, M. and A. Krapp: 1999, 'The interaction between elevated carbon dioxide and nitrogen nutrition: the physiological and molecular background'. *Plant Cell and Environment* **22**, 583–621.

Tans, P.: 2012, 'Recent Mauna Loa CO_2'. Online, 2012/09/13. URL http://www.esrl.noaa.gov/gmd/ccgg/trends/mlo.html.

Taub, D.: 2010, 'Effects of Rising Atmospheric Concentrations of Carbon Dioxide on Plants'. *Nature Education Knowledge* **1**, 21.

Taub, D. and X. Wang: 2008, 'Why are nitrogen concentrations in plant tissues lower under elevated CO_2? A critical examination of the hypothesis'. *Journal of Integrative Plant Biology* **50**, 1365–1374.

Thomas, R. and B. Strain: 1991, 'Root Restriction as a Factor in Photosynthetic Acclimation of Cotton Seedlings Grown in Elevated Carbon Dioxide.'. *Plant Physiology* **96**, 627–634.

Thornley, J.: 1998, 'Dynamic Model of Leaf Photosynthesis with Acclimation to Light and Nitrogen'. *Annals of Botany* **81**, 421–430.

Thornley, J.: 2002, 'Instantaneous canopy photosynthesis: Analytical expressions for sun and shade leaves based on exponential light decay down the canopy and an acclimated non-rectangular hyperbola for leaf photosynthesis'. *Annals of Botany* **89**, 451–458.

Thornley, J.: 2004, 'Acclimation of photosynthesis to light and canopy nitrogen distribution: An interpretation'. *Annals of Botany* **93**, 473–475.

Thornley, J. and J. France: 2007, *Mathematical models in agriculture: Quantitative methods for the plant, animal and ecological sciences.* CABI, 2. Edition.

Tubiello, F., J. Amthor, K. Kenneth J. Boote, M. Donatelli, W. Easterling, G. Fischer, R. Gifford, M. Howden, J. Reilly, and C. Rosenzweig: 2007, 'Crop response to elevated CO_2 and world food supply A comment on Food for Thought ... by Long et al., Science 312:1918-1921, 2006'. *European Journal of Agronomy* **26**, 1918–1921.

van Keulen, H., J. Goudriaan, L. Stroosnijder, E. Lantinga, and H. van Laar: 1992, *Simulation of Crop Growth for Potential and Water-Limited Production Situations (as applied to Spring Wheat).* Simulation Reports CABO-TT No. 27, vol. 27. Centre for Agrobiological Research and Department of Theoretical Production Ecology, Wageningen Agricultural University, The Netherlands.

van Keulen, H. and H. van Laar: 1982, 'Modelling of Agricultural Production: Weather, Soils and Crops'. *Simulation Monographs, Pudoc, Wageningen, The Netherlands* pp. 117–129.

van Noije, T., H. Eskes, F. Dentener, D. Stevenson, K. Ellingsen, M. Schultz, O. Wild, M. Amann, C. Atherton, D. Bergmann, I. Bey, K. Boersma, T. Butler, J. Cofala, J. Drevet, A. Fiore, M. Gauss, D. Hauglustaine, L. Horowitz, I. Isaksen, M. Krol, J.-F. Lamarque, M. Lawrence, R. Martin, V. Montanaro, J.-F. Müller, G. Pitari, M. Prather, J. Pyle, A. Richter, J. Rodriguez, N. Savage, S. Strahan, K. Sudo, S. Szopa, and M. van Roozendael: 2006, 'Multi-model ensemble simulations of tropospheric NO_2 compared with GOME retrievals for the year 2000'. *Atmospheric Chemistry and Physics* **6**, 2943–2979. Online, 2012/04/17 URL http://www.atmos-chem-phys.net/6/2943/2006/.

Voet, D., J. Voet, and C. Pratt: 2010, *Lehrbuch der Biochemie.* VCH Verlagsgesellschaft mbH, Weinheim, Germany, 2. Edition.

von Sengbusch, P.: 2003, 'Botanik online - Die Internetlehre - The Internet Hypertextbook'. Online, 2012/07/03. Online, 2012/09/16 URL http://www.biologie.uni-hamburg.de/b-online/d24/24b.htm.

Wagner, F., L. Kouwenberg, T. van Hoof, and H. Visscher: 2004, 'Reproducibility of Holocene atmosphere CO_2 records based on stomatal frequency'. *Quaternary Science Reviews* **23**, 1947–1954.

Wall, G., R. Neal, T. Brooks, B. Kimball, P. J. Pinter, R. LaMorte, F. Adamsen,

D. Hunsaker, G. Wechsung, F. Wechsung, S. Grossman-Clarke, S. Leavitt, A. Matthias, and A. Webber: 2000, 'Acclimation response of spring wheat in a free-air CO_2 enrichment (FACE) atmosphere with variable soil nitrogen regimes. 2. Net assimilation and stomatal conductance of leaves.'. *Photosynthesis Research* **66**, 79–95.

Wand, S., G. Midgley, and M. Jones: 1999, 'Response of wild C_4 and C_3 grass (*Poaceae*) species to elevated atmospheric CO_2 concentration: a meta-analytic test of current theories and perceptions'. *Global Change Biology* **5**, 723–741.

Wang, E.: 1997, 'Development of a generic process-oriented model for simulation of crop growth'. Ph.D. thesis, Institut für Landwirtschaftlichen und Gärtnerischen Pflanzenbau - Fachgebiet für Ackerbau und Informatik im Pflanzenbau, TU München.

Wang, E. and T. Engel: 2000, 'SPASS: a generic process-oriented crop model with versatile windows interfaces'. *Environmental Modelling & Software* **15**, 179–188.

Wang, Y., M. Frei, Q. Song, and L. Yang: 2011, 'The impact of atmospheric CO_2 concentration enrichment on rice quality - A research review'. *Acta Ecologica Sinica* **31**, 277–282.

Wang, Y. and P. Jarvis: 1990, 'Description and validation of array model MAESTRO.'. *Agricultural and Forest Meteorology* **51**, 257–280.

Webber, A., G. Nie, and L. S.P.: 1994, 'Acclimation of photosynthetic proteins to rising atmospheric CO_2'. *Photosynthesis Research* **39**, 413–425.

Weber, H. and L. Zimmermann: 2004, *2. KLIWA-Symposium am 03. und 04.05.2004 in Würzburg: Fachvorträge Klimaveränderung und Konsequenzen für die Wasserwirtschaft.*, Heft 4. Arbeitskreis KLIWA - www.kliwa.de (Landesanstalt für Umwelt, Messungen und Naturschutz Baden-Württemberg, Bayerisches Landesamt für Wasserwirtschaft, Deutscher Wetterdienst).

Wittig, V., C. Bernacchi, X.-G. Zhu, C. Calfapietra, R. Ceulemans, P. DeAngelis, B. Gielen, F. Miglietta, P. Morgan, and S. Long: 2005, 'Gross primary production is stimulated for three *Populus* species grown under free-air CO_2 enrichment from planting through canopy closure.'. *Global Change Biology* **11**, 644–656.

Wullschleger, S.: 1993, 'Biochemical limitations to carbon assimilation in C_3 plants - a retrospective analysis of the A/C_i curves from 109 species'. *Journal of Experimental Botany* **44**, 907–920.

Wullschleger, S., R. Norby, and C. Gunderson: 1992, 'Growth and maintenance respiration in leaves of *Liriodendron tulipifera* L. exposed to long-term carbon dioxide enrichment in the field'. *New Phytologist* **121**, 515–523.

Yin, X. and H. van Laar: 2005, *Crop Systems Dynamics - An Ecophysiological Simulation Model for Genotype-by-Environment Interactions*. Wageningen Academic Publishers, Wageningen, The Netherlands.

Yin, X., M. van Oijen, and A. Schapendonk: 2004, 'Extension of a biochemical model for the generalized stoichiometry of electron transport limited C_3 photosynthesis'. *Plant Cell and Environment* **27**, 1211–1222.

Zeldovich, Y. and Y. Raizer: 1967, *Physics of Shock Waves and High Temperature Hydrodynamic Phenomena*. Academic, San Diego, California.

Zhu, C., J. Zhu, Q. Zeng, G. Liu, Z. Xie, H. Tang, J. Cao, and Z. Zhao: 2009, 'Elevated CO_2 accelerates flag leaf senescence in wheat due to ear photosynthesis which causes greater ear nitrogen sink capacity and ear carbon sink limitation'. *Functional Plant Biology* **36**, 291–299.

Zhu, X.-G., Q. Song, and D. Ort: 2012, 'Elements of a dynamic systems model of canopy photosynthesis'. *Current Opinion in Plant Biology* **15**, 237–244.

Folgende in begutachteten Fachzeitschriften eingereichte und veröffentlichte Manuskripte sind in der vorliegenden Arbeit enthalten:

Kapitel 2

Biernath C., Gayler S., Bittner S., Klein, C., Högy P., Fangmeier A. und Priesack E. 2011: Evaluating the ability of four crop models to predict different environmental impacts on spring wheat grown in open-top chambers. *European Journal of Agronomy*, 35: 71–82.

Kapitel 3

Biernath C., Bittner S., Klein C., Gayler S., Hentschel R., Hoffman P., Högy P., Fangmeier A. and Priesack E. 2013: Modeling Acclimation of leaf photosynthesis to increasing atmospheric CO_2 concentration. *European Journal of Agronomy*, 48: 74-87.

Kapitel 4

Bittner S., Gayler S., Biernath C., Winkler J. B., Seifert S., Pretzsch, H. and Priesack E. 2012: The performance of a voxel-based canopy light model based on terrestrial laser scans. *Canadian Journal of Remote Sensing*, 38: 619-628.

C. J. Biernath hat die Manuskripte “Biernath et al. 2011. Evaluating the ability of four crop models to predict different environmental impacts on spring wheat grown in open-top chambers” und Biernath et al. “Modeling Acclimation of leaf Photosynthesis to Increasing Atmospheric CO_2 Concentration” als Erstautor erstellt, die zugrundeliegenden Simulationen durchgeführt und statistisch ausgewertet, die Modellentwicklung geleistet und die Messdaten aufbereitet. Die Modellentwicklung umfasste hierbei den Test der GECROS Implementierung in Expert-N, die Erweiterung des GECROS Modells zur Berechnung der Photosynthese für n Blattschichten des Bestandes, die Implementierung eines dynamischen Umsatzmodells (Turnovermodell) für photosynthetisch aktiven Stickstoff in der Pflanze sowie des Zielkonflikts bei der Verwendung des biologisch abgebauten photosynthetisch aktiven Stickstoffs alternativ für das Wachstum oder für die Optimierung des Photosyntheseapparates. Am Manuskript Bittner et al. war C. J. Biernath als Koautor beteiligt. Er hat mit S. Bittner die Inhalte des Manuskripts diskutiert, das Manuskript überarbeitet und für die Einreichung bei Fachjournalen vorbereitet.

2 Evaluating the ability of four crop models to predict different environmental impacts on spring wheat grown in open-top chambers

Published in the European Journal of Agronomy.

Biernath C., Gayler S., Bittner S., Klein, C., Högy P., Fangmeier A. und Priesack E. 2011: Evaluating the ability of four crop models to predict different environmental impacts on spring wheat grown in open-top chambers. *European Journal of Agronomy*, 35: 71–82.

Europ. J. Agronomy 35 (2011) 71–82

Contents lists available at ScienceDirect

European Journal of Agronomy

journal homepage: www.elsevier.com/locate/eja

Evaluating the ability of four crop models to predict different environmental impacts on spring wheat grown in open-top chambers

Christian Biernath[a,*], Sebastian Gayler[b], Sebastian Bittner[a], Christian Klein[a], Petra Högy[c], Andreas Fangmeier[c], Eckart Priesack[a]

[a] Helmholtz Zentrum München, German Research Center for Environmental Health, Institute of Soil Ecology, Modeling Soil-Plant-Systems, Ingolstädter Landstraße 1, D-85764 Neuherberg, Germany
[b] WESS - Water & Earth System Science Research Institute c/o Universität Tübingen, Center for Applied Geoscience, Sigwartstraße 10, D-72076 Tübingen, Germany
[c] Universität Hohenheim, Institute for Landscape and Plant Ecology, Area Plant Ecology and Ecotoxicology, August-v.-Hartmann-Straße 3, D-70599 Stuttgart, Germany

ARTICLE INFO

Article history:
Received 15 October 2010
Received in revised form 1 April 2011
Accepted 6 April 2011

Keywords:
Triticum aestivum L.
Wheat
Elevated CO_2
Crop growth simulation
Crop model

ABSTRACT

We used the modeling package Expert-N to investigate the ability of four generic-mechanistic crop models that were originally developed under field conditions to simulate the plant growth of spring wheat grown in open-top chambers (OTC) under different environmental conditions. We focus on the impacts of water limitation and elevated atmospheric CO_2 concentration on biomass production. Expert-N facilitates the comparison of the components of agro-ecosystem models because it allows the exchange of single modules while leaving the rest of the model unchanged. The crop growth part of the models SPASS, CERES-Wheat, SUCROS and GECROS were combined with the Penman–Monteith equation for potential evapotranspiration, the HYDRUS-1D model for water transport and the LEACHN model for nitrogen transport and turnover simulation. The models were applied to a data set provided by OTC experiments with spring wheat (*Triticum aestivum* L. cv. 'Minaret') that was grown under two atmospheric CO_2 concentrations (ambient/elevated), two irrigation schemes (non-limited water supply/water limitation) and two soil types (Cambisol/Chernosem) in two subsequent vegetation periods (1998/1999). Based on the model calibration using experimental and literature data, the best simulation results describing the impact of the considered environmental conditions were obtained using the SUCROS model followed by the SPASS, GECROS and CERES models. The study depicts the shortcomings of the underlying processes in all of the models. These shortcomings need to be addressed when models are applied on regional scales or for prediction under climate change conditions.

1. Introduction

Plants assimilate carbon from atmospheric CO_2 via photosynthesis. From a pre-industrial level of approximately 280 ppm (Siegenthaler et al., 2005), recent CO_2 concentrations now amount to 390 ppm (Tans, 2009) and are predicted to yield 450 ppm in the year 2030 (Alcamo et al., 2007; OECD EO, 2008). Because CO_2 is not substrate saturated at current atmospheric CO_2 concentrations, CO_2 enrichment commonly boosts crop yields of C_3 cereals, such as wheat, and thus increases food and feed production. Throughout the last two decades, this view was supported by various experiments using climate chamber, open-top chamber (OTC) and free-air-CO_2-enrichment (FACE) technology (Amthor, 2001; Fangmeier et al., 1999; Högy et al., 2009; Wullschleger et al., 1992). Although most studies have demonstrated positive effects on the aboveground biomass production of wheat under CO_2 enrichment (Ewert et al., 2002; Fangmeier et al., 2000; Poorter et al., 1996), several studies have suggested a reduction in the crop biomass under elevated CO_2 due to interactions with other environmental factors (Long et al., 2005,2006). Long et al. (2006) and Schimmel (2006) summarized that CO_2 fertilization effects on plant production have been overestimated as they account for up to 13% of wheat grown in FACE experiments in contrast to the 31–36% observed in chamber-based studies. Nevertheless, Ziska and Bunce (2007) have shown that differences of the CO_2 responses on plant production between several experimental systems were less significant if the data were normalized to the different levels of CO_2 enrichment. Moreover, elevated CO_2 inhibits the nitrate assimilation from soil (Bloom et al., 2010) that may be largely responsible for CO_2 acclimation and, in turn, decreases in grain protein quality (Högy and Fangmeier, 2008). Furthermore, CO_2 fertilization effects on plants using the C_3 metabolism are only expected if the environment is not limited by temperature or water supply. Extreme weather events, such as the prolonged periods of limited water supply predicted by climate scenarios for Europe (McGregor et al., 2005; Parizek et al., 2004), could interact with CO_2-induced impacts on crop growth in the future.

* Corresponding author. Tel.: +49 89 3187 3119; fax: +49 89 3187 3376.
E-mail address: christian.biernath@helmholtz-muenchen.de (C. Biernath).

1161-0301/$ – see front matter © 2011 Elsevier B.V. All rights reserved.
doi:10.1016/j.eja.2011.04.001

Throughout the last decades, various crop models have been developed that describe physiological processes and the cycling of water and nutrients in terrestrial agro-ecosystems. Model types can be characterized as static or dynamic, deterministic or stochastic and empirical or mechanistic (Dent and Blackie, 1979; Thornley and France, 2007). To date, model development for complex system simulations aims to be dynamic rather than static, deterministic rather than stochastic and mechanistic rather than empirical (Wang, 1997). Empirical models are direct descriptions of measurements, and they define the characteristics of a system in a simple way. At some points it is inevitable to use empirical sub-models, including when the physical processes are not well understood. In crop science, the typical use of empirically determined development stages and the thermal time leads to a principal empirical model approach. The advantages of empirical models include the little effort needed for calibration and their robustness. A mechanistic model would encompass the necessary physics, chemistry and physiology to describe the crop growth processes from seed initiation to senescence. Mechanistic models offer more options to improve the system and to understand processes and their interactions. They are therefore commonly favored for modeling climate change (Thornley and France, 2007; van Wijk et al., 2002). In practice, simulation models are mechanistic to varying degrees, with inevitable empiricisms built into the sub-models.

Cross comparison between models is a well-established tool for model evaluation (Ewert et al., 2002; Jamieson et al., 1998, 2000; Porter et al., 1993; Priesack and Gayler, 2006; Rastetter, 1996; van Wijk et al., 2002; Yin and Struik, 2010). Cross comparison shows the quality of model components and indicates which components need more intense scientific attention. Moreover, these comparisons assist the model user to evaluate modeling outputs, particularly when the models are used for regionalization or for climate change simulations.

The four crop models in this study were chosen because of the different degree to which they include mechanistic approaches to model genotype-by-environment interactions and because of the different approaches to simulate effects of CO_2 on crop growth. The selected models are CERES-Wheat 2.0 (Ritchie and Godwin, 1987; Ritchie et al., 1987), SUCROS2 (Goudriaan and van Laar, 1994; Groot, 1987; Spitters et al., 1989; van Keulen et al., 1992; van Keulen and van Laar, 1982), SPASS (Wang, 1997; Wang and Engel, 2000) and GECROS (Yin and van Laar, 2005). For simplicity, the four models are further abbreviated with CERES, SUCROS, SPASS and GECROS. In SUCROS and CERES, the CO_2 response is simply controlled by an empirical increase of the light use efficiency (LUE). The SPASS model assumes a constant initial slope where photosynthesis is entirely CO_2 limited with a switch to a horizontal maximum photosynthesis rate, and the GECROS model applies the non-rectangular hyperbolic response to CO_2 concentrations of the Farquhar model (Farquhar et al., 1980). The objective of this study was to test the four crop growth models included in the Expert-N modeling package in terms of their ability to simulate aboveground biomass production, grain yield and yield quality of spring wheat under various environmental conditions. For comparison, only the plant models were exchanged, and the models of water flow, nitrogen transport and heat transfer were the same for all four crop models. We therefore analyzed

(i) if the impacts of atmospheric CO_2 and water shortage on biomass production can be adequately simulated by each of the four different crop growth models and
(ii) if a more mechanistic modeling approach for the CO_2-induced responses on crop growth is an improvement compared to the established models that include empirical assumptions.

2. Material and methods

2.1. The Expert-N model package

The model package Expert-N was developed to provide models for the simulation of soil-plant-atmosphere systems. The modular design helps to combine simulation models from the available components that were implemented in the Expert-N package. These components include sub-models to simulate soil water flow, soil heat transfer, turnover and transport of soil carbon and nitrogen, soil management and crop growth (Priesack, 2006; Priesack and Bauer, 2003). The output of different crop growth sub-models describes phenological development, photosynthesis, canopy formation, growth of aboveground and root biomass, crop senescence, transpiration and nitrogen uptake. These sub-models include corresponding routines of the generic plant models CERES, SUCROS, SPASS and GECROS.

In contrast to the original crop growth models, the sub-models calculating soil processes such as water flow, heat transfer, and nitrogen transport were replaced within the Expert-N package by corresponding sub-models. In this way, the model package Expert-N facilitates the comparison of crop growth models because they can now be based on the same model components that represent the soil processes. In the following simulations, we applied the soil water flow model similar to HYDRUS 1D (Simunek et al., 1998), the soil heat transfer and soil nitrogen transport description using LEACHN (Hutson and Wagenet, 1992) and the soil carbon and nitrogen turnover simulation method according to the SOILN model (Johnsson et al., 1987).

2.2. Crop growth sub-models

CERES was developed for agricultural practice to simulate crop development and grain yield (Ritchie and Godwin, 1987; Ritchie et al., 1987). The model was designed for use under extremely different environments, including those with limited water availability (Otter-Nacke et al., 1986; Otter-Nacke and Ritchie, 1989). A number of cultivar specific coefficients explain the variability between cultivars. The CO_2 assimilation rates are calculated as a non-linear function of the absorbed photosynthetic active radiation (PAR) and a genotype specific LUE (Priesack, 2006). The model is independent of the leaf CO_2 concentration. To consider the effect of the atmospheric CO_2 concentration on plant growth, the model was modified to increase the light saturated photosynthetic capacity by 20% as the CO_2 concentration increases by 200 ppm (Tubiello et al., 1999).

The SUCROS model was developed to quantify the aboveground biomass production of crops. Although in SUCROS1, plant growth is dependent on temperature and radiation, it is further limited by the availability of water in SUCROS2. The SUCROS version implemented in Expert-N also considers nitrogen-limited growth, assuming a maximal uptake for each crop species and the partitioning of nitrogen according to the partitioning key given by van Keulen and Seligman (1987). The CO_2 assimilation rates are a hyperbolic function of the absorbed PAR (Goudriaan and van Laar, 1994). To consider the CO_2 effect, SUCROS was altered to be similar to CERES. Thus, grain numbers were calculated similar to CERES and SPASS from the stem weight at anthesis.

The SPASS model is a hybrid model composed of parts of CERES and SUCROS. For example, crop senescence is simulated using the relative death rate based on the SUCROS model, and partitioning of nitrogen follows the parameterization according to Penning de Vries et al. (1989). The CO_2 assimilation rates are calculated similarly to those in SUCROS by a hyperbolic function. The maximum photosynthetic rates and LUE are affected by the intercellular CO_2 concentration. For this purpose, based on a maximum

photosynthetic rate at a reference concentration of atmospheric CO_2, a reduction factor is described for optimal temperature and nitrogen conditions. This factor reduces maximum gross photosynthesis based on a Blackman-response that describes an initial constant increase at CO_2 limitation of photosynthesis and switches to a horizontal maximum when photosynthetic rates are no more limited by CO_2 concentrations (Priesack, 2006; Wang, 1997). In C_3 species, the maximum rate of leaf photosynthesis is nearly proportional to the atmospheric CO_2 concentration and holds up to a level of about 700 ppm (Penning de Vries et al., 1989).

The GECROS model is a succeeded the SUCROS models and was developed to better describe the interactions between genotype and environment. Therefore, the input parameters are mainly genotype-by-environment specific measurable parameters. The model deals with the interactions of CO_2 and other environmental factors on photosynthesis based on the biochemical Farquhar model (Farquhar et al., 1980). The assimilation rates are either limited by rubisco activity or rubisco biphosphate regeneration. In both cases, the assimilation rates are affected by the intercellular CO_2 concentration, and the model assumes an optimal criterion for the root-shoot ratios of nitrogen and carbon. Apart from temperature, radiation and water availability the nitrogen supply also determines crop growth (Yin and van Laar, 2005).

2.3. Data sets for model input and testing

The experimental data used in this study are part of the "IMPETUS" project that are presented in Schütz and Fangmeier (2001). The data were obtained from OTC experiments carried out at the Justus-Liebig-Universität Gießen, Germany. The experiment provides data of two vegetation periods (1998 and 1999) on the development stages and the aboveground biomass fractions of spring wheat grown at a density of 350 plants m^{-2} under different environmental conditions. The plants were exposed to two different atmospheric CO_2 concentrations (ambient and elevated) and two different water supply levels (limited and non-limited). The influences of two soil types (Cambisol and Chernozem) on crop growth were analyzed in 1998. The environmental conditions of the treatments were applied as presented in Table 1. The OTC system is described in detail by Fangmeier et al. (1991).

2.4. Model calibration

The models were parameterized using the available measurements of the reference treatment (ambient CO_2, non-limited water supply, Cambisol) in 1999 and data from the literature if the experiments could not provide the required parameters. According to Hunt et al. (1993), the model calibration was conducted iteratively. First, the crop phenological development of the four crop models was calibrated to the reference treatment. This was subsequently followed by adjusting the coefficients that describe crop growth and grain development. The adapted parameter values are presented in Table 2. Genotype-specific parameters were used when measurements were available from the experiment or could be obtained from the literature. The rest of the model parameters were taken from the original model documentations. Subsequently, calibrated models were applied to the remaining treatments of 1998 and 1999.

2.5. Statistical measures

The ability of the model to match the observations was tested by two statistical criteria: the model efficiency index (ME) after Willmott (1982) and the normalized root mean square error (NRMSE). The ME is a method to evaluate the modeling performance in a range between 0 and 1. A value close to 1 indicates high modeling efficiency. The NRMSE evaluates the average relative deviation between the simulation and the measurements in a range between 0 for a perfect match of simulation and measurement and $+\infty$ indicating no match at all. The definitions of the statistical measures are supplied in Appendix A.

ME and NRMSE were calculated for each model, each treatment and each replicate for the observables growth stage, total aboveground biomass and leaf area index (LAI). To include the variability of ME and NRMSE values between the individual treatments, the arithmetic means $\overline{ME}$ and $\overline{NRMSE}$ for the single observable over all treatments were also calculated. In addition, the arithmetic means of the statistical measurements over all considered plant variables and treatments, $\overline{\overline{ME}}$ and $\overline{\overline{NRMSE}}$, provide aggregated indices that facilitate comparisons of the model performance. In case of the yield parameters for grain yield, thousand grain weight and grain numbers measured once per year at crop maturity, only $\overline{ME}$ and $\overline{\overline{ME}}$ were calculated.

Differences between the different metrics were tested by the Kruskal–Wallis one way analysis of variance on ranks followed by the Student–Newman–Keuls test. A value of $p \leq 0.05$ was accepted as statistically significant.

3. Simulation results

Fig. 1 presents the simulation results of all four models together with measured data of the reference treatment. Table 3 presents the results of the statistical evaluation of those output variables that were measured repeatedly during the vegetation period for all treatments. Table 4 lists the simulation results and corresponding measurements of model outputs, for which only one measurement at the end of the vegetation exists, and it depicts the values of $\overline{ME}$ for these variables.

3.1. Overall behavior and model performance

Based on the values of $\overline{\overline{ME}}$ and $\overline{\overline{NRMSE}}$, a rough assessment of the performance of the models with respect to the crop growth variables presented in Table 3 is possible:

$\overline{\overline{ME}}$: SUCROS (0.85) > GECROS (0.84) > CERES (0.82) > SPASS (0.80).
$\overline{\overline{NRMSE}}$: SPASS (0.28) < SUCROS (0.30) < GECROS (0.43) < CERES (0.56).

Results for the grain yield parameters (Table 3) were as follows:

$\overline{\overline{ME}}$: SPASS (0.73) > SUCROS (0.56) > CERES (0.49) > GECROS (0.40).

The simulated development stages were within the standard deviations of the measurements for all four crop models (Fig. 1). The $\overline{ME}$ values were greater than 0.96, and the $\overline{NRMSE}$ values were below 0.15 (Table 3). During early growth stages, the CERES development rates were higher than in GECROS. The development rates of SUCROS were between those of the CERES and GECROS simulations. The performance of the simulations of the development stages was significantly better in the SPASS ($\overline{ME} = 0.99/\overline{NRMSE} = 0.09$) and SUCROS (0.99/0.15) simulations. However, the $\overline{ME}$ (0.98) of GECROS was significantly better than that of the CERES (0.96) simulations. CERES reached the development stage 20 two weeks earlier than GECROS. The simulation of the total aboveground biomass was within the standard deviations of the measurements except for the final harvest, which was underestimated (Fig. 1). In the case of both green leaf biomass and LAI,

Table 1
Experimental conditions of the applied data sets (Schütz and Fangmeier, 2001).

Cultivar	*Triticum aestivum* L. cv. 'Minaret'		
Year	1998	1998	1999
Soil type	Chernozem	Cambisol	Cambisol
Soil texture	Clay loam (Lt)	Loamy sand (Sl)	Loamy sand (Sl)
Soil depth [cm]	40 cm (pot system)	40 cm (pot system)	50 cm (plot system)
N-Fertilization [kg N ha^{-1}]	200	200	200
Irrigation (nw) [mm]	718 ± 67	789 ± 115	433 ± 5
Irrigation (lw) [mm]	377 ± 40	477 ± 48	102 ± 2
ambient CO_2 [ppm]	Ø380.4 ± 27.1	Ø380.4 ± 27.1	Ø383.7 ± 32.3
elevated CO_2 [ppm]	Ø634.1 ± 69.2	Ø634.1 ± 69.2	Ø672.7 ± 120.0
Organic C content [%]	2.44	0.812	0.812
Organic N content [%]	0.24	0.081	0.081
Texture (S/U/C) [%]	35/44/21	67/22/11	67/22/11
Porosity [%]	57	52	52
Field capacity (pF 1.8)	45	40	40
Wilting point (pF 4.2)	30	17	17
Plot size [m^2]	0.27	0.27	1.765
Lateral canopy border conditions	Shading fences	Shading fences	Border strip
Average PAR [MJ m^{-2} day^{-1}]	9.9 ± 4.6	9.9 ± 4.6	10.2 ± 3.6
Location of the experiments	50.6°N, 8.7°E, Gießen, Germany		

Soil type according to FAO classification. Soil textures as described in AG Boden (1994); the air flow rate within the OTC amounted to 19,000 m^3 h^{-1}; nw: non-limited water supply, lw: water limitation.

Table 2
Values of crop growth model parameters.

Parameter		Unit	Value	Reference
CERES				
P5	Grain filling period coefficient		4	
P1D	Day length coefficient		3.25	
P1V	Vernalization coefficient		0.3	
fPhint	Phyllochrome interval		80	Ritchie and Godwin (1987)
G1	Kernel number coefficient		4	Godwin et al. (1990)
G2	Kernel weight coefficient		3	Godwin et al. (1990)
LUE	Light use efficiency, ambient CO_2		7.5	Ritchie and Godwin (1987)
	Light use efficiency, elevated CO_2		9.0	Ritchie and Godwin (1987)
GECROS				
YGV	Growth efficiency of vegetative organs	g C g^{-1} C	0.79	Penning de Vries et al. (1989)
CFV	C fraction in vegetative-organ biomass	g C g^{-1}	0.45	Tubiello et al. (1999)
LWIDTH	Leaf width	m	0.012	Bos and Neuteboom (1998)
LNCI	Initial critical shoot N concentration	g N g^{-1}	0.0555	Brooks et al. (2000)
RNCMIN	Min N concentration in root	g N g^{-1}	0.0076	Rroco and Mengel (2000)
STEMNC	Min N concentration in stem	g N g^{-1}	0.005	Abreu et al. (1993)
SEEDW	Weight of a single seed	g $seed^{-1}$	0.038	Diepenbrock et al. (1999)
SEEDNC	Standard seed N concentration	g N g^{-1}	0.0242	Weigel and Manderscheid (2005)
HTMX	Max plant height	m	0.9	
CDMHT	Proportionality factor between stem biomass and plant height	g m^{-2} m^{-1}	450	
MTDV	Min thermal days for vegetative phase	day	22	
MTDR	Min thermal days for reproductive	day	32	
EAJMAX	Activation energy of J_{max}	J mol^{-1}	23,100	Alonso et al. (2009)
BLD	Leaf angle from horizontal		25	Simon (1999)
NUPTX	Max N-uptake rate	g N m^{-2} day^{-1}	0.5	
SLNMIN	Min specific leaf nitrogen	g N g^{-1}	0.2	
RDMX	Max root depth, 1998	cm	40	
	Max root depth, 1999	cm	50	
SPASS				
D_v	Physiological development days before anthesis	day	37	
D_r	Physiological development days after anthesis	day	24	
V_{nd}	Vernalization requirement	day	0	
W	Photoperiod sensitivity factor	day^{-1}	0.25	
$R_{gfill,max}$	Max grain filling rate	mg grain $^{-1}$ day^{-1}	1.75	
x_{grain}	Number of grains	g grains $stem^{-1}$	25	
	Basis parameterization for N allocation			Penning de Vries et al. (1989)
SUCROS				
TbaseV	Base temperature of development Rate before anthesis	C	0	
DVRV	Development rate before anthesis	C day^{-1}	0.4	
TbaseR	Base temperature of development rate after anthesis	C	0	
$DVRR^{-1}$	Development rate after anthesis	C day^{-1}	0.48	
LUE	Light use efficiency, ambient CO_2	g MJ^{-1}	0.45	Ritchie and Godwin (1987)
LUE	Light use efficiency, elevated CO_2	g MJ^{-1}	0.54	Ritchie and Godwin (1987)
	Basis parameterization of N allocation			van Keulen and Seligman (1987)

Table 3
Model efficiency index (ME) and normalized root mean square error (NRMSE) of the simulations with the respective model for the development stage, total aboveground biomass (TAGB) and leaf area index (LAI). $\overline{ME}$ and $\overline{NRMSE}$ represent the arithmetic means of each column, and $\overline{\overline{ME}}$ and $\overline{\overline{NRMSE}}$ represent the arithmetic mean of the observed ME and NRMSE values of a single crop model.

Treatment	Growth stage ME/NRMSE	TAGB ME/NRMSE	LAI ME/NRMSE	Growth stage ME/NRMSE	TAGB ME/NRMSE	LAI ME/NRMSE
	CERES			*SPASS*		
nw/aCO$_2$/Ch/98	0.95/0.23	0.81/0.14	0.86/0.66	0.98/0.13	0.81/0.14	0.76/0.77
nw/eCO$_2$/Ch/98	0.97/0.17	0.75/0.18	0.53/2.72	0.99/0.10	0.59/0.29	1.00/0.13
nw/aCO$_2$/Ca/98	0.97/0.16	0.68/0.27	0.90/0.49	0.99/0.12	0.55/0.31	0.68/0.94
nw/eCO$_2$/Ca/98	0.98/0.15	0.64/0.37	0.91/0.52	0.99/0.11	0.52/0.50	0.70/0.90
lw/aCO$_2$/Ch/98	0.95/0.21	0.34/0.75	0.60/2.17	0.98/0.12	0.00/0.27	1.00/0.12
lw/eCO$_2$/Ch/98	0.97/0.18	0.64/0.38	0.55/2.55	0.99/0.11	0.07/0.31	0.99/0.16
lw/aCO$_2$/Ca/98	1.00/0.16	0.59/0.28	0.57/2.40	1.00/0.12	0.39/0.26	0.99/0.14
lw/eCO$_2$/Ca/98	0.98/0.15	0.98/0.04	0.67/1.72	0.99/0.11	0.44/0.31	0.94/0.40
nw/aCO$_2$/Ca/99	0.97/0.16	0.93/0.14	0.91/0.33	0.99/0.12	0.79/0.21	0.86/0.35
nw/eCO$_2$/Ca/99	0.94/0.09	0.86/0.23	0.88/0.38	1.00/0.02	0.74/0.35	0.89/0.53
lw/aCO$_2$/Ca/99	0.94/0.09	0.80/0.24	0.76/0.75	1.00/0.04	0.61/0.32	0.91/0.32
lw/eCO$_2$/Ca/99	0.94/0.09	0.83/0.22	0.84/0.56	0.99/0.04	0.68/0.33	0.86/0.45
$\overline{ME} \pm SD$	0.96 ± 0.02^{A}	0.74 ± 0.17	0.75 ± 0.15^{A}	0.99 ± 0.01^{B}	0.52 ± 0.26	0.88 ± 0.11^{B}
$\overline{NRMSE} \pm SD$	0.15 ± 0.04^{A}	0.27 ± 0.18	1.27 ± 0.96^{A}	0.09 ± 0.04^{B}	0.30 ± 0.09	0.42 ± 0.30^{B}
	$\overline{\overline{ME}} = 0.820.17$, $\overline{\overline{NRMSE}} = 0.560.75$			$\overline{\overline{ME}} = 0.800.26$, $\overline{\overline{NRMSE}} = 0.280.22$		
	GECROS			*SUCROS*		
nw/aCO$_2$/Ch/98	0.98/0.17	0.73/0.31	0.63/0.84	0.98/0.23	0.79/0.15	0.81/0.67
nw/eCO$_2$/Ch/98	0.98/0.16	0.74/0.28	0.98/0.31	0.99/0.17	0.75/0.15	0.97/0.39
nw/aCO$_2$/Ca/98	0.96/0.21	0.48/0.61	0.62/1.07	0.99/0.16	0.64/0.22	0.73/0.82
nw/eCO$_2$/Ca/98	0.97/0.17	0.56/0.60	0.67/0.78	0.99/0.15	0.58/0.36	0.77/0.74
lw/aCO$_2$/Ch/98	0.97/0.17	0.65/0.39	0.85/0.56	0.98/0.21	0.26/1.04	0.98/0.30
lw/eCO$_2$/Ch/98	0.98/0.16	0.95/0.10	0.65/2.00	0.99/0.18	0.52/0.56	0.98/0.32
lw/aCO$_2$/Ca/98	0.99/0.21	0.70/0.27	0.76/0.66	0.98/0.16	0.41/0.48	0.98/0.27
lw/eCO$_2$/Ca/98	0.97/0.18	0.73/0.27	0.86/0.84	0.99/0.15	0.83/0.11	1.00/0.12
nw/aCO$_2$/Ca/99	0.96/0.21	0.89/0.19	0.87/0.35	0.99/0.16	0.80/0.20	0.90/0.36
nw/eCO$_2$/Ca/99	1.00/0.02	0.78/0.29	0.96/0.24	1.00/0.09	0.70/0.30	0.92/0.33
lw/aCO$_2$/Ca/99	1.00/0.04	0.93/0.18	0.90/0.33	1.00/0.09	0.70/0.27	0.98/0.18
lw/eCO$_2$/Ca/99	1.00/0.02	0.90/0.20	0.93/0.36	0.99/0.09	0.71/0.26	0.95/0.29
$\overline{ME} \pm SD$	$0.980.01^{C}$	0.750.15	$0.780.13^{A}$	$0.990.01^{B}$	0.640.17	$0.920.09^{B}$
$\overline{NRMSE} \pm SD$	$0.140.07^{A}$	0.310.15	$0.840.61^{C}$	$0.150.04^{A}$	0.340.26	$0.400.22^{B}$
	$\overline{\overline{ME}} = 0.840.15$, $\overline{\overline{NRMSE}} = 0.430.46$			$\overline{\overline{ME}} = 0.850.19$, $\overline{\overline{NRMSE}} = 0.300.22$		

Bold letters indicate the reference treatment; nw: non-limited water supply; lw: water limitation; aCO$_2$: ambient; eCO$_2$: elevated atmospheric CO$_2$ concentrations; Ch: Chernozem soil; Ca: Cambisol soil; 98: 1998; 99: 1999; SD: standard deviation of $\overline{ME}$ and $\overline{\overline{ME}}$, respectively; A, B and C indicate significant differences ($p < 0.05$; Student–Newman–Keuls).

Table 4
Comparison of measurements and simulations of grain yield parameters.

Yield parameter	Treatment	Measured ± SD	CERES Sim	GECROS Sim	SPASS Sim	SUCROS Sim
Grain yield [g m^{-2}]	nw/aCO$_2$/Ch/1998	575 ± 84	537.2	433.3	498.2	594.8
	nw/eCO$_2$/Ch/1998	809 ± 146	639.3	422.7	779.1	743.0
	nw/aCO$_2$/Ca/1998	790 ± 50	569.3	290.4	550.2	620.4
	nw/eCO$_2$/Ca/1998	1107 ± 180	682.9	522.8	785.9	705.2
	lw/aCO$_2$/Ch/1998	301 ± 40	539.3	446.2	514.9	684.2
	lw/eCO$_2$/Ch/1998	441 ± 239	640.7	619.1	765.7	791.2
	lw/aCO$_2$/Ca/1998	401 ± 29	569.6	320.5	530.2	684.1
	lw/eCO$_2$/Ca/1998	657 ± 63	682.9	630.1	777.6	772.8
	nw/aCO$_2$/Ca/1999	566 ± 98	582.1	557.3	479.2	608.3
	nw/eCO$_2$/Ca/1999	832 ± 241	681.5	648.5	819.1	705.5
	lw/aCO$_2$/Ca/1999	530 ± 145	372.0	540.1	302.4	479.0
	lw/eCO$_2$/Ca/1999	648 ± 120	448.0	661.2	501.2	542.9
	$\overline{ME}$		0.50	0.33	0.69	0.22
Thousand grain weight [g]	**nw/aCO$_2$/Ca/1999**	32.9 ± 4.8	43.9	32.2	39.7	35.6
	nw/eCO$_2$/Ca/1999	35.9 ± 2.3	42.8	38.0	42.0	35.7
	lw/aCO$_2$/Ca/1999	33.4 ± 2.8	36.2	31.3	32.4	37.9
	lw/eCO$_2$/Ca/1999	37.1 ± 1.5	37.6	37.9	32.5	38.1
	$\overline{ME}$		0.44	0.55	0.83	0.67
Grain number [m^{-2}]	nw/aCO$_2$/Ca/1999	17,143 ± 1386	13,382	17,378	12,162	17,173
	nw/eCO$_2$/Ca/1999	22,957 ± 5732	16,072	17,143	19,664	19,785
	lw/aCO$_2$/Ca/1999	15,645 ± 3308	10,364	17,391	9421	12,626
	lw/eCO$_2$/Ca/1999	17,434 ± 1352	12,027	17,472	15,564	14,238
	$\overline{ME}$		0.52	0.31	0.67	0.78

Bold letters indicate the reference treatment. nw: unlimited water supply; lw: water limitation; aCO$_2$: ambient, eCO$_2$: elevated atmospheric CO$_2$ concentrations; Ch: Chernozem; Ca: Cambisol. SD: Standard deviation, Sim: Simulation.

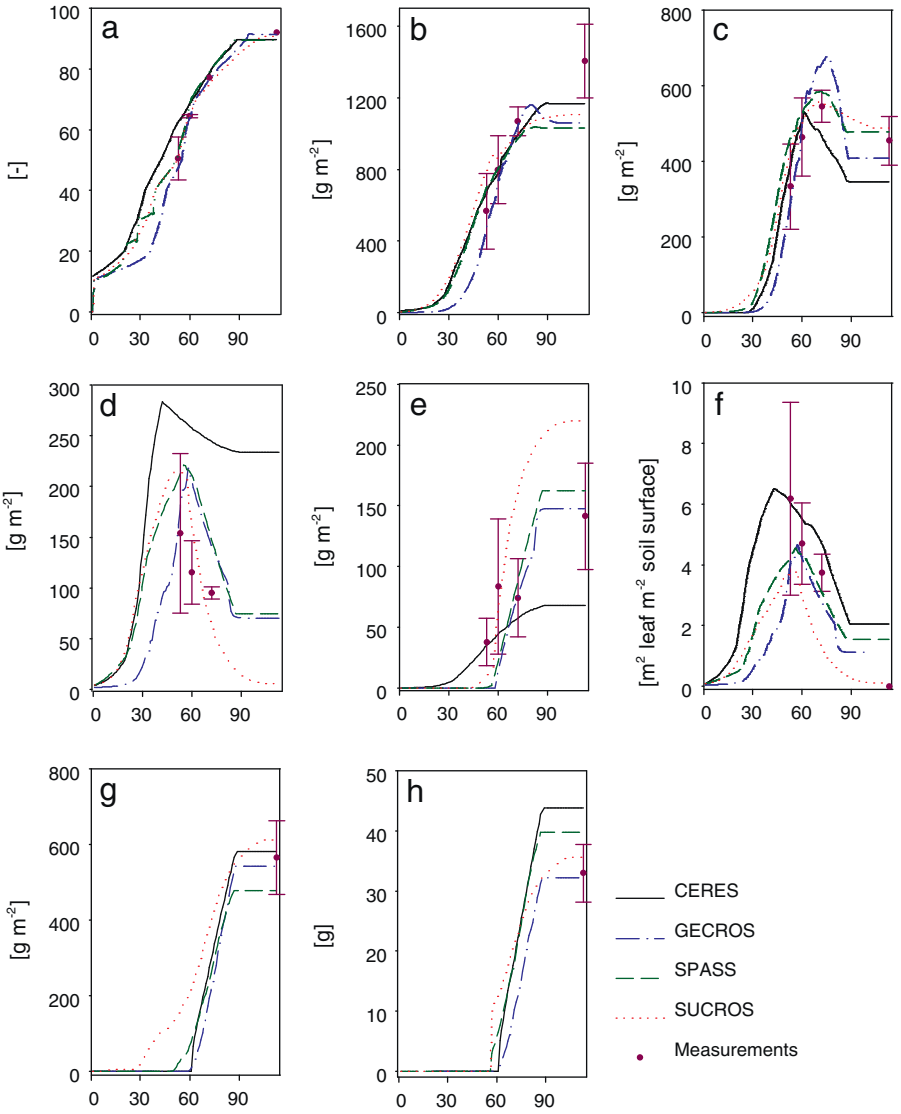

Fig. 1. Simulation results and dynamics of the reference treatment (wet, ambient CO_2, Cambisol, 1999) after calibration. *X*-axis units are the days after sowing. (a) Development stage; (b) total aboveground biomass DW; (c) stem DW; (d) green leaf DW; (e) senescent leaf DW; (f) LAI; (g) grain yield; (h) thousand grain weight. Abbreviations: DW – dry weight, LAI – leaf area index. Error bars are standard deviations of the measurements.

the variability of the measurements was high, particularly for the first harvest. The four models do not generally agree with the measurements, especially in the case of some high NRMSE values (above 1.00). These were observed in the CERES and GECROS simulations concerning the state variables stem biomass, green leaf biomass and LAI, in the SPASS simulations for the stem biomass and in the SUCROS simulations for the total aboveground and stem biomass. The $\overline{ME}$ and $\overline{NRMSE}$ values for the LAI simulations were significantly the best with SUCROS (0.92/0.40) and SPASS (0.88/0.42), respectively, which were primarily based on better simulations in 1998. The performance of LAI simulations by GECROS (0.78/0.84) was better than those by CERES (0.75/1.27; Table 3).

3.2. Environmental conditions

The observations and the simulations showed general dependency of the total aboveground biomass on environmental conditions (Table 5), but the simulated and measured effects varied strongly between the treatments. The sensitivity of the responses on environmental conditions due to the treatments was also observed for the leaf senescence, development stages, green leaves and yield.

3.2.1. Atmospheric CO_2 concentration

Generally, the four crop models agreed with the assumption that elevated atmospheric CO_2 concentrations increase plant growth. Nevertheless, some weaknesses were obtained for the accuracy of the simulations with any of the four crop models. None of the four crop models could simulate the strong variation of the CO_2 effect on total aboveground biomass, which was measured in the OTC with respect to the development stage in 1999. The simulations by the four models under different CO_2 concentrations basically increased the total aboveground biomass and grain yield. The response of the *CERES* and *SUCROS* simulations to elevated CO_2 increased the grain yields and total aboveground biomass rather constantly by 18% (CERES) and 16% (SUCROS). This increase was unaffected by other environmental conditions or the development stage of the crop. In interaction with the other environmental factors, a more sensitive CO_2 response was observed for the GECROS and SPASS simulations. The measured effect of the environmental variable on aboveground biomass varied in the treatments between the development

Table 5
(A) Ratio of the total aboveground biomass under elevated CO_2 concentration to total aboveground biomass under ambient CO_2 concentration for six treatments differing in water availability, soil type and year. (B) Ratio of the total aboveground biomass under unlimited water supply to the total aboveground biomass under water limitation for six treatments differing in atmospheric CO_2 concentration, soil type and year.

	DS	Measurement	CERES	GECROS	SPASS	SUCROS
(A) Relative effect of elevated CO_2						
nw/Ch/1998	65	1.28	1.18	1.49	1.45	1.36
	92	1.27	1.19	1.26	1.58	1.30
nw/Ca/1998	65	1.12	1.18	1.45	1.36	1.14
	92	1.38	1.18	1.36	1.43	1.15
lw/Ch/1998	65	1.35	1.17	1.49	1.37	1.14
	92	1.63	1.19	1.26	1.49	1.16
lw/Ca/1998	65	1.50	1.18	1.51	1.37	1.14
	92	1.58	1.18	1.49	1.45	1.14
nw/Ca/1999	44–57	1.14	1.18	1.36	1.58	1.14
	64–65	1.05	1.18	1.28	1.56	1.14
	77	1.00	1.19	1.18	1.57	1.15
	92	1.31	1.18	1.17	1.64	1.16
lw/Ca/1999	44–57	0.96	1.16	1.37	1.61	1.11
	64–65	1.43	1.15	1.29	1.56	1.11
	77	1.10	1.16	1.26	1.60	1.12
	92	1.10	1.18	1.20	1.64	1.12
(B) Relative effect of water limitation						
aCO_2/Ch/1998	65	0.58	1.01	0.99	1.05	1.18
	92	0.51	1.00	0.96	1.04	1.16
eCO_2/Ch/1998	65	0.61	1.00	0.99	0.99	1.00
	92	0.65	1.00	0.96	0.98	1.04
aCO_2/Ca/1998	65	0.68	1.00	1.07	0.99	1.00
	92	0.55	1.00	1.31	0.97	1.06
eCO_2/Ca/1998	65	0.92	1.00	1.12	0.99	1.00
	92	0.64	1.00	1.43	0.99	1.05
aCO_2/Ca/1999	44–57	0.90	0.88	1.00	0.82	0.82
	64–65	0.67	0.81	1.00	0.77	0.77
	77	0.79	0.86	0.84	0.81	0.79
	92	0.88	0.76	0.77	0.74	0.79
eCO_2/Ca/1999	44–57	0.76	0.86	1.00	0.84	0.80
	64–65	0.90	0.79	1.00	0.77	0.75
	77	0.88	0.84	0.90	0.83	0.77
	92	0.74	0.76	0.79	0.73	0.76

Bold letters indicate the reference treatment; nw: non-limited water supply; lw: water limitation; aCO_2: ambient; eCO_2: elevated atmospheric CO_2 concentrations; Ch: Chernozem soil; Ca: Cambisol soil; DS: development stage (Zadok et al., 1974).

stages 65 and 92. This effect was not strongly expressed in the simulations of all four crop models.

An earlier development of green leaf biomass under elevated CO_2 was simulated using GECROS, CERES and SPASS. Leaf senescence under elevated CO_2 concentrations was delayed in the simulations of each of the four crop models compared to the OTC measurements. SPASS and GECROS simulations showed an increase of senescent leaf biomass under elevated CO_2 conditions. While on average senescent leaf biomass was simulated best by SPASS under all different environmental conditions, the best response of leaf senescence to CO_2 enrichment was simulated using GECROS.

In *SPASS* simulations, elevated CO_2 increased total aboveground biomass and grain yields by 53% on average. In particular, the impact of elevated CO_2 on the stem biomass and grain yield ranged from a minimum increase of 43% up to 71%. On average, the CO_2 effect on grain yield was much more strongly expressed in 1999 (68%) than in 1998 (49%).

GECROS simulations showed a higher CO_2 fertilization effect on the grain yield when the water supply was limited. The highest sensitivity to CO_2 concentration on grain yields was simulated using GECROS. Elevated CO_2 increased the grain yield on average by 42%. However, the degree of the CO_2-induced response interacted strongly with the availability of water, resulting in a decrease by 2% up to an increase by 97%. Elevated CO_2 increased grain yields on average by 53% under water limitation, but only by 31% when water supply was not limited. Elevated CO_2 increased the thousand grain weight by 6 g, and the reduction due to water limitation was small (<1 g). At approximately 26% on average for all treatments, the increase observed in the measurements of total aboveground biomass resembled the average increase of the GECROS simulations. In 1999, the GECROS simulations clearly indicated that the CO_2 effect depended on the development stage. The effect was stronger in the earlier development stages (DC 44–65) than at later development stages (DC 77–92). Ongoing plant development weakened the positive CO_2 fertilization effect on total aboveground biomass by 16% on average (from 48% at heading to 34% at maturity in 1998 and from 36% to 18% in 1999, respectively). GECROS also indicated a slightly increased CO_2 fertilization effect on total aboveground biomass when the water supply was limited (Tables 3 and 4).

3.2.2. Water supply

The total aboveground biomass and the grain yield were differently affected by limited and non-limited water supply in the two years. In 1998, the significant reductions of total aboveground biomass and grain yields that were observed in the OTC experiments under water limitation could not be simulated by any of the four crop models. In 1999, the simulation results of all models were

in agreement with the observation that water limitation decreases the grain yield. In 1999, the measured reduction of the total aboveground biomass under water limitation was simulated adequately by the CERES, SPASS and SUCROS models throughout the vegetation period. In the GECROS simulations, this reduction did not occur until flowering, but then a drop of 22% was simulated for the water limited treatments until maturity.

In 1999, the grain numbers were significantly reduced by CERES, SPASS and SUCROS under water limitation. GECROS, however, simulated rather constant grain numbers. The thousand grain weights were reduced by water limitation in CERES, SPASS and SUCROS simulations (Table 4).

4. Discussion

The four crop models were evaluated focusing on three aspects: (A) the overall model performance, (B) the adequate description of the basic processes and (C) the applicability to the different environmental conditions. Furthermore, we analyzed the potential of each of the models for its use to simulate crop growth under climate change conditions at the regional scale.

4.1. Overall model performance

The NRMSE and ME values were comparable to other crop growth simulation studies (Niu et al., 2009; Priesack and Gayler, 2006; Wegehenkel and Mirschel, 2006). Single high NRMSE values showed that the four models tested in the present study cannot reliably predict all plant variables under the different environmental conditions of the OTC experiments. The statistical metrics based on ME and NRMSE values indicated that SPASS and SUCROS performed best for the simulation of the OTC experiments. The similarity of the simulation results between these two models was not surprising as the model of canopy light absorption is the same. The models differ primarily in their treatment of photosynthesis (see Section 2). Thus, the maximum photosynthetic rates are increased under elevated atmospheric CO_2 in SUCROS based on empirical data, although in SPASS the photosynthetic rates are calculated depending on intercellular CO_2 concentrations. For the OTC experiments, the application of the SPASS photosynthesis model caused overestimations of aboveground biomass growth under the elevated atmospheric CO_2 concentration.

The CERES model is a model often used for crop growth simulations, and it is an extensively analyzed, intrinsic component of the DSSAT and CROPSIM models (Bannayan et al., 2003; Hunt and Pararajasingham, 1995; Jamieson et al., 1998; Jones et al., 2003; Porter et al., 1993; Timsina and Humphreys, 2006). Originally, CERES was developed to simulate grain yield and aboveground biomass. Most authors find a good agreement between the simulations of these two variables (Heng et al., 2000); however, Jamieson et al. (1998) observed underestimations of aboveground biomass. In the present study, the CERES simulations were of high quality for the grain yield and aboveground biomass, based on considerably low parameterization effort.

The genotype specific parameterization of GECROS and the physical model description of plant growth processes are advantages in modeling studies that aim to understand the principal processes of wheat growth and particularly the reaction to environmental variables (Yin and Struik, 2010). However, this requires a higher parameterization effort due to the high number of genotype specific calibration parameters. This is a consequence of the Farquhar photosynthesis model among other contributing factors (Farquhar et al., 1980; Yin and van Laar, 2005). Besides the high parameterization effort, a significant weakness is that some parameters have constant values. The examples in the Farquhar photosynthesis model include the maximum carboxylation rate, the quantum use efficiency and the carbon respiration coefficient (Farquhar et al., 1980). However, these parameters may change under different environmental conditions even for a single genotype. Photosynthetic parameters may change for acclimation to different atmospheric CO_2 concentrations (Medlyn et al., 1999; Rastetter, 1996). Wittenbach (1979) found that even the development stage of a crop may alter these parameters.

In each of the models, crop development is based on temperature sums. The duration of a particular development stage is controlled by a crop species and the variety-specific number of degree-days (GECROS, SUCROS, SPASS) or the phyllochron that determines photothermal days for successive leaf development (CERES). This assumption is only valid, however, for optimum conditions of plant growth. Besides temperature, plant development is driven by factors such as atmospheric CO_2 concentration and water and nitrogen availabilities. Nord and Lynch (2009) reviewed the impacts of phenological development on the soil resource acquisition and the utility and remobilization of nitrogen within a plant. Slight differences in phenology modeling may cause a considerable difference with regard to the overall performance of model components. Development rates may be shortened by nitrogen deficiency (Gayler et al., 2002; Landivar et al., 2010; Marschner, 1995), delayed by excessive nitrogen supply (Angus and Moncur, 1985) or affected if water supply is suboptimal (Blum, 1996; Husain and Aspinal, 1970). Doraiswamy and Thompson (1982) suggested a model to include a water stress index that modifies the development rates of spring wheat. However, none of the four crop models accounts for interactions of such factors other than temperature on development rates. Therefore, the observed acceleration of development rates under elevated CO_2 treatments were not simulated by each of the models.

The soil nutrient and water availability for plant growth depend on the rooted soil depth. In plant growth models, an important factor is the root-front velocity, the rate at which roots extend to depth with time. The interplay between the root system formation and the aboveground biomass development is driven by the amount of water and nutrients taken up by the roots for shoot growth and by the amount of carbon that is partitioned to the roots from photosynthetic activity. In soils, the root system formation is very sensitive to environmental factors and genotype (species and variety) (Hoffman and Kolb, 1997; Weaver, 1926).

In contrast to Jamieson et al. (1998) and Savin et al. (1994), who showed differences of root penetration between SUCROS and CERES, we observed no significant differences for the downward root-front velocity. Because of the artificial root growth limitation by the shallow and homogenous soil profiles of the OTC experiments, possible differences between the root growth models are not expressed in the root-front velocity simulations. This resulted in a rapid rooting of the complete profile depth in the models. As a result, similar quantities of plant available water were provided for crop growth in all models. Differences were only observed in the water limited treatments in 1999. In the SUCROS, CERES and SPASS simulations, the root growth ceased if the soil water content of one soil layer fell below the water content of the permanent wilting point. As a consequence, the rooting depth was always less than 34 cm in the SUCROS, CERES and SPASS simulations. In GECROS, however, the root penetration was unaffected by the soil water content, which caused rapid rooting of the complete soil profile. Root-front velocity was calculated assuming an exponential root distribution in the soil profile modeled by an empirical extinction coefficient.

The actual transpiration rates determine the water uptake. Because of the delayed LAI development during early growth, the transpiration rates were smaller in the GECROS simulations, and consequently, less water was extracted from the soil than in the

simulations of the other models. Both the lower transpiration rates during early growth and the deeper rooting depth in GECROS simulations resulted in wetter soil conditions, particularly in the upper layers. Although water limitation restricted the transpiration rates and the rooting depth in SUCROS, CERES and SPASS simulations in mid-June and again in mid-July, GECROS simulations were only influenced during the second period of water limitation.

Although the intrinsic mechanisms of crop growth are generally the same independent of any environmental conditions, we stress that OTC are artificial systems that influence crop growth to an extent that remains unknown on the basis of the applied set of data. However, Ziska and Bunce (2007) showed that the CO_2 effects on crop growth between field and enclosure studies are small. Detailed descriptions of potential disagreements between measurements and simulation results based on OTC data are given by van Oijen and Ewert (1999). Both chamber and pot effects (Arp, 1991; Passioura, 2002; Pinter et al., 2000) cannot be ruled out because no comparable measurements under field conditions are available. Simulations of experiments that provide data from field and OTC may be useful for the evaluation of possible differences. We believe that such differences could be simulated using different soil parameters and root growth limitations.

4.2. Basic processes and mechanisms

In this section, we analyze the underlying processes that determine the assimilation rates, the LAI development and the grain numbers.

The carbon assimilation is dependent on PAR absorption and its consequent conversion into sugars. The simulations have shown that the light absorption was of major importance particularly during early crop growth (data not shown). Until anthesis, for example, the highest PAR absorption was simulated by CERES, which was approximately five times higher than in the GECROS simulation. Thus, the higher simulated PAR absorption during early plant growth caused higher carbon assimilation rates, resulting in increased leaf area development and light absorption. This positive feedback mechanism works until the incoming light is completely absorbed by the canopy or until the onset of senescence. In CERES, the simulation of this positive feedback loop is based on the simple model for light absorption where only direct beam and a single extinction coefficient ($k = 0.85$) are assumed. Due to the relatively high extinction coefficient, most light is absorbed by the top leaves of the canopy. This is an advantage when the LAI is small during early growth. The consequence is rapid leaf development that later caused overestimations of LAI. With increasing LAI, the absorbed radiation and the assimilation rates per unit leaf area declined in the CERES simulations. Porter et al. (1993) previously tested the CERES light absorption model and showed that simple variation of the extinction coefficient changes the simulation results but does not increase the model performance. A positive feedback loop between increasing LAI and light absorption also exists in GECROS at least until flowering, as long as the LAI development is carbon gain limited. At low leaf areas, the quantities of absorbed PAR are small, but with increasing LAI, higher amounts of PAR are absorbed at comparable smaller LAI values than in the CERES simulations. The more complex light absorption model that distinguishes between sunlit and shaded leaves and between different extinction coefficients for direct, scattered and diffuse light causes this outcome. The absorption of direct, scattered and diffuse light is modeled in SUCROS and SPASS in a way similar to GECROS. However, the direct beam extinction coefficient is constant in SUCROS and SPASS, whereas in GECROS, it is calculated dependent of the leaf angle and the sum of the green and the senescent leaf area. Elevated CO_2 concentration increased the mean assimilation rates per leaf area in the CERES, SPASS and SUCROS simulations but not in GECROS (Fig. 2). In GECROS, the slightly higher assimilation rates under elevated CO_2 increased the LAI from low to full expansion, but higher LAI values did not necessarily result in higher assimilation rates under CO_2 enrichment. Consequently, the average value of CO_2 assimilation rates per leaf area under elevated CO_2 was lower. In GECROS and SPASS, the dependency of the temperature-sensitive assimilation rates on the intercellular CO_2 concentrations resulted in a more dynamic interplay with the atmospheric CO_2 concentration. This contrasted with CERES and SUCROS, in which elevated CO_2 always increased the assimilation rates due to the higher parameter values for the maximal photosynthesis rates.

The calculation of the grain number is essential for the simulation of grain quality parameters, such as the concentrations of nutrients or protein. The mechanisms of grain number determinations were not fully understood until now (Fischer, 2008; Sinclair and Jamieson, 2006). In CERES, SPASS and SUCROS, the grain number is determined by the stem weight at flowering multiplied by a constant empirical factor, but the results varied between the three models. The best results were achieved by the SUCROS simulations, in which the best results for stem weights at different development stages were achieved. This indicates that the empirical estimation of the grain number from the stem weight at a certain development stage could be a suitable tool but that it depends on accurate predictions of stem biomass. The accuracies of the stem biomass predictions varied strongly between the different crop models, and the simulated grain number also varied between the models and the treatments. In GECROS, the grain number is dynamically determined by the grain nitrogen concentration at different development stages. In 1999, GECROS simulated constant grain numbers per area for all treatments ($17{,}346 \pm 142$ grains m^{-2}). Optimum nitrogen concentrations in the grains were achieved even if the water supply was limited. The nitrogen uptake rates are determined by the nitrogen availability in the rooted soil layers and the actual demand for nitrogen in the crop organs, which is limited by a daily crop specific maximum nitrogen uptake rate. Because C-assimilation was increased in the simulations under elevated CO_2 concentrations, the plants assimilated more nitrogen from the soil to achieve optimum nitrogen concentrations in the biomass. This simulation result was not in agreement with the experimental observation that C/N ratios increased in plants under elevated CO_2 due to acclimation (Fangmeier et al., 1999). Consequently, neither the CERES, SPASS and SUCROS models nor the GECROS model adequately described the determination of the grain number under OTC conditions.

4.3. Reaction to the different environmental conditions in the OTC experiments

If only yield and total aboveground biomass are considered, the CERES simulations were high quality, and the model can therefore be recommended for up-scaling yield and total aboveground biomass at regional levels and in climate change studies. However, quantities such as leaf senescence, LAI, stem and leaf biomass were almost unaffected by the different environmental conditions in the CERES simulations. Based on statistical and phenological interpretation, the simulations of highest quality under the different environmental conditions were found for SUCROS. However, the model weakness resulted in the overexpression of leaf senescence.

In most studies, positive effects were observed on the aboveground biomass production of C_3 species under elevated CO_2 (Ewert et al., 2002; Fangmeier et al., 2000; Poorter et al., 1996). As expected, this CO_2 effect was observed in the simulation results using four different crop models, but the models were unable to simulate the special conditions of the OTC experiments adequately. Clearly, the CO_2 response and its interaction with other environmental factors were more sensitive in the case of the two more

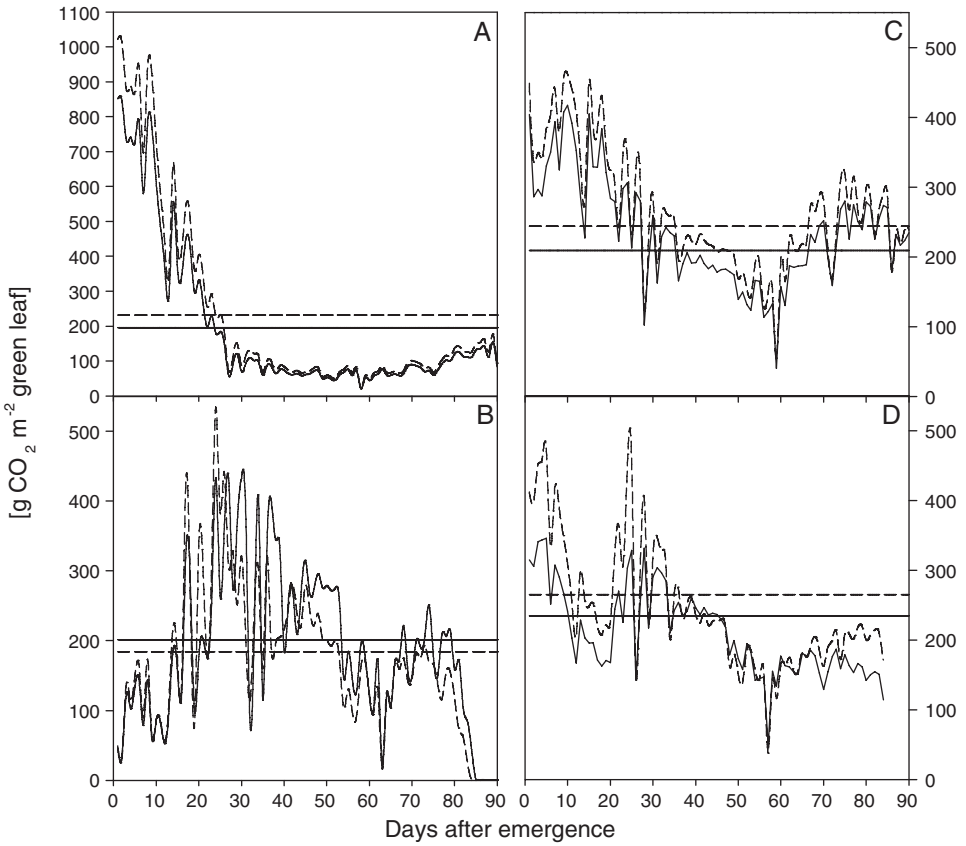

Fig. 2. Assimilation rates normalized by the leaf area index for ambient (straight lines) and elevated (dashed lines) atmospheric CO_2 concentrations (well watered treatments in 1999). Horizontal lines represent the averaged values over the vegetation period. A: CERES, B: GECROS, C: SUCROS, D: SPASS. Note the different ordinate scales.

mechanistic approaches by SPASS and GECROS. However, the SPASS simulations strongly overestimated biomass accumulation under elevated CO_2. In contrast, such overestimations of the CO_2 response were not simulated by GECROS, but the observed growth dynamics of the different OTC experiments were not described with sufficient quality. Despite this weakness, the GECROS simulations were in accordance with the finding by Ewert et al. (2002), Manderscheid and Weigel (2007); Tubiello and Ewert (2002), who reported that the effects of longer periods of water limitation in summer can be weakened by elevated CO_2.

In most of the simulations, the measured thousand grain weights were increased by elevated CO_2 and a non-limited water supply. Based on the $\overline{ME}$ value, the simulation of the thousand grain weight by SPASS ($\overline{ME} = 0.83$) performed best, followed by SUCROS ($\overline{ME} = 0.67$). In SUCROS and SPASS, the thousand grain weights are calculated as the ratio of yield to grain number. The yield is calculated from the fraction of assimilates partitioned to the grains. These fractions are provided by tabular functions. In 1999, the dynamic interplay of CO_2 and water availability was best simulated by GECROS. GECROS needs the genotype-specific final grain weight as a target input parameter, which regulates the strength of the sink for assimilate partitioning within the shoot. CERES performed more poorly than the other models ($\overline{ME} = 0.44$). In CERES, the growth rate of grains is driven by temperature and water deficit but is not affected by elevated CO_2.

5. Conclusions

Four crop models were calibrated to an experimental OTC dataset of different environmental conditions. The performance of the models in describing the impact of the considered effects of water availability and CO_2 concentration followed the order SUCROS > SPASS > GECROS > CERES. Hence, the more mechanistic models, GECROS and SPASS, do not generally lead to better model performance when describing the reaction of the plant to environmental conditions.

Nevertheless, this manuscript described the importance of using more physiologically based models to analyze the underlying processes of crop growth. We identified processes of plant growth that need further improvement, particularly in the case of CO_2 assimilation. A major weakness of CERES is the simple model of light absorption that does not consider diffuse and scattered light. As a consequence, biomass production was overestimated during the juvenile phase. The SUCROS model turned out to be quite robust for the simulation of wheat growth under the different environmental conditions of the OTC experiments. However, additional benefit for understanding the photosynthesis processes cannot be expected. The SPASS model overestimated the CO_2 assimilation rates under elevated CO_2 concentration, resulting in the overestimation of biomass, particularly of stem biomass. The Farquhar model used in GECROS is rather complex and based on a high parameterization effort. Some of these parameters might vary with the development stage or alter with changing environmental conditions. Dynamic interactions between the atmospheric CO_2 concentration and other environmental conditions on wheat growth were identified in the OTC experiments. Such dynamic interactions were also simulated by the more mechanistic models that consider intercellular CO_2 concentrations. However, the differences of the CO_2 response dynamics between the measurements and the simulations showed that further research and model improvement is important to understand the complex interaction of climate change and environmental conditions on crop growth responses.

Acknowledgments

The study was funded by the German Research Foundation (DFG) as part of the Joint Research Project 'Regional Climate Change' (PAK 346) at the Universität Hohenheim and the Helmholtz Zentrum München. We thank Dr. Hagen Scherb for his advice on statistical analysis. We thank two anonymous reviewers for their constructive criticisms that significantly helped to improve the manuscript.

Appendix A.

1. We define the ME after Willmott (1982) as

$$ME = 1 - \frac{\sum_{i=1}^{n}(P_i - O_i)^2}{\sum_{i=1}^{n}(|P_i - \bar{O}| + |O_i - \bar{O}|)^2} \quad (1)$$

where $\bar{O}$ denote for the mean values of the measured values O_i. The corresponding simulated values to O_i are P_i.

2. The NRMSE is given by

$$\mathrm{NRMSE} = \frac{\sqrt{(1/n)\sum_{i=1}^{n}(P - O_i)^2}}{\bar{O}} \quad (2)$$

The NRMSE describes the average relative deviation between the simulation and the measurements.

References

Abreu, J.D.M., Flores, I., Abreu, F.D., Madeira, M., 1993. Nitrogen uptake in relation to water availability in wheat. Plant Soil. 154 (1), 89–96.

Alcamo, J., Moreno, J., Nováky, B., Bindi, M., Corobov, R., Devoy, R., Giannakopoulos, C., Martin, E., Olesen, J., Shvidenko, A., 2007. Europe. Climate Change 2007: Impacts, Adaptation and Vulnerability. Contribution of Working Group II to the Fourth Assessment Report of the Intergovernmental Panel on Climate Change ,. Cambridge University Press, Cambridge, pp. 541–580.

Alonso, A., Perez, P., Martinez-Carrasco, R., 2009. Growth in elevated CO_2 enhances temperature response of photosynthesis in wheat. Physiol. Plant. 135 (2), 109–120.

Amthor, J., 2001. Effects of atmospheric CO_2 concentration on wheat yield: review of results from experiments using various approaches to control CO_2 concentration. Field Crop. Res. 73, 1–34.

Angus, J., Moncur, M., 1985. Models of growth and development of wheat in relation to plant nitrogen. Aust. J. Agric. Res. 36, 537–544.

Arp, W., 1991. Effects of source-sink relations on photosynthetic acclimation to elevated CO_2. Plant. Cell Environ. 14 (8), 869–875.

Bannayan, M., Crout, N., Hoogenboom, G., 2003. Application of the CERES-wheat model for within-season prediction of winter wheat yield in the United Kingdom. Agron. J. 95, 114–125.

Bloom, A., Burger, M., Asensio, J., Cousins, A., 2010. Carbon dioxide enrichment inhibits nitrate assimilation in wheat and Arabidopsis. Science 328 (5980), 899–903.

Blum, A., 1996. Crop responses to drought and the interpretation of adaptation. J. Plant Growth Regul. 20, 135–148.

Bos, J., Neuteboom, J., 1998. Growth of individual leaves of spring wheat (*Triticum aestivum* L.) as influenced by temperature and light intensity. Ann. Bot. Lond. 8, 141–149.

Brooks, T., Wall, G., Pinter Jr., P., Kimball, B.A., LaMorte, R., Leavitt, S., Matthias, A., Adamsen, F., Hunsaker, D., Webber, A., 2000. Acclimation response of spring wheat in a free-air CO_2 enrichment (FACE) atmosphere with variable soil nitrogen regimes 3. Canopy architecture and gas exchange. Photosynth. Res. 66, 97–108.

Dent, J., Blackie, M., 1979. Systems Simulation in Agriculture. Applied Science Publishers Ltd., London, UK.

Diepenbrock, W., Fischbeck, G., Heyland, K.-U., Knauer, N., 1999. Nutzpflanzenkunde. In: Spezieller Pflanzenbau, 3, neubearbeitete und ergänzte Edition. Eugen Ulmer, Stuttgart, Germany.

Doraiswamy, P., Thompson, D., 1982. A crop moisture stress index for large areas and its application in the prediction of spring wheat phenology. Agric. Meteorol. 27, 1–15.

Ewert, F., Rodriguez, D., Jamieson, P., Semenov, M., Mitchell, R., Goudriaan, J., Porter, J., Kimball Jr., B., Manderscheid, P.P., Weigel, R., Fangmeier, H., Fereres, A., Villalobos, E.F., 2002. Effects of elevated CO_2 and drought on wheat: testing crop simulation models for different experimental and climatic conditions. Agr. Ecosyst. Environ. 93, 249–266.

Fangmeier, A., Chrost, B., Hoegy, P., Krupinska, K., 2000. CO_2 enrichment enhances flag leaf senescence in barley due to greater grain nitrogen sink capacity. Environ. Exp. Bot. 44, 151–164.

Fangmeier, A., Stein, W., Jäger, J., 1991. Advantages of an open-top chamber plant exposure system to assess the impact of atmospheric trace gases on vegetation. Vereinigung für Angewandte Botanik 66, 97–105.

Fangmeier, A., Temmerman, L.D., Mortensen, L., Kemp, K., Burke, J., Mitchell, R., van Oijen, M., Weigel, H., 1999. Effects of nutrients on grain quality in spring wheat crops grown under elevated CO_2 concentrations and stress conditions in the European multiple-site experiment 'ESPACE-wheat'. Eur. J. Agron. 10, 215–229.

Farquhar, G., von Caemmerer, S., Berry, J., 1980. A biochemical model of photosynthetic CO_2 assimilation in leaves of C3 species. Planta 149, 78–90.

Fischer, R., 2008. The importance of grain or kernel number in wheat: a reply to Sinclair and Jamieson. Field Crop. Res. 105 (1–2), 15–21.

Gayler, S., Wang, E., Priesack, E., Schaaf, T., Maidl, F.-X., 2002. Modelling biomass growth, N-uptake and phenological development of potato crop. Geoderma 105, 367–383.

Godwin, D., Ritchie, J., Singh, U., Hunt, L., 1990. A User's Guide to CERES-Wheat – V2. 10. International Fertilizer Development Center, Muscle Shoals, AL, USA.

Goudriaan, J., van Laar, H., 1994. Modelling Potential Crop Growth Processes. Kluwer Academic Publishers, Dordrecht, the Netherlands.

Groot, J., 1987. Simulation of Nitrogen Balance in a System of Winter Wheat and Soil. Simulation Report CARBO-TT No. 13. Centre for Agrobioloigical Research (8CABO) and Department of Theoretical Production Ecology, Agricultural University Wageningen, the Netherlands.

Heng, L., Baethgen, W., Moutoonnet, P., 2000. The collection of a minimum dataset and the application of DSSAT for optimizing wheat yield in irrigated cropping systems. In: Optimizing Nitrogen Fertilizer Application to Irrigated Wheat. IAEA TECDOC-1164, 245 pp. (7–17).

Hoffman, T., Kolb, F., 1997. Effects of barley yellow dwarf virus on root and shoot growth of winter wheat seedlings grown in aeroponic culture. Plant Dis. 81, 497–500.

Högy, P., Fangmeier, A., 2008. Effects of elevated atmospheric CO_2 on grain quality of wheat. J. Cereal Sci. 48, 580–591.

Högy, P., Wieser, H., Köhler, P., Schwadorf, K., Breuer, J., Franzaring, J., Muntifering, R., Fangmeier, A., 2009. Effects of elevated CO_2 on grain yield and quality of wheat: results from a three-year FACE experiment. Plant Biol. 11 (Suppl. 1), 60–69.

Hunt, L., Pararajasingham, S., 1995. Cropsim-wheat: a model describing the growth and development of wheat. Can. J. Plant Sci. 75, 619–632.

Hunt, L., Pararajasingham, S., Jones, J., Hoogenboom, G., Imamura, D., Ogoshi, R., 1993. GENCALC: software to facilitate the use of crop models for analyzing field experiments. Agron. J. 85, 1090–1094.

Husain, I., Aspinal, D., 1970. Water stress and apical morphogenesis in barley. Ann. Bot. 34, 393–407.

Hutson, J., Wagenet, R., 1992. LEACHM: Leaching Estimation and Chemistry Model: A Process-Based Model of Water and Solute Movement, Transformations, Plant Uptake and Chemical Reactions in the Unsaturated Zone. Version 3.0. Tech. Rep. Research Series No. 93-3, Department of Soil, Crop and Atmospheric Sciences, Cornell University, Ithaca, NY.

Jamieson, P., Berntsen, J., Ewert, F., Kimball, B., Olesen Jr., J., Porter, P.P., Semenov, J.M., 2000. Modelling CO_2 effects on wheat with varying nitrogen supplies. Agric. Ecosyst. Environ. 82, 27–37.

Jamieson, P., Porter, J., Goudriaan, J., Ritchie, J., van Keulen, H., Stol, W., 1998. A comparison of the models AFRCWHEAT2, CERES-wheat, Sirius, SUCROS2 and SWHEAT with measurements from wheat grown under drought. Field Crop. Res. 55, 23–44.

Johnsson, H., Bergstroem, L., Bergstroem, P., Jansson, P., Paustian, K., 1987. Simulated nitrogen dynamics and losses in a layered agricultural soil. Agric. Ecosyst. Environ. 18, 333–356.

Jones, J., Hoogenboom, G., Porter, C., Boote, K., Batchelor, W., Wilkens, P., Sing, U., Gijsman, A., Ritchie, J., 2003. The DSSAT cropping system model*1. Eur. J. Agron. 18 (3–4), 235–265.

Landivar, J., Reddy, K.R., Hodges, H., 2010. Physiological simulation of cotton growth and yield. In: Physiology of Cotton. Springer, Dordrecht/Heidelberg/London/New York.

Long, S., Ainsworth, E., Leakey, A., Morgan, P., 2005. Global food insecurity. Treatment of major food crops with elevated carbon dioxide or ozone under large-scale fully open-air conditions suggests recent models may have overestimated future yields. Philos. Trans. R. Soc. B 360, 2011–2020.

Long, S., Ainsworth, E., Leakey, A., Nosberger, J., Donald, R., 2006. Food for thought: lower-than-expected crop yield stimulation with rising CO_2 concentrations. Science 312 (5782), 1918–1921.

Manderscheid, R., Weigel, H., 2007. Drought stress effects on wheat are mitigated by atmospheric CO_2 enrichment. Agron. Sustainable Dev. 27, 679–687.

Marschner, H., 1995. Mineral Nutrition of Higher Plants, 2nd edition. Academic Press, London.

McGregor, G., Ferro, C., Stephenson, D., 2005. Projected Changes in Extreme Weather and Climate Events in Europe. Springer, Berlin/Heidelberg/Germany, p. 303.

Medlyn, B., Badeck, F., Pury, D.D., Barton, C., Broadmeadow, M., Ceulemans, R., Angelis, P.D., Forstreuter, M., Jach, M., Kellomaki, S., Laitat, E., Marek, M., Philippot, S., Rey, A., Strassemeyer, J., Laitat, K., Liozon, R., Portier, B., Roberntz, P., Wang, K., Jarvis, P., 1999. Effects of elevated [CO_2] on photosynthesis in European forest species: a meta-analysis of model parameters. Plant Cell Environ. 22, 1475–1495.

Niu, X., Easterling, W., Hays, C., Jacobs, A., Mearns, L., 2009. Reliability and input-data induced uncertainty of the EPIC model to estimate climate change impact on sorghum yields in the U.S. Great Plains. Agric. Ecosyst. Environ. 129, 268–276.

Nord, E., Lynch, J., 2009. Plant phenology: a critical controller of soil resource acquisition. J. Exp. Bot. 60 (7), 1927–1937.
OECD EO, 2008. Environmental Outlook to 2030, http://www.oecd.org/environment/outlookto2030 (accessed 09.06.10).
Otter-Nacke, S., Godwin, D., Ritchie, J., 1986. Testing and Validating the CERES-Wheat Model in Diverse Environments. Agristar Tech. Rep.YM-15-00407, JSC-202-44. Johnson Space Center, Houston, USA.
Otter-Nacke, S., Ritchie, J., 1989. Crop growth simulation model. In: Farm Resource Management Program. Annual Report 1988. ICARDA , Aleppo, Syria, pp. 99–110.
Parizek, B., Richard, R., Alley, B., 2004. Implications of increased Greenland surface melt under global-warming scenarios: ice-sheet simulations. Quaternary Sci. Rev. 23 (9–10), 1013–1027.
Passioura, J., 2002. Soil conditions and plant growth. Plant Cell Environ. 25 (2), 311–318.
Penning de Vries, F., Jansen, D., ten Berge, H., Bakema, A., 1989. Simulation of Ecophoysiological Processes of Growth in Several Annual Crops. Pudoc, Wageningen, the Netherlands.
Pinter, P.J., Kimball, B., Wall, G., LaMorte, R., Hunsaker, D., Adamsen, F., Frumau, K., Vugts, H., Hendrey, G., Lewin, K., Nagy, J., Johnson, H., Wechsung, F., Leavitt, S., Thompson, T., Matthias, A., Brooks, T., 2000. Free-air CO_2 enrichment (FACE): blower effects on wheat canopy microclimate and plant development. Agric. Forest. Meterol. 103, 319–333.
Poorter, H., Roumet, C., Campbell, B., 1996. Interspecific variation in the growth response of plants to elevated CO_2: a search for functional types. In: Carbon Dioxide, Populations, and Communities. Academic Press, San Diego, CA, USA, pp. 375–412.
Porter, J., Jamieson, P., Wilson, D., 1993. A comparison of the wheat crop simulation models AFRCWHEAT2. CERES wheat and SWHEAT for non-limiting conditions of growth. Field Crop. Res. 33, 131–157.
Priesack, E., 2006. Expert-N Dokumentation der Modellbibliothek – FAM-Bericht 60. Forschungsverbund Agrarökosysteme München – Erfassung, Prognose und Bewertung nutzungsbedingter Veränderungen in Agrarökosystemen und deren Umwelt. Hyronimus Buchproduktions GmbH, München, Germany.
Priesack, E., Bauer, C., 2003. Expert-N Datenmanagement – FAM-Bericht 59. Forschungsverbund Agrarökosysteme München – Erfassung, Prognose und Bewertung nutzungsbedingter Veränderungen in Agrarökosystemen und deren Umwelt. Hieronimus Buchproduktions GmbH, München, Germany. Priesack, E., Gayler, S., Hartmann, H.P., 2006. The impact of crop growth sub-model choice on simulated water and nitrogen balances. Nutr. Cycl. Agroecosyst. 75 (1–3), 1–13.
Rastetter, E., 1996. Validating models of ecosystems response to global change. Bioscience 46, 190–198.
Ritchie, J., Godwin, D., 1987. CERES Wheat 2.0, http://nowlin.css.msu.edu/indexritchie.html (accessed 11.05.10).
Ritchie, J., Godwin, D., Otter-Nacke, S., 1987. CERES-WHEAT. A simulation model of wheat growth and development. Unpublished model documentation.
Rroco, E., Mengel, K., 2000. Nitrogen losses from entire plants of spring wheat (*Triticum aestivum*) from tillering to maturation. Eur. J. Agron. 13, 101–110.
Savin, R., Hallb, A., Satorrea, E., 1994. Testing the root growth subroutine of the CERES-wheat model for two cultivars of different cycle length. Field Crop. Res. 38 (3), 125–133.
Schimmel, D., 2006. Climate change and crop yields: beyond Cassandra. Science 312 (5782), 1889–1890.
Schütz, M., Fangmeier, A., 2001. Growth and yield responses of spring wheat (*Triticum aestivum* L. cv Minaret) to elevated CO_2 and water limitation. Environ. Pollut. 114 (2), 187–194.
Siegenthaler, U., Stocker, T., Monnin, E., Luthi, D., Schwander, J., Stauffer, B., Raynaud, D., Barnola, J.-M., Fischer, H., Masson-Delmotte, V., Jouzel, J., 2005. Stable carbon cycle-climate relationship during the late pleistocene. Science 310 (5752), 1313–1317.
Simon, M., 1999. Inheritance of flag-leaf angle, flag-leaf area and flag-leaf area duration in four wheat crosses. Theor. Appl. Genet. 98, 310–314.
Simunek, J., Huang, K., van Genuchten, M., 1998. The HYDRUS Code for Simulating the One-Dimensional Movement of Water, Heat, and Multiple Solutes in Variably-Saturated Media. Version 6.0. Tech. Rep. U.S. Salinity Laboratory, USDA, ARS.
Sinclair, T., Jamieson, P., 2006. Grain number, wheat yield, and bottling beer: an analysis. Field Crop. Res. 98 (1), 60–67.
Spitters, C., van Keulen, H., van Kraalingen, D., 1989. Simulation and Systems Management in Crop Protection. Simulation Monographs, vol. 32. Pudoc, Wageningen, pp. 147–181.
Tans, P., 2009. Trends in Carbon Dioxide, http://www.esrl.noaa.gov/gmd/ccgg/trends/ (accessed 17.05.10).
Thornley, J., France, J., 2007. Mathematical Models in Agriculture – Quantitative Methods for the Plant, Animal and Ecological Sciences, 2nd edition. Cromwell Press, Trowbridge, UK.
Timsina, J., Humphreys, E., 2006. Applications of CERES-rice and CERES-wheat in research, policy and climate change studies in Asia: a review. Int. J. Agric. Res. 1 (3), 202–225.
Tubiello, F., Ewert, F., 2002. Simulating the effects of elevated CO_2 on crops: approaches and applications for climate change. Eur. J. Agron. 18, 57–74.
Tubiello, F., Mahato, T., Morton, T., Druitt, J., Volk, T., Marino, B., 1999. Growing wheat in biosphere 2 under elevated CO_2: observations and modelling. Ecol. Eng. 13, 273–286.
van Keulen, H., Goudriaan, J., Stroosnijder, L., Lantinga, E., van Laar, H., 1992. Simulation of Crop Growth for Potential and Water-Limited Production Situations (as Applied to Spring Wheat). Simulation Reports CABO-TT No. 27, vol. 27. Centre for Agrobiological Research and Department of Theoretical Production Ecology, Wageningen Agricultural University, The Netherlands, pp. 27–72.
van Keulen, H., Seligman, N., 1987. Simulation of Water Use, Nitrogen Nutrition and Growth of a Spring Wheat Crop. Pudoc, Wageningen, the Netherlands.
van Keulen, H., van Laar, H., 1982. Modelling of Agricultural Production: Weather, Soils and Crops. Simulation Monographs, Pudoc, Wageningen, the Netherlands, pp. 117-129.
van Oijen, M., Ewert, F., 1999. The effects of climatic variation in Europe on the yield response of spring wheat cv 'Minaret' to elevated CO_2 and O_3: an analysis of open-top chamber experiments by means of two crop growth simulation models. Eur. J. Agron. 10, 249–264.
van Wijk, M., Bouten, W., Verstraten, J., 2002. Comparison of different modelling strategies for simulating gas exchange of a Douglas-fir forest. Ecol. Model. 158, 63–81.
Wang, E., 1997. Development of a generic process-oriented model for simulation of crop growth. Ph.D. Thesis. Institut für Landwirtschaftlichen und Gärtnerischen Pflanzenbau – Fachgebiet für Ackerbau und Informatik im Pflanzenbau, TU München, Herbert Utz Verlag, München, Germany.
Wang, E., Engel, T., 2000. SPASS: a generic process-oriented crop model with versatile windows interfaces. Environ. Model. Software 15, 179–188.
Weaver, J., 1926. Root Development of Field Crops. McGraw Hill, New York.
Wegehenkel, M., Mirschel, W., 2006. Crop growth, soil water and nitrogen balance simulation on three experimental field plots using the Opus model – a case study. Ecol. Model. 190, 116–132.
Weigel, H., Manderscheid, R., 2005. CO_2 enrichment effects on forage and grain nitrogen content of pasture and cereal plants. J. Crop Improve. 13 (1), 73–89.
Willmott, C., 1982. Some comments on the evaluation of model performance. Bull. Am. Meteorol. Soc., 64.
Wittenbach, V., 1979. Ribulose bisphosphate carboxylase and proteolytic activity in wheat leaves from anthesis through senescence. Plant Physiol. 64, 884–887.
Wullschleger, S., Norby, R., Gunderson, C., 1992. Growth and maintenance respiration in leaves of *Liriodendron tulipifera* L. exposed to long-term carbon dioxide enrichment in the field. New Phytol. 121, 515–523.
Yin, X., Struik, P., 2010. Modelling the crop: from system dynamics to systems biology. J. Exp. Bot. 61, 2171–2183.
Yin, X., van Laar, H., 2005. Crop Systems Dynamics – An Ecophysiological Simulation Model for Genotype-by-Environment Interactions. Wageningen Academic Publishers, Wageningen, the Netherlands.
Zadok, J., Chang, T., Konzak, C., 1974. A decimal code for the growth stages of cereals. Weed Res. 14, 415–421.
Ziska, L.H., Bunce, J.A., 2007. Predicting the impact of changing CO_2 on crop yields: some thoughts on food. New Phytol. 175 (4), 607–618.

3 Modeling acclimation of leaf photosynthesis to atmospheric CO_2 enrichment

Published in the European Journal of Agronomy.

Biernath C., Bittner S., Klein C., Gayler S., Hentschel R., Hoffman P., Högy P., Fangmeier A. and Priesack E. 2013: Modeling Acclimation of leaf photosynthesis to increasing atmospheric CO_2 concentration. *European Journal of Agronomy*, 48: 74-87.

Europ. J. Agronomy 48 (2013) 74–87

Contents lists available at SciVerse ScienceDirect

European Journal of Agronomy

journal homepage: www.elsevier.com/locate/eja

Modeling acclimation of leaf photosynthesis to atmospheric CO_2 enrichment

Christian Biernath[a,*], Sebastian Bittner[a], Christian Klein[a], Sebastian Gayler[b], Rainer Hentschel[a,c], Peter Hoffmann[a], Petra Högy[d], Andreas Fangmeier[d], Eckart Priesack[a]

[a] Helmholtz Zentrum München, German Research Center for Environmental Health, Institute of Soil Ecology, Modeling Soil-Plant-Atmosphere Systems, Ingolstädter Landstraße 1, 85764 Neuherberg, Germany
[b] Water & Earth System Science (WESS) Competence Cluster, c/o University of Tübingen, Hölderlinstr. 12, 72074 Tübingen, Germany
[c] Leibnitz-Zentrum für Agrarlandschaftsforschung e. V., Institute for Landscape Biogeochemistry, Eberswalder Straße 84, 15374 Müncheberg, Germany
[d] University of Hohenheim, Institute for Landscape and Plant Ecology, Plant Ecology and Ecotoxicology, August-v.-Hartmann-Straße 3, 70599 Stuttgart, Germany

ARTICLE INFO

Article history:
Received 18 May 2012
Received in revised form 13 February 2013
Accepted 22 February 2013

Keywords:
Elevated CO_2
Rubisco turnover
Canopy photosynthesis
Acclimation
Wheat
Plant model

ABSTRACT

In this study, we developed and analyzed a new model for the simulation of photosynthetic active nitrogen (N_P) turnover dynamics in crops and assessed its impact on the acclimation of canopy photosynthesis to atmospheric CO_2 enrichment. Typical canopy models assume a vertical exponential decline of light interception following the Beer–Lambert law and vertical distributions of leaf N_P contents directly proportional to the light distribution. This assumption is often inconsistent with experimental observations. We therefore modified and extended the photosynthesis model of the GECROS crop model to consider the trade-off that occurs between the use of degraded N_P for plant growth and the synthesis of new N_P. This model extension thus enabled the examination of the CO_2-induced down-regulation of photosynthesis hypothesis using a crop model. The simulation results of the original and modified GECROS model were compared and evaluated based upon measurements of field-grown spring wheat. The modified GECROS model better simulated the dynamics of crop growth under varying atmospheric CO_2 concentrations. Furthermore, the application of different temperature functions to N_P degradation strongly influenced the simulation results, revealing the necessity for improving the understanding of the temperature dependence of N_P turnover for different crop species and varieties. In conclusion, the redistribution of nitrogen within the plant and its alternative use either for growth or the optimization of the photosynthetic apparatus is an important mechanism for crop growth acclimation to regionally changing climatic conditions and in particular, atmospheric CO_2 enrichment.

1. Introduction

Recent atmospheric CO_2 measurements have revealed levels of 393 ppm, which are expected to increase by 2 ppm per year during this century in a best-case scenario (Tans, 2012; OECD, 2012). Atmospheric CO_2 is the substrate for photosynthetic carbon assimilation in plants. Since the emergence of C_3 photosynthesis during early geological periods, plants have experienced higher and lower mean atmospheric CO_2 concentration ($[CO_2]$) compared with present levels (Berner, 1998). In a canopy, the $[CO_2]$ outside of the leaf may fluctuate due to wind speed, turbulence and diurnal variations in soil and plant respiration and photosynthetic carbon fixation (Monteith and Unsworth, 1990). In C_3 plants such as wheat (*Triticum aestivum* L.), leaf photosynthesis is not substrate-saturated under actual $[CO_2]$. Together with increasing $[CO_2]$, the diffusion gradients between the atmosphere and reactive sites in the cells of green leaves increase. Thus, one expects that a higher availability of CO_2 at the reactive sites would increase biomass growth and the possible adaption of the plant to the changing environment (Chen et al., 1995; Poorter et al., 1997; Körner and Bazzaz, 1996).

To analyze crop acclimation, many experiments have been conducted using various plant species and management systems (Amthor, 2001; Ainsworth and Long, 2005; Poorter, 1993). The reported characteristics of canopy responses to higher $[CO_2]$ vary strongly and include greater biomass production, decreased tissue nitrogen concentrations, altered yield quality, and increased nitrogen-use and water-use efficiencies (Högy and Fangmeier,

* Corresponding author. Tel.: +49 089 31873119; fax: +49 089 31872800.
E-mail address: christian.biernath@helmholtz-muenchen.de (C. Biernath).

1161-0301/$ – see front matter © 2013 Elsevier B.V. All rights reserved.
http://dx.doi.org/10.1016/j.eja.2013.02.008

2008; Yamasaki et al., 2002; Borjigidai et al., 2006; Hikosaka et al., 2006). The presence of decreased tissue nitrogen concentrations is a key factor in the explanation of canopy acclimation. However, plant growth is based upon diverse processes involving nitrogen uptake and metabolism. Therefore, the mechanisms that cause lower tissue nitrogen concentrations under elevated [CO_2] remain poorly understood (Bloom et al., 2010; Taub and Wang, 2008).

Various hypotheses exist to explain the lower nitrogen concentrations in plant leaves under elevated [CO_2] (Taub and Wang, 2008). The new canopy acclimation model presented in this study is based upon the "down-regulation of the photosynthesis" hypothesis (Gifford et al., 2000; Fangmeier et al., 1999, 2000). As part of this hypothesis, Fangmeier et al. (1999, 2000) suggested that lower grain protein concentrations under elevated [CO_2] are the consequence of lower protein concentrations in leaves. Because photosynthetic enzymes make up a large fraction of the total nitrogen in C_3 species, this reduction is largely a result of decreased Rubisco concentrations (Ainsworth and Long, 2005; Evans and Seemann, 1989). Moreover, to understand plant acclimation to elevated [CO_2], the interleaving between structural adjustments, such as stem growth or lamina expansion, and physiological adjustments, such as increased nitrogen- and water-use efficiencies and sink strength, must be addressed (Diaz, 1995). Therefore, holistic concepts are necessary to explain the effects of [CO_2] on physiological and structural changes and their interactions with plant growth (Murthy and Dougherty, 1997; Pritchard et al., 1999). However, the mechanisms of the interactions between canopy acclimation and environmental factors (such as nitrogen and water availability) or climate change (temperatures and precipitation distribution patterns) remain uncertain. To date, it has not been possible to sufficiently describe canopy acclimation to rising [CO_2].

To analyze crop acclimation, we used the source-sink-regulated crop growth simulator GECROS (Yin and van Laar, 2005), in which carbon assimilation rates are simulated based on Michaelis–Menten kinetics to account for the competition of CO_2 and O_2 at the reactive site of the Rubisco enzyme (Farquhar et al., 1980; von Caemmerer and Farquhar, 1981) and Rubisco content within the leaves. Biernath et al. (2011) successfully used GECROS to simulate the dynamic interactions between plant growth, [CO_2], soil type and plant available water. Our new model is an extension of the GECROS model, which assumes exponential profiles of photosynthetic active nitrogen (N_P [g m^{-2}], predominantly Rubisco enzyme) distribution within the canopy (Yin et al., 2000) by adding a dynamic model of N_P turnover (Thornley, 1998, 2004). The simulation of dynamic N_P turnover enables the estimation of the redistribution of green leaf nitrogen and its subsequent optional disposal either for growth or for the reorganization of the photosynthetic apparatus. Thornley (1998) suggests that this is a promising approach to modeling canopy acclimation to increasing [CO_2]. This model was previously applied by Thornley and Cannell (2000a,b) to describe the observed downward acclimation of the maximal leaf photosynthesis rate when exposed to elevated [CO_2] over longer periods for both a forest and grassland ecosystem. Recently, it was adopted as a more teleonomic model by Bertheloot et al. (2011) to simulate the nitrogen economy of wheat after anthesis. All of these models combine the Thornley (1998, 2004) model either with rectangular or non-rectangular hyperbola to describe the leaf photosynthetic response to [CO_2] levels and levels of incident light (Thornley and Cannell, 2000a,b; Bertheloot et al., 2011; Johnson et al., 2010; Thornley and France, 2007).

In contrast, our new model combines the approach of Thornley (1998, 2004) and the photosynthesis model of Farquhar et al. (1980) with extensions by Yin and van Laar (2005) and Yin et al. (2004) to achieve a better description of the [CO_2] response mechanism of the biochemical process of CO_2 assimilation. Here, a linear relationship between N_P and leaf nitrogen content is assumed according to De Pury and Farquhar (1997). The crop growth model was embedded in the ecosystem model package Expert-N (Priesack, 2006; Priesack et al., 2006; Priesack and Bauer, 2003) to take advantage of its mechanistic models of soil carbon and nitrogen turnover, including soil solute transport, and for better comparability with previous studies (Gayler et al., 2002; Biernath et al., 2011).

The two main objectives of our study were (i) to analyze the extent to which a trade-off between nitrogen usage either for structural growth or optimal leaf photosynthesis could explain canopy acclimation to changing atmospheric [CO_2] and (ii) compare simulations using a static vertical distribution of leaf nitrogen (Yin and van Laar, 2005) with simulations using the new model that considers N_P turnover and, hence, the redistribution of nitrogen in the canopy.

2. Materials and methods

In our new model of plant nitrogen turnover, we consider a nitrogen cycle that is composed of six rates [g m^{-2} d^{-1}]: remobilized nitrogen from aboveground biomass provided for growth ($N_{R\rightarrow G}$), remobilized nitrogen from non-photosynthetic tissue provided for growth ($N_{X\rightarrow G}$), nitrogen assimilated by the roots ($N_{U\rightarrow G}$), nitrogen that exceeds demands for growth and is directed to the synthesis of photosynthetic active nitrogen ($N_{G\rightarrow P}$), nitrogen left over from photosynthetic active nitrogen synthesis ($N_{G\rightarrow R}$), and nitrogen derived from photosynthetic active nitrogen degradation ($N_{P\rightarrow R}$). These processes transfer nitrogen between three pools [g m^{-2}]: non-photosynthetic nitrogen in plants that is mostly fixed in structural plant compartments (N_X), nitrogen in the photosynthetic apparatus (N_P), and excess nitrogen, which consists of mobile nitrogen species that are neither needed for photosynthesis nor growth (N_R). Abbreviations, variables, constants, units, and values used for the development and testing of the new model are given in Appendix (Table A.1).

2.1. Simulation model

In the present study, the photosynthesis model of the crop growth simulator GECROS (Yin and van Laar, 2005) was modified and extended to improve crop growth simulations under various environmental conditions and in particular, explain potential canopy acclimation to atmospheric CO_2 enrichment. GECROS is a canopy crop model developed to simulate interactions between crop growth and environmental conditions. The crop model simulates field scale crop monocultures maintained to be free of pests and weeds (Yin and van Laar, 2005). Leaf photosynthesis is simulated using a two-leaf approach that distinguishes between sunlit and shaded leaves (De Pury and Farquhar, 1997; Wang and Leuning, 1998; Yin and van Laar, 2005), assuming exponential vertical profiles of intercepted light and N_P distribution throughout the canopy. The root-shoot partitioning of nutrients is computed to maximize the carbon gain of the crops, which is based upon the root-shoot functional balance theory (Charles-Edwards, 1976; Yin and Schapendonk, 2004). The partitioning of nutrients within the shoot is determined using target concentrations that determine the sink strength of crop organs. The GECROS model is described in detail in Yin and van Laar (2005). We extracted the GECROS plant model components and embedded them into the ecosystem model package Expert-N (Priesack et al., 2006; Priesack, 2006; Priesack and Bauer, 2003; Gayler et al., 2002; Biernath et al., 2011), which allows for a more mechanistic modeling of soil water, carbon, heat, and water dynamics compared with the more simple GECROS soil capacity model. Only the GECROS plant growth modules were executed, while the GECROS soil model was replaced by more mechanistic models to simulate soil water and

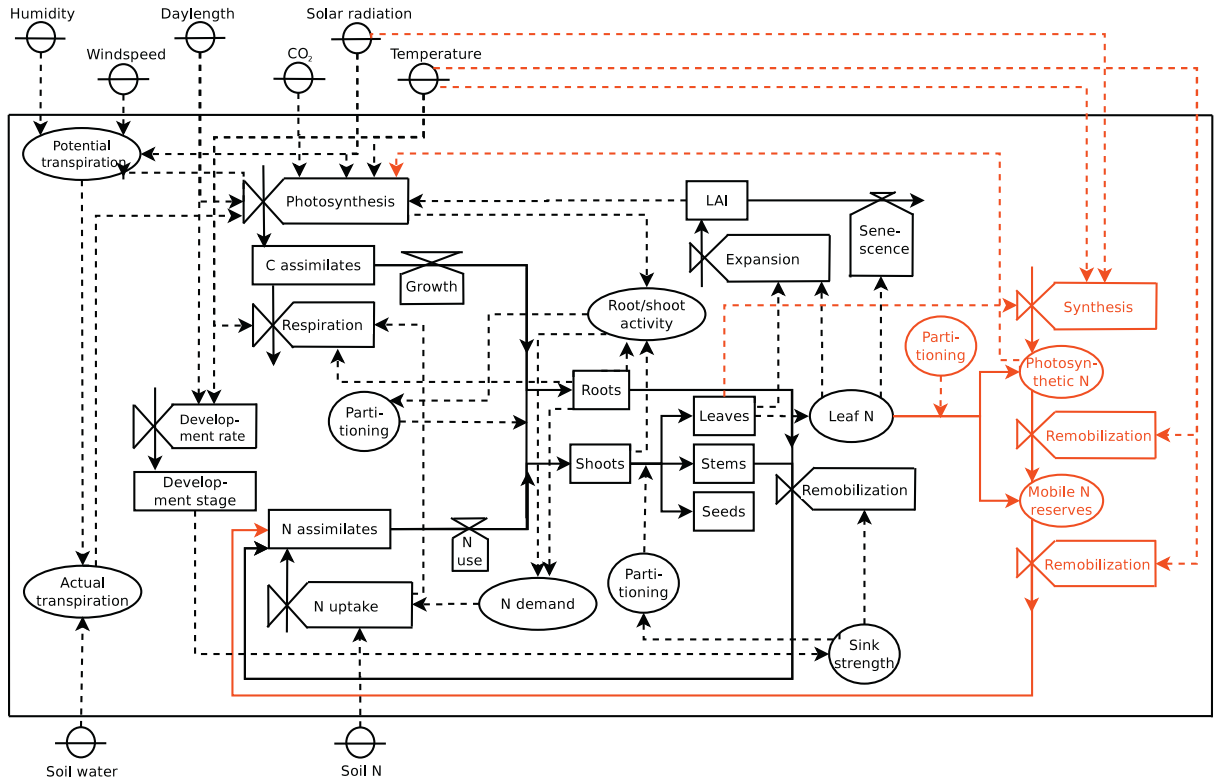

Fig. 1. Relational diagram of the Exert-N plant submodel GECROS (based on Yin and van Laar, 2005) modified to allow turnover of photosynthetic active nitrogen to the purpose of modeling the acclimation to atmospheric CO_2 enrichment. The symbols used in the diagram were introduced by Forrester (1961). State variables are represented by boxes, rate variables by valves, intermediate variables by ellipses, environmental variables by small crossed circles, material flows by solid-line arrows and information flows by dashed-line arrows.

nitrogen dynamics (Simunek and Huang, 1998; Hutson and Wagenet, 1992; Johnsson et al., 1987). In preparation for subsequent model adaptions, we replaced the continuous two-leaf approach for simulating light interception and vertical leaf nitrogen distribution by a numerical multilayer approach. This approach yields identical results compared with the two-leaf approach of the original GECROS model, as long as the same light and nitrogen profiles in the canopy are assumed. Hereafter, the configuration of Expert-N with the crop model GECROS computing leaf photosynthesis with a multilayer approach is referred to as XN-G.

2.1.1. Plant nitrogen cycle

The XN-G photosynthesis model was further extended using a dynamic plant nitrogen turnover module (adopted from Thornley, 1998, 2004) to allow the dynamic simulation of nitrogen redistribution within the canopy and acclimation of leaf photosynthesis and plant growth to changing environmental conditions. We refer to this new model as XN-GN (Fig. 1). A list of all of the symbols used in the following presentation of the extended module is provided at the end of this chapter. For all other equations pertaining to the GECROS model, we referred to Yin and van Laar (2005). Three different nitrogen pools are considered to simulate nitrogen cycling in the plant (Fig. 2). The fluxes of nitrogen between these pools are estimated from the source and sink strength of the plant, turnover rates of nitrogen pools and light supply. The simulation of the spatial and temporal dynamics of photosynthetically active nitrogen is based upon two main assumptions:

(a) The Beer–Lambert law is valid for the simulation of light extinction in homogenous crop canopies. The distribution of N_P in the canopy is more strongly affected by the specific location of a photosynthetically active site within the canopy than the canopy constitution and architecture of a single plant. Following the light extinction curve the exponential decline with canopy depth is the target N_P distribution in the canopy.

(b) Remobilized nitrogen substrate due to N_P turnover ($N_{R\rightarrow G}$), nitrogen substrate remobilized from the root and from non-photosynthetic aboveground tissues ($N_{X\rightarrow G}$) and nitrogen supply from root uptake ($N_{U\rightarrow G}$) are partitioned to root and shoot growth. Nitrogen partitioned to the shoot is first used for

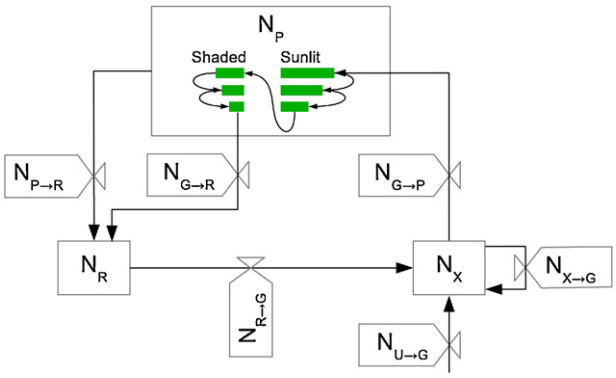

Fig. 2. Model of the plant internal nitrogen cycle. N_X: nitrogen in non-photosynthetic plant tissue, N_P: Nitrogen in the photosynthetic apparatus N_R: nitrogen either remobilized from the photosynthetic apparatus or exceeding the capacity for optimization of the photosynthetic apparatus. $N_{X\rightarrow G}$: flux of nitrogen remobilized from non-photosynthetic tissue, $N_{R\rightarrow G}$: flux of N_R for repartitioning to organ growth, $N_{U\rightarrow G}$: flux of nitrogen absorbed from the soil by the roots, $N_{G\rightarrow P}$: flux of nitrogen to optimize the photosynthetic apparatus, $N_{G\rightarrow R}$: flux of nitrogen that exceeds the capacity for the optimization of the photosynthetic apparatus, $N_{P\rightarrow R}$: flux of nitrogen remobilized by N_P degradation. Valves are fluxes, boxes are pools, and arrows are material flows. Green horizontal bars indicate canopy layers which distinguish between sunlit and shaded leaves.

structural biomass production and grain filling. Nitrogen substrate ($N_{R\to G}$, $N_{X\to G}$ and $N_{U\to G}$) that exceeds demands for growth is directed to N_P synthesis in the leaves ($N_{G\to P}$). If there is still nitrogen left over, i.e., if $N_{G\to P}$ exceeds the demand for N_P synthesis ($N_{G\to R}$), then it is stored in a nitrogen reserve pool (N_R) for subsequent availability for redistribution within the plant. Nitrogen substrate derived from N_P degradation ($N_{P\to R}$) is also stored in N_R.

The non-photosynthetic nitrogen (N_X) used for plant growth and canopy expansion is the sum of the nitrogen partitioned to the different crop organs. It can be described by

$$\frac{dN_X}{dt} = N_{U\to G} + N_{R\to G} + N_{X\to G} - N_{G\to P} = \frac{dN_{X,stem}}{dt} + \frac{dN_{X,grain}}{dt} + \frac{dN_{X,leaf}}{dt} + \frac{dN_{X,root}}{dt} \quad (1)$$

where $N_{U\to G}$ is the nitrogen assimilation rate calculated from soil nitrogen availability, root activity, and plant nitrogen demand (Yin and van Laar, 2005).

The computation of nitrogen partitioning to the different crop organs is described in detail by Yin and van Laar (2005), Yin and Schapendonk (2004) and Priesack and Gayler (2009). The change in N_P is then given by

$$\frac{dN_P}{dt} = N_{G\to P} - N_{G\to R} - N_{P\to R} \quad (2)$$

Similarly, the change in N_R is calculated by

$$\frac{dN_R}{dt} = N_{P\to R} + N_{G\to R} - N_{R\to G} \quad (3)$$

The nitrogen flux that exceeds the capacity of the canopy to synthesize N_P is

$$N_{G\to R} = N_{G\to P} - \sum_{i=1}^{m} N_{G\to P,i}^{syn,su} - \sum_{i=1}^{m} N_{G\to P,i}^{syn,sh} \quad (4)$$

where $N_{G\to P,i}^{syn,su}$ [g m^{-2} d^{-1}] and $N_{G\to P,i}^{syn,sh}$ [g m^{-2} d^{-1}] are N_P that is synthesized in the sunlit and shaded leaves, respectively, of the ith canopy layer, and m is the number of canopy layers.

The flux of nitrogen provided for storage in N_R is

$$N_{P\to R} = \sum_{i=1}^{m} N_{P\to R,i}^{su} + \sum_{i=1}^{m} N_{P\to R,i}^{sh} \quad (5)$$

where $N_{P\to R,i}^{su}$ [g m^{-2} d^{-1}] and $N_{P\to R,i}^{sh}$ [g m^{-2} d^{-1}] are the flux of degraded N_P in the sunlit and shaded leaves of the ith canopy layer, respectively.

The rate of nitrogen provided for N_P synthesis is then given by

$$N_{G\to P} = \sum_{i=1}^{m} N_{G\to P,i}^{syn,su} + \sum_{i=1}^{m} N_{G\to P,i}^{syn,sh} \quad (6)$$

The rate of remobilized nitrogen from the mobile nitrogen storage pool is calculated from

$$N_{R\to G} = N_R \cdot c_{G,N_R} \quad (7)$$

where c_{G,N_R} is a constant growth factor [d^{-1}] to determine the nitrogen flux from N_R to N_X.

2.1.2. Vertical nitrogen profile

In our model, we assume that new N_P is only synthesized in a leaf layer if the actual amount of photosynthetic active nitrogen in this layer does not exceed its expected target content, which is calculated from the total nitrogen content in the leaves and follows the exponential profile of light interception, which is calculated from the Beer–Lambert law (Monsi and Saeki, 2005) by

$$I(L_i) = I_0 \cdot (e^{-k\cdot(L_i+L_{c,i})} - e^{-k\cdot L_i}) \quad (8)$$

where I_0 [W m^{-2}] is the incoming radiation I [W m^{-2}] at the top of the canopy, k [m^2 m^{-2}] is the light extinction coefficient, L_i [m^{-2} m^{-2}] is the leaf area index of the ith canopy layer and $L_{c,i} = \sum_{j=0}^{i-1} L_j$. The light absorbed by the ith canopy layer is then calculated based upon (Yin and van Laar, 2005) as described in Priesack and Gayler (2009). Light interception in every layer i is further divided into direct beam interception and diffuse light interception (Kropff, 1993; Yin and van Laar, 2005). The fractions of sunlit and shaded leaves are calculated from

$$f_i^{su} = e^{-k_{dir}(L_i+L_{c,i})} \quad (9)$$

and

$$f_i^{sh} = 1 - f_i^{su} \quad (10)$$

where k_{dir} is the extinction coefficient of direct beam radiation and depends on the elevation of the sun over the horizon, corresponding with the fractions in the respective leaf layers. The light interception by sunlit leaves in a layer, I_i^{su} [W m^{-2}], is then the sum of direct beam and diffuse radiation interception, whereas the light interception by shaded leaves, I_i^{sh} [W m^{-2}], is restricted to diffuse radiation.

The target distribution N_P^{tar} is recalculated at each time point from the total amount of nitrogen in the green leaves assuming an exponential distribution of N_P (Yin and van Laar, 2005; Yin et al., 2000)

$$N_{P,i}^{tar} = \left[\frac{n_0}{k_n}\cdot e^{-k_n\cdot L_{c,i}} - \frac{n_0}{k_n}\cdot e^{-k_n\cdot(L_i+L_{c,i})} - n_b\cdot L_i\right] \quad (11)$$

$$N_{P,i}^{tar,su} = \left[n_0\cdot\frac{(e^{-(k_n+k_{dir})\cdot L_{c,i}} - e^{-(k_n+k_{dir})\cdot(L_i+L_{c,i})})}{(k_n+k_{dir})} - n_b\cdot\frac{(e^{-k_{dir}\cdot L_{c,i}} - e^{-k_{dir}\cdot(L_i+L_{c,i})})}{k_{dir}}\right] \quad (12)$$

$$N_{P,i}^{tar,sh} = N_{P,i}^{tar} - N_{P,i}^{tar,su} \quad (13)$$

where $N_{P,i}^{tar}$ is the target photosynthetic active leaf nitrogen content of the ith canopy layer, L_i [m^2 m^{-2}] is L of the ith canopy layer, and $L_{c,i}$ [m^2 m^{-2}] is the cumulative L above the ith layer. n_0 [g m^{-2}] is the nitrogen amount at the top of the canopy, and n_b [g m^{-2}] is the minimal amount of nitrogen for photosynthesis. k_n [m^2 m^{-2}] is the nitrogen extinction coefficient, and k_{dir} [m^2 m^{-2}] is the beam radiation extinction coefficient. In GECROS the estimation of n_0 is based upon the exponential profile which is described in detail in Yin and van Laar (2005, Eq. 40 in page 35). The nitrogen extinction coefficient k_n is computed following the relations of Yin et al. (2003) as described in Yin and van Laar (2005).

The actual photosynthetic active nitrogen content in XN-GN after seed emergence is initially

$$N_{P,i}^{act}(t=0) = N_{P,i}^{tar}(t=0) \quad (14)$$

After initialization, the actual N_P content of the sunlit leaves of the ith canopy layer $N_{P,i}^{act,su}$ [g m^{-2}] is computed by

$$\frac{dN_{P,i}^{act,su}}{dt} = N_{G\to P,i}^{syn,su} - N_{G\to R,i}^{su} \quad (15)$$

and $N_{P,i}^{act,sh}$[gm^{-2}] for the shaded leaves by

$$\frac{dN_{P,i}^{act,sh}}{dt} = N_{G\to P,i}^{syn,sh} - N_{G\to R,i}^{sh} \quad (16)$$

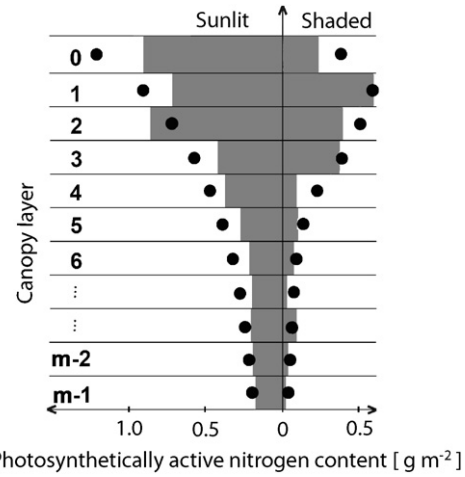

Fig. 3. Schematic vertical distribution of N_P contents within the canopy of XN-GN. Black dots are the fitted exponential declines of the N_P contents [g N_P per m^2 ground per canopy layer] with canopy depth using the XN-G model. For the XN-GN model, the black dots are the target N_P contents to compute the actual N_P contents (grey bars) of the ith canopy layer. Each canopy layer contains the same proportion of the leaf area index. The x-axes scale is representative for $m = 10$ canopy layers.

The dynamics of N_P turnover are calculated following (Thornley, 1998, 2002, 2004). The synthesis of N_P is a photosynthetically active radiation-driven process that requires $N_{G\to P}$. The synthesis of new N_P follows first-order kinetics and initially occurs in the sunlit and then the shaded leaves (Fig. 3).

$$N^{syn,su}_{G\to P,i} = c_{G,N_P} \cdot W_i \cdot f^{su}_i \cdot \frac{I^{su}_i}{I^{su}_i + m_I} \cdot \frac{N_{G\to P}}{N_{G\to P} + m_N} \quad (17)$$

$$N^{syn,sh}_{G\to P,i} = c_{G,N_P} \cdot W_i \cdot (1 - f^{su}_i) \cdot \frac{I^{sh}_i}{I^{sh}_i + m_I} \cdot \frac{N_{G\to P}}{N_{G\to P} + m_N} \quad (18)$$

W_i [g m^{-2}], I^{su}_i and I^{sh}_i [W m^{-2}] are the green leaf weight and photosynthetic active radiation that intercepts the sunlit and shaded leaves of the ith canopy layer, respectively. c_{G,N_P} [d^{-1}] is a growth constant of photosynthetic active nitrogen. m_I [W m^{-2}] and m_N [g N g^{-1} d^{-1}] are Michaelis–Menten coefficients that control the impacts of intercepted photosynthetic active radiation and available $N_{G\to P}$ on the synthesis of N_P.

$N_{G\to P}$ for N_P synthesis is distributed to the sunlit leaves of each canopy layer, starting at the top layer and finishing at the bottom layer. The remaining $N_{G\to P}$ is available for N_P synthesis in the shaded leaves and distributed similarly to that in the sunlit leaves from the top down (Fig. 3). Excess $N_{G\to P}$ not needed for N_P synthesis is stored in the N_R pool.

The degradation of N_P is constant over a period of approximately five days (Thornley, 1998); however, it is possibly affected by leaf temperature. The amount of N_P transformed into new substrate nitrogen per time point for each canopy layer i is defined by

$$N^{su}_{P\to R,i} = c_{D,N_P} \cdot N^{act,su}_{P,i} \cdot f(T^{su}_i) \quad (19)$$

$$N^{sh}_{P\to R,i} = c_{D,N_P} \cdot N^{act,sh}_{P,i} \cdot f(T^{sh}_i) \quad (20)$$

where c_{D,N_P} [d^{-1}] is the N_P degradation constant, and $f(T^{su}_i)$ and $f(T^{sh}_i)$ are the effects of the leaf temperatures of the sunlit and shaded leaves in the ith canopy layer on N_P degradation in relation to three different temperature functions proposed by Thornley and France (2007), respectively. If no temperature function was considered the temperature function was set to $f(T) = 1$.

Together with the newly absorbed nitrogen assimilated by the roots, the N_R pool first provides nitrogen for the redistribution to new biomass production. Subsequently, nitrogen not needed for growth is utilized for the synthesis of new N_P. Finally, nitrogen not needed for N_P synthesis is available for redistribution to plant organs (Fig. 2).

The presented model distinguishes between sunlit and shaded leaves in the canopy. This approach is directly based on the two-leaf approach to compute the canopy photosynthesis in the original GECROS model (Yin and van Laar, 2005). For the model development this approach was adopted to keep the differences to the original model minimal. We assume that the acclimation of the depth distribution of the photosynthetic capacity within the canopy is less strong affected by the diurnal light profile than by the live cycle of the plant throughout the vegetation period.

2.2. Dataset for model calibration and model testing

For the model calibration and testing, we used data sets obtained by Högy et al. (in press) in a mini-FACE experiment conducted in Stuttgart–Hohenheim, Germany, in 2008. Spring wheat (*Triticum aestivum* L. cv. 'Triso') was grown at a sowing density of 360 plants per m^2. The soil was a slightly stagnic Luvisol that formed from banked limestone (Muschelkalk) covered with loess (silt). The field experiment consisted of 15 FACE plots with surface areas of 2 m^2 each. Two different atmospheric CO_2 concentration levels (ambient and elevated) were applied throughout the vegetation period (from April 22nd to August 4th, 2008). In the simulations, single daily mean values were applied for each plot. Included were three treatments with five replicates each: (1) ambient [CO_2] with FACE ring construction (418±19 ppm), (2) elevated [CO_2] with FACE ring construction (569 ± 156 ppm), and (3) reference treatment without FACE ring construction (418 ± 17 ppm).

2.3. Model calibration

In all simulations, the same parameter values were used for XN-G and XN-GN. The parameters were calibrated using the XN-G model. The values of the additional parameters affecting N_P turnover in XN-GN were adopted from (Thornley, 2004) without modifications. The required GECROS parameter values could be measured in the mini-FACE experiment or were taken from the literature. The target values for model calibration were the measured values of the crop developmental stages, dynamics of leaf area development, and both the dry masses of the total above-ground biomass and yield at final harvest. Data from the reference treatment were used for the model calibration only and were not included in further model evaluations. The adapted crop specific parameter values used to run the GECROS model are presented in Appendix (Table A.2). Subsequently, the calibrated model was applied to simulate the crop growth of each FACE ring.

2.4. Statistics

The ability of the model to match the observations was tested by two statistical criteria: the model efficiency index (ME) according to Willmott (1982), and the normalized root mean square error (NRMSE) according to Wallach and Goffinet (1989). The ME is a method used to evaluate modeling performance using a range of between 0 and 1. A value of close to 1 indicates a good match between the measured and simulated values. The NRMSE evaluates the average relative deviation between the simulation and measurements in a range of between 0 for a perfect match and $+\infty$ indicating no match at all.

We define the ME by

$$ME = 1 - \frac{\sum_{i=1}^{n}(P_i - O_i)^2}{\sum_{i=1}^{n}(|P_i - \overline{O}| + |O_i - \overline{O}|)^2} \quad (21)$$

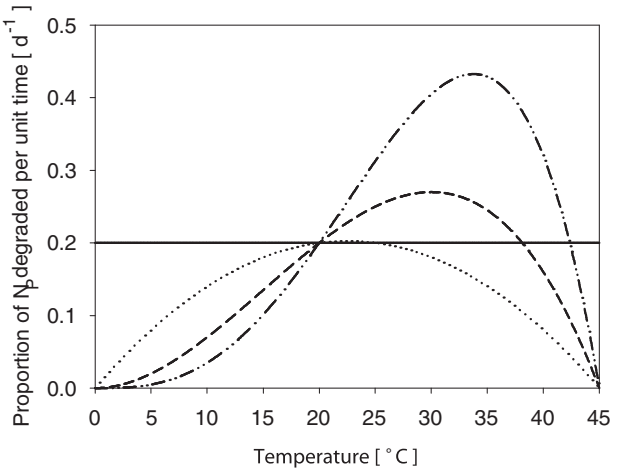

Fig. 4. N_P degradation in relation to temperature response. No temperature response: continuous line. Temperature response using Eq. 23 for Υ_1 (υ=1; dotted), Υ_2 (υ=2; dashed), Υ_3 (υ=3, dash-dotted). N_P^{act}=1 g m^{-2}, c_{D,N_P}=0.2, T_r = 20 °C, T_0 = 0 °C and $T_{0'}$ = 45 °C, and ϑ=1. Based on Thornley and France (2007).

where n is the number of measurement points, and $\overline{O}$ represents the mean values of the measured values O_i. The corresponding simulated values to O_i are P_i.

The NRMSE is given by

$$NRMSE = \frac{\sqrt{(1/n)\sum_{i=1}^{n}(P_i - O_i)^2}}{\overline{O}} \quad (22)$$

3. Simulation results

First, we tested the impact of CO_2 enrichment on the simulation results by increasing the atmospheric CO_2 concentration stepwise by 100 ppm from 400 to 700 ppm. Second, we analyzed the effect of the temperature function (Eq. 23) for three different curvatures Υ_1, Υ_2 and Υ_3 (Fig. 4) on the simulation results of XN-GN. Third, the calibrated models were applied to the conditions of the mini-FACE experiment.

3.1. Impacts of atmospheric CO_2 concentrations

The impacts of CO_2 on simulated vertical distributions of photosynthetic active nitrogen (N_P) are shown in Fig. 5 for different pre-anthesis and post-anthesis crop growth stages with intervals of seven days. Overall, the N_P contents decreased with canopy depth in all of the model variations. Using the XN-G model, the N_P contents decreased exponentially with the highest contents at the top of the canopy in principle. In simulations using XN-GN, such exponential profiles hardly occurred. Because of its dependence on both the growth stage and environmental conditions, the vertical N_P distributions deviated more or less from the exponential decrease with canopy depth.

In most cases, the distribution of N_P contents with canopy depth declined, with stronger gradients observed in the XN-GN simulations. This means that the N_P contents were higher in the upper canopy layers but much lower in the lower parts of the canopy compared to XN-G simulations. The convex curvature of N_P contents visible in XN-GN simulations in the upper third of the canopy increased with increasing [CO_2]. This indicates a more pronounced green effect in the top layers of the canopy under higher [CO_2] due to higher chlorophyll contents (Fig. 5).

Using both models, the total aboveground biomass production increased with increasing [CO_2] from 1800 g m^{-2} at 400 ppm to 2011 g m^{-2} at 700 ppm using the XN-G model and from 1743 g m^{-2} to 2025 g m^{-2} in simulations using XN-GN. However, using XN-GN, the total aboveground biomass production was 3% lower when the [CO_2] was below 550 ppm, but with higher [CO_2], it was approximately 1% higher compared with simulations using the XN-G model. Overall, the total aboveground biomass production increased by 15% using XN-GN but only by 10% with XN-G (Fig. 6A). [CO_2] enrichment had no effect on grain yields, which were constant at approximately 755 g m^{-2} using XN-G. An increase of up to 5% in grain yields was observed in the XN-GN simulations, in which they increased from 747 g m^{-2} at 400 ppm to 778 g m^{-2} at 500 ppm and then decreased to 760 g m^{-2} at 700 ppm. The protein concentrations of the grains decreased with increasing [CO_2] in both models. In general, the protein concentrations of the grains were higher using XN-G compared with XN-GN, amounting to 12.5% compared with 12.1% at a [CO_2] of 400 ppm and 10.7% compared with 10.4% at a [CO_2] of 700 ppm (Fig. 6A).

3.2. Impact of different temperature functions

Following Thornley and France (2007), the temperature functions that affect N_P degradation were computed using

$$f(T_i) = \frac{(T_i^{act} - T_0)^{\upsilon} \cdot (T_{0'} - T_i^{act})^{\vartheta}}{(T_r - T_0)^{\upsilon} \cdot (T_{0'} - T_r)^{\vartheta}} \quad (23)$$

where T_i^{act} [°C] is the actual leaf temperature of the ith canopy layer, and T_0 [°C] and $T_{0'}$ [°C] are the lowest and highest possible leaf temperatures that allow enzyme activity, respectively. T_r [°C] is the reference temperature at which the value of $f(T)$ equals one. The form of the curve is defined by υ[−] and ϑ[−]. The effect of ϑ was not part of this study and therefore fixed to 1. The effects of the three different temperature functions were tested by changing υ. In accordance with Thornley and France (2007), for T_r = 20 °C, T_0 = 0 °C and $T_{0'}$ = 45 °C, the shapes of the curves can be described as quadratic (υ = 1 ; referred to as temperature function Υ_1), cubic (υ = 2 ; Υ_2) or quartic (υ = 3 ; Υ_3). The curvatures of Υ_2 and Υ_3 increased in a sigmoid fashion from T_0 to the optimum temperatures for protein turnover but decreased steeply from the optimum temperatures to $T_{0'}$ (Fig. 4).

Fig. 6B shows the effects of the applications of the different leaf temperature functions on controlling N_P turnover using the XN-GN model. The different temperature functions caused significant changes in the availability of N_P within the canopy due to the trade-off between the structural growth and physiological optimization of the photosynthetic apparatus, which affected the formation of crop biomass and grain protein concentrations. Regarding the total aboveground biomass and grain yields, the differences between the simulations by XN-GN, XN-GN for Υ_1 and XN-GN for Υ_2 were small. The Υ_3 value from XN-GN showed that the simulated increase of the total aboveground biomass was 5% lower when [CO_2] increased from 400 to 500 ppm, and the increase in the grain yields was significantly higher. Most significant were the decreases in protein concentrations with increasing [CO_2]. Similar declines of 1.6% and 1.5% were simulated by XN-G and XN-GN between 400 and 700 ppm. In the same range of [CO_2], protein concentrations decreased by 1.5%, 1.3% and 2.1% using the temperature functions Υ_1, Υ_2 and Υ_3 for the calculation of N_P turnover in XN-GN, respectively. Between 400 and 500 ppm, any of the three temperature functions doubled the decrease simulated by both XN-G and XN-GN to 0.7–0.8%. Between 500 and 600 ppm, no decrease in protein concentrations was observed using Υ_1 and Υ_2, but the grain protein concentrations decreased by 0.9% using Υ_3. Between 600 and 700 ppm the protein concentrations decreased by 1%, 0.6% and 0.3% using Υ_1, Υ_2 and Υ_3, respectively.

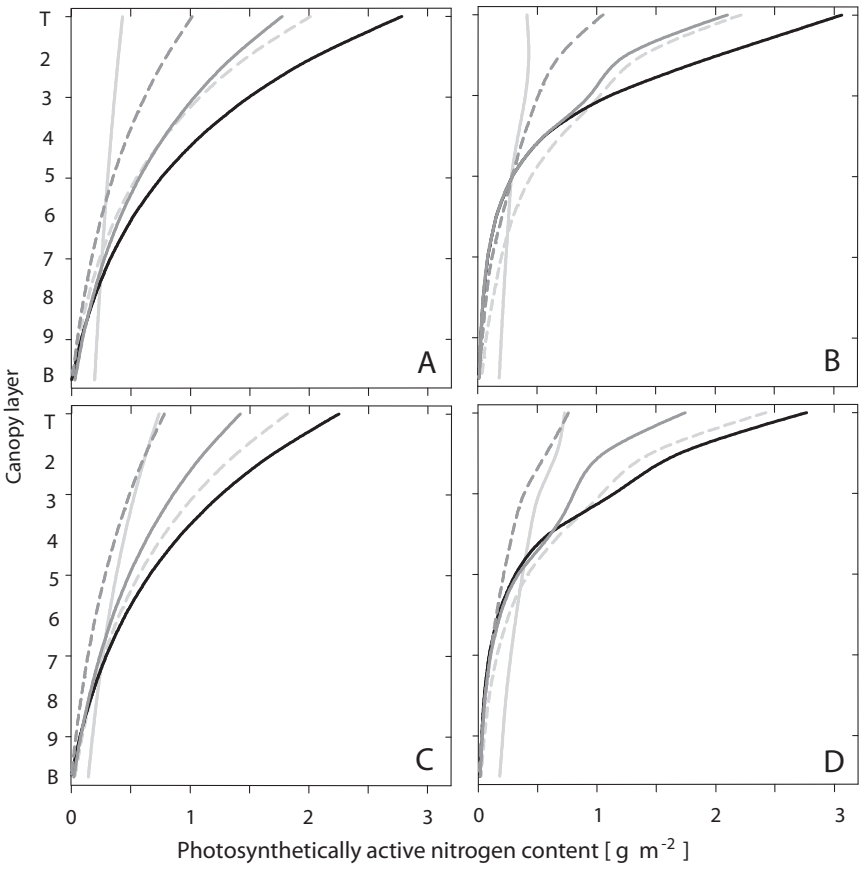

Fig. 5. Each of the four plots shows the vertical simulated distributions of N_P contents [g N_P per m^2 ground per canopy layer] at five different developmental stages (grey, solid lines: "tillering"; grey, dashed lines: "booting"; black, solid lines: "anthesis"; dark grey, solid lines: "development of seeds"; dark grey, dashed lines: "ripening") for two different atmospheric CO_2 concentrations, and the two models. A: XN-G, 400 ppm; B: XN-GN, 400 ppm; C: XN-G, 600 ppm; D: XN-GN, 600 ppm. $m = 10$ canopy layers, where T is the top and B the bottom layer.

3.3. Model performance

The simulations showed that both models, XN-G and XN-GN, responded differently to the daily changing mean atmospheric CO_2 concentrations measured in the ambient and elevated [CO_2] treatments. The mostly lower NRMSE and higher ME values indicate that the acclimation to elevated [CO_2] was better in the XN-GN simulations. As indicated by the high ME values (>0.99), crop biomass growth was well simulated by both models. For the examined crop variables, the deviations between the measurements and simulations were generally smaller than 30% ($NRMSE < 0.3$). Some higher NRMSE values were observed in the case of green leaf biomass only. The weakest NRMSE values ($NRMSE > 0.8$) were found using the XN-G model. Both models simulated decreasing grain protein concentrations with increasing [CO_2], but the decrease in the grain protein concentration per ppm was lower in XN-GN. However, for both models, the protein concentrations of the grains at maturity were largely underestimated by the simulations as indicated by weak ME values (Table 1).

In the simulations, the increases in [CO_2] from 418 to 569 ppm on average increased the maximal stem biomass from 905 g m^{-2} to 1051 g m^{-2} and 930 g m^{-2} to 1069 g m^{-2} using XN-G and XN-GN,

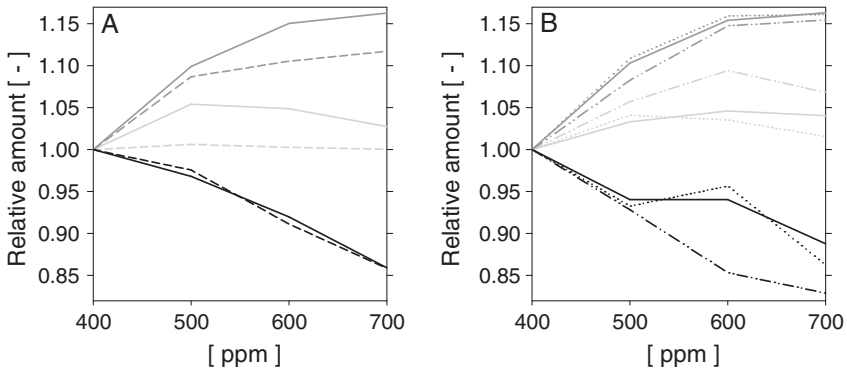

Fig. 6. Impact of the atmospheric CO_2 concentration on crop traits. The values are normalized to the simulation values at 400 ppm. Dark grey lines: total above-ground biomass, grey lines: grain yields, black lines: grain protein concentrations. (A) XN-G (dashed) vs. XN-GN (solid). (B) XN-GN including the effect of different temperature functions on photosynthetic active nitrogen turnover. Υ_1 (dotted), Υ_2 (solid) Υ_3 (dash-dotted).

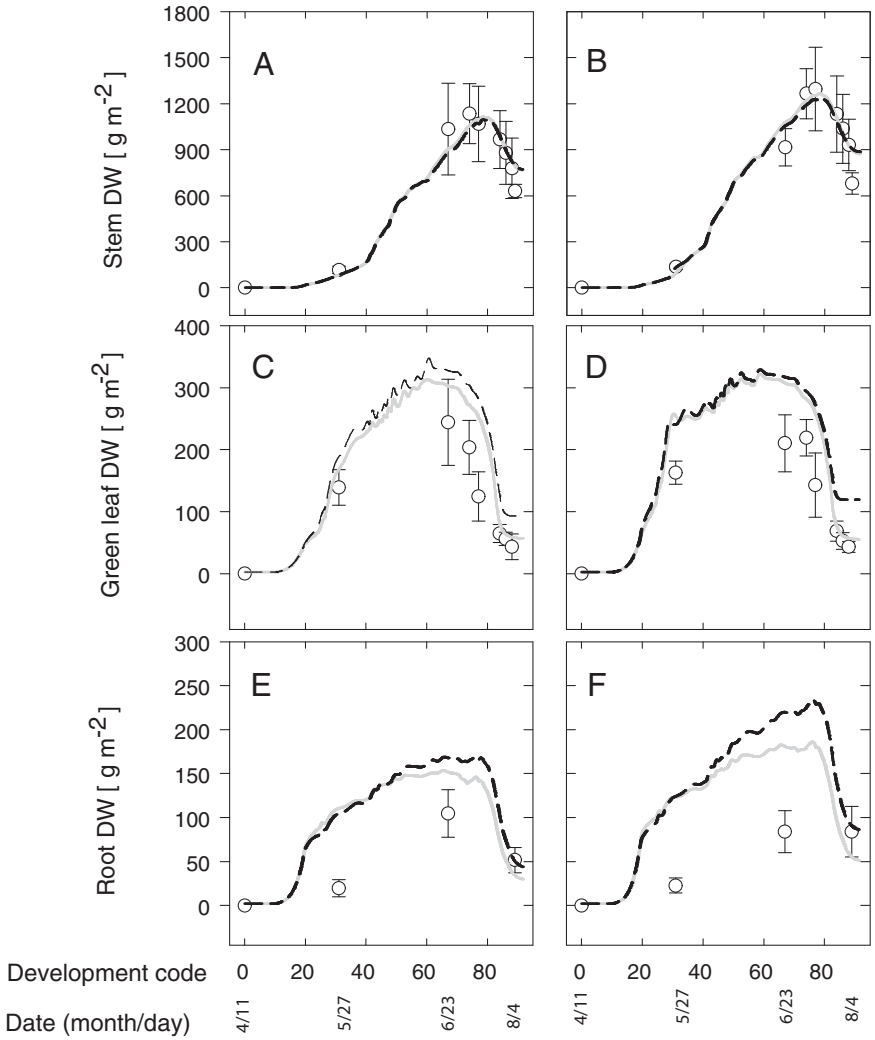

Fig. 7. Dynamics of the simulated wheat biomass using XN-G (black, dashed lines) and XN-GN (grey lines). Panels A, C and E correspond with ambient [CO_2], and panels B, D and F correspond with elevated [CO_2]. Circles and error bars are measurements from the mini-FACE experiment and respective standard deviations. DW is dry weight. Development code following (Meier, 1997).

Table 1
Statistical evaluation of the ability of the different photosynthesis sub-models in XN-G to simulate spring wheat grown under FACE conditions. Abbreviations: A: XN-G; B: XN-GN; BΥ_1, BΥ_2, and BΥ_3: XN-GN where the degradation of photosynthetic active nitrogen is affected by different functions of the leaf temperature. The curvatures are described as Υ_1 = quadratic, Υ_2 = cubic, and Υ_3 = quartic. "Ambient" and "elevated" are the two [CO_2] treatments. NRMSE is the normalized root mean square error (Wallach and Goffinet, 1989) and ME is the modeling efficiency (Willmott, 1982). ME values of the stems, leaves, and grain yield do not significantly differ from 1.00.

	[CO_2]	Stem	Leaf	Grain yield	Grain protein	
		NRMSE	NRMSE	NRMSE	NRMSE	ME
A	Ambient	0.32	0.89	0.10	0.18	0.35
	Elevated	0.24	0.88	0.26	0.18	0.15
B	Ambient	0.33	0.66	0.09	0.20	0.32
	Elevated	0.24	0.69	0.25	0.17	0.16
BΥ_1	ambient	0.33	0.70	0.09	0.21	0.28
	Elevated	0.24	0.68	0.25	0.17	0.16
BΥ_2	ambient	0.37	0.64	0.10	0.18	0.35
	Elevated	0.24	0.70	0.26	0.16	0.16
BΥ_3	ambient	0.33	0.58	0.11	0.16	0.36
	Elevated	0.24	0.68	0.26	0.15	0.15

respectively, the maximal leaf biomass decreased from 326 g m^{-2} to 293 g m^{-2} and 301 g m^{-2} to 281 g m^{-2}, respectively, and the maximal root biomass increased from 171 g m^{-2} to 235 g m^{-2} and 154 g m^{-2} to 186 g m^{-2}, respectively (Fig. 7). The simulated grain yields increased from 702 g m^{-2} to 734 g m^{-2} and from 710 g m^{-2} to 738 g m^{-2}, respectively, and the grain protein concentrations decreased from 12.4% to 11.5% and 12.0% to 11.6%, respectively. In the measurements from the field experiment the yield increased from 752 ±73 g m^{-2} to 833±82 g m^{-2} and the grain protein concentrations decreased from 14.9 ±0.4% to 13.8 ±0.7% (Högy et al., in press). The use of different temperature functions to drive N_P degradation in XN-GN altered the effects of [CO_2] on the simulated maximal stem biomass by +17.9% in the case of Υ_1, +18.3% for Υ_2, and +21.8% for Υ_3. The maximal leaf biomass was altered by −9.4% in simulations using Υ_1, −7.9% using Υ_2, and +10.1% using Υ_3. The grain yields were increased by +5.5% using Υ_1, +4.7% using Υ_2, and +6.9% using Υ_3. The grain protein concentrations decreased from 12.0% to 11.5% in the case of Υ_1, 12.3% to 11.7% for Υ_2, and 12.6% to 11.8% for Υ_3.

Overall, the improved NRMSE and ME values (Table 1) are correlated with better performance of XN-GN in the simulation of spring wheat biomass production in a free-air CO_2 enrichment system and in particular, the simulations under elevated [CO_2]. Moreover, using

XN-GN, the influence of the temperature function on N_P turnover and crop growth was significant. The use of Υ_1 led to improved simulation results compared with Υ_3 in cases involving stem biomass and grain yield. The leaf biomasses and protein concentrations of the grains were best simulated using Υ_3. The overall optimal simulation results were obtained when N_P degradation depended on a quartic function (Υ_3) of the leaf temperature.

4. Discussion

In this study we present a new model (XN-GN) to describe canopy acclimation to atmospheric [CO_2] enrichment. The difference between the XN-G and the XN-GN models is based on the vertical distribution of photosynthetic active nitrogen contents in the canopy. In the XN-G model the vertical N_P contents are generally assumed optimal and follow the exponential light extinction given by Beers' law. The XN-GN model uses the fitted exponential optimum N_P profile as target only to partition nitrogen to the photosynthetic apparatus, however, limited by the availability of nitrogen assimilates, the leaf biomass, and the intercepted light. Dynamic redistribution of photosynthetic nitrogen to growth follows after enzyme degradation. As a consequence, the XN-G model allows acclimation to [CO_2] enrichment on the morphological level (growth) only. The XN-GN model allows a dynamic acclimation on both levels, the morphological and the biochemical (optimization of the photosynthetic apparatus). Interactions of [CO_2] and nitrogen were not analyzed because no nitrogen limitation occurred in the experiment.

4.1. Overall model behavior

The statistical values were comparable to other crop growth studies (Niu et al., 2009; Wegehenkel and Mirschel, 2006; Priesack et al., 2006; Biernath et al., 2011). The XN-GN simulations had mostly better ME and NRMSE values than the XN-G simulations, which is remarkable because the XN-G model was used for the calibration, and the same parameterization was subsequently applied in both the XN-G and XN-GN simulations. The improved simulation results show that the dynamic model could partially explain canopy acclimation and improved crop growth simulations under [CO_2] enrichment. Based on the calibration to XN-G the total aboveground biomass decreased from 1800 (XN-G) to 1743 g m^{-2} (XN-GN) at 400 ppm [CO_2]. To achieve flexibility by a new dynamic for acclimation we extended the model which thus cannot reach the optimal exponential N_P profile in the canopy. Because the XN-G model is optimal regarding the vertical N_P profile the new model is suboptimal and consequently the total aboveground biomass is lower in XN-GN simulations at ambient [CO_2]. In both models, the increases in stem biomass were most sensitive to rising [CO_2], which is in agreement with findings from other [CO_2] enrichment studies (Kimball et al., 1995, 2001; Högy et al., 2009a). However, these findings contrast with the measurements by Högy et al. (in press) where the ears were most sensitive to [CO_2]. In GECROS, the crop organs are functional rather than physiological compartments (Yin and van Laar, 2005). In this sense, the ears are composed of leaves (glumes), stems (axes) and grains (with the onset of grain filling), and thus, the physiological function of ears is developmental stage-dependent.

We disagree with Laisk and Edwards (2009), who claimed that the photosynthesis model by Farquhar et al. (1980) and von Caemmerer and Farquhar (1981) fails to estimate assimilation rates when calculations are based upon the Rubisco contents of leaves. In the present study, the crop biomass was well simulated, which indicates appropriate assimilation rates. However, we agree that the equilibrium assumption for the distribution of Rubisco within the canopy is an oversimplification of plant growth under changing environmental conditions. Thus, crop model performance can be improved by applying a dynamic model for Rubisco turnover and interactive redistribution, accounting for the trade-off between optimal nitrogen availability for photosynthesis and growth.

The dynamics of wheat growth and thus crop acclimation, to the varying CO_2 levels of the FACE treatments were more adequately simulated using XN-GN. While nitrogen uptake increased under [CO_2] enrichment similarly by 7% using both models, the absolute nitrogen uptake was smaller using the XN-GN model. This is in agreement with the increase in the maximal root biomass under [CO_2] enrichment observed in the simulations by both models. The induction of increases in root biomass following [CO_2] enrichment has been previously described by van Vuuren et al. (1997) and Wechsung et al. (1995). However, the root biomass was significantly smaller in the XN-GN simulations, in which it was reduced by 10% at ambient [CO_2] and 21% under elevated [CO_2] compared with the XN-G simulations (Fig. 7). The validation of the dynamics of the root biomass simulations is difficult because the measurements are typically upscaled from a soil core device to field scale and thus possibly biased (Wechsung et al., 1995). Correspondingly, the total aboveground biomass production showed a stronger increase in the XN-GN simulations with [CO_2] enrichment. This result is based upon 2% lower transpiration rates compared with those of the XN-G simulations. Consequently, the efficiencies of nitrogen and water use were approximately 2% higher in the XN-GN simulations; additionally, carbon assimilation was lower. The maintenance costs for the photosynthetic apparatus were lower because N_P reduction occurred, particularly in the deeper canopy layers where carbon assimilation is more expensive due to a low PAR abundance, which reduces the photosynthetic capacity. The lower levels of total aboveground biomass in XN-GN simulations under ambient [CO_2] are a consequence of the dynamic acclimation of the plant. Such dynamic acclimation leads to a suboptimal vertical N_P distribution in the canopy compared to the fitted optimum vertical profile given by the exponential function. While the simulations using both models were of similar quality for the ambient [CO_2] treatments, XN-GN better simulated the elevated [CO_2] treatments of the FACE experiment (Table 1). In XN-GN, the acclimation to elevated [CO_2] is based on a dynamic distribution of N_P in the canopy and the ability of the plant to reuse the nitrogen allocated in the photosynthetic apparatus for growth. Therefore, N_P is distributed more effectively within the canopy with respect to the abundance of PAR and available amino acids for N_P synthesis. The result is an increase in the efficiency of the photosynthetic apparatus due to concurrent lower respiration costs and higher carbon fixation rates. The water and nitrogen use efficiencies increased in both models with rising [CO_2] but they were also higher using the new XN-GN model. This result strongly indicates that the dynamic model, together with its coupling to the Farquhar photosynthesis model, improves crop growth simulations under changing environmental conditions.

The altered depth distribution of N_P affected both light attenuation and the maintenance costs of the photosynthetic apparatus due to the higher N_P contents at the top of the canopy and in the sunlit leaves and lower contents at the bottom and in the shaded leaves using the XN-GN model. Thus, the harvest of incoming PAR is more effective, and maintenance costs are reduced in canopy regions where the interception of PAR is low. The efficiency of the photosynthetic apparatus increases due to the N_P dynamics and ability to use the nitrogen that exceeds the demand of the photosynthetic apparatus for biomass growth. This finding correlates with the hypothesis of decreased nitrogen demand under higher [CO_2], which assumes that plants can sustain their growth under lower shoot nitrogen concentrations (Conroy, 1992) due to increased nitrogen-use efficiencies (Stitt and

Krapp, 1999) since nitrogen uptake is partially regulated by sink demand (BassiriRad et al., 2001). The simulation results led to conclusions similar to those of Davey et al. (1999), Stitt and Krapp (1999) and Gifford et al. (2000), who found that increased nitrogen efficiency for biomass production under elevated [CO_2] is the product of increased photosynthetic nitrogen efficiency, resulting from the increased carboxylation efficiency of Rubisco and a decreased investment in N_P. Moreover, in XN-G, there is no redistribution of leaf nitrogen before the onset of leaf senescence. However, Feller and Fischer (1994) found that Rubisco degradation occurs during the early phases of canopy development. XN-GN allows for pre-anthesis redistribution because of the turnover of N_P and redistribution of the amino acids that exceed the maximum capacity for N_P synthesis in the canopy. In the simulations using XN-GN, the ratio between the N_R and N_P contents was 1:5 after emergence; this ratio rose to 4:5 at anthesis until ripeness, revealing the large amount of nitrogen available for redistribution and thus the structural and physiological acclimation to CO_2 enrichment. Moreover, XN-GN allows for leaves with low N_P contents to have the potential to synthesize new N_P if the availability of mobile nitrogen in the plant exceeds the demand for more dominant sinks, such as grain filling. This mechanism correlates with the observations by Imai et al. (2008), who observed that nitrogen influx in rice leaves promoted active Rubisco synthesis and counteracted leaf senescence even at late stages. Both the newly absorbed nitrogen from the soil and redistributable nitrogen species are available for growth before they are available for the recycling of N_P. Thus, XN-GN allows for the interactive canopy acclimation between structural and physiological canopy compartments to changing environmental conditions, which (Diaz, 1995) considered to be key elements of leaf acclimation.

The theoretical maximum N_P content of a leaf layer is limited by the same exponential distribution used in the XN-G model because no additional nitrogen is distributed to the leaf layer when the optimal levels are reached. Using the XN-GN, model the exponential profile is valid for plants under optimum growth conditions when the canopy reaches its maximum expansion (before the onset of senescence). Generally, during growth, the reallocation of carbon and nitrogen within the plant allows a more economic use of those resources. Therefore, in the XN-GN simulations, the observed N_P profiles did not reach the optimal exponential distribution but changed their shape dynamically. The depth distribution can be described by different polynomial fits. The highest N_P contents were not necessarily observed in the top layer of the canopy due to dilution by canopy expansion. Such vertical nitrogen distribution patterns in the canopy that varied from the exponential profile were previously described by Anten et al. (1995). Thus, we conclude that the predictions of canopy photosynthesis are likely to fail in models in which the N_P distribution is a fixed function of the total leaf nitrogen content (Johnson et al., 2010; Yin et al., 2000; Yin and van Laar, 2005; Kull, 2002) when crop acclimation to changing environmental conditions is simulated.

Due to the compartment approach of the nitrogen cycling module, amino acids derived from N_P degradation are immediately ready for redistribution throughout the whole plant in the XN-GN model. This could be an oversimplification because at least a portion of the recently degraded N_P is used for N_P synthesis at the site of degradation in the canopy instead of redistributed within the whole plant. To address this spatial component of the nitrogen cycle, the model could be extended by incorporating an additional resistance function, which retains a portion of the amino acids in the canopy layer in which they degraded, leaving the other portion available for redistribution throughout the plant for growth and the acclimation of the photosynthetic apparatus.

4.2. Rubisco turnover

Rubisco turnover is an important source for the redistribution of nitrogen throughout the plant (Hirel and Gallais, 2006). Despite a number of efforts to analyze Rubisco synthesis and degradation (Makino et al., 1984; Esquivel et al., 1998; Feller et al., 2008), the mechanisms of Rubisco turnover in leaves remain poorly understood (Houtz and Portis, 2003; Diaz et al., 2008; Feller et al., 2008). Turnover refers to the flow of amino acids through proteins, which is the balance between protein synthesis and degradation (Huffaker and Peterson, 1974). The site of Rubisco turnover in the leaf is within and/or outside of the chloroplast. Davies (1982) estimated leaf protein turnover rates to be 0.14 d^{-1} but found that turnover was considerably accelerated under stress conditions. This is in agreement with Peterson et al. (1973), who found that the protein turnover rates in barley leaves depend on environmental conditions and range from 0.06 to 0.38 d^{-1}. The different relationships between leaf protein turnover and leaf temperature were observed between different species of desert annuals (Smrcka and Szarek, 1986) and even between different rice varieties (Bose et al., 1999). Due to the limited knowledge available regarding species or even variety-typical mechanisms of protein turnover and responses to changing environmental conditions, we applied the parameterization of the turnover model as proposed by Thornley (1998). The temperature-unaffected Rubisco turnover value of 0.2 d^{-1} applied in this study is therefore in the range measured by Peterson et al. (1973). The temperature function Υ_1 was only able to prolong the flux of amino acids through proteins for temperatures above and below $T_r = 20\,^{\circ}C$ but not accelerate it. The temperature functions Υ_2 and Υ_3 were able to cause a prolongation for temperatures below T_r and high temperatures close to $T_{0'} = 45\,^{\circ}C$ but also caused significant acceleration for temperatures above T_r (Thornley and France, 2007). Using Υ_2 the range proposed by Peterson et al. (1973) was well-covered by the temperature function, which explains the good performance of the simulation results (in the range of 0.06–0.3 d^{-1} for temperatures between 5 °C and 43 °C). Using Υ_3, these limits were generally lower for temperatures below 10 °C, which increased N_P turnover to up to 50 days and higher for temperatures between 26 °C and 38 °C with turnover times of only 2 days. The consequence was an altered capacity for canopy acclimation due to the different partitioning of nitrogen either to growth or the optimization of photosynthesis, which is caused by a more static photosynthetic apparatus at low temperatures and rapid turnover under higher temperatures, which are usually favorable for biochemical reactions, such as photosynthesis. Therefore, the application of different temperature functions to affect N_P turnover strongly influenced the redistribution of N_P within the canopy. The best simulation results were obtained using Υ_3. This finding is not surprising because the response of enzyme activity to temperature typically increases slowly with temperatures above 0 °C, reaches its optimum at 30–40 °C and rapidly declines above 40 °C. Thus, protein turnover could perform an important regulatory role in the temperature adaption of the canopy (Smrcka and Szarek, 1986). We assume that the remobilization of nitrogen from N_P for redistribution within the canopy is an important process of crop acclimation to changing environmental conditions, such as [CO_2] and light. Thus, turnover is an advantage because the N_P distribution using XN-GN acclimates to both environmental changes and the nutritional state of the leaf. Assuming that the exponential N_P distribution is optimal a canopy acclimates such that carbon assimilation is most effective by accumulating N_P in canopy regions with higher PAR abundances. This indicates that detailed knowledge regarding the temperature response of N_P turnover could significantly improve crop growth simulations. Altogether, this is a clear indication that the redistribution of N_P within the canopy

must be addressed to analyze canopy acclimation to elevated CO_2.

4.3. Effect of canopy acclimation to [CO_2] on crop growth and yield quality

The sensitivity analysis showed that an increase in total aboveground biomass with increasing [CO_2] can be simulated with both models. Enriching [CO_2] from 400 to 500 ppm increased the total aboveground biomass by 8.7% using XN-G and 9.9% using XN-GN. The grain yields remained constant in the XN-G simulations but increased with increasing [CO_2] (from 400 to 500 ppm) using the XN-GN model. In C_3 species, photosynthesis is not yet substrate-saturated when the [CO_2] increases from 400 to 500 ppm. Hence, if no other factors than [CO_2], such as soil nitrogen availability, limit plant growth, we would expect increases in both the total aboveground biomass and grain yields (Fangmeier et al., 1996; Mitchell et al., 1993) as simulated in the XN-GN simulations. A decrease in grain protein has been reported from many [CO_2] enrichment studies (Erbs et al., 2010; Högy et al., in press; Högy et al., 2009a,b; Högy and Fangmeier, 2008; Taub et al., 2008; Wieser et al., 2008; Fangmeier et al., 1999; Kimball et al., 2001). Both XN-G and XN-GN simulated a similar reduction in grain protein concentrations with increasing [CO_2]. Using XN-GN, the grain protein content was 0.5% lower than in the XN-G simulation, regardless of [CO_2]. The lower protein concentrations in the XN-GN simulations were due to the lower leaf N_P contents available for redistribution for grain filling after anthesis and lower amounts of nitrogen redistributable from the reduced root biomass. In the GECROS model, the grains are the dominant sinks for nitrogen following the end of the grain-number-determining period. Because nitrogen uptake in this growth stage is already strongly reduced, most of the nitrogen necessary for grain filling must be remobilized from the green leaves during senescence. In the case of high biomass production, however, a large proportion is irretrievably fixed into structural plant components. These results are in agreement with Fangmeier et al. (1999, 2000, 2002), who stated that the down-regulation of leaf proteins decreases nitrogen availability so that it cannot be redistributed to nitrogen sinks, such as the storage organs.

4.4. Impact of carbon accumulation on leaf photosynthesis

Based on the results of this study, we suggest that the down-regulation of the assimilation rates in C_3 crops is due to the decreased Rubisco contents in the leaves. However, canopy acclimation could not completely be explained by the proposed model. Thus, other mechanisms may also play a role in canopy acclimation to higher [CO_2]. For example, the presented model does not account for reduced Rubisco concentrations which is part of the dilution by carbohydrates hypothesis in which the potential inhibition of leaf photosynthesis is affected by carbohydrate accumulation (Gifford et al., 2000; Kuehny et al., 1991; Wong, 1990). However, further model extension seems possible by accumulating recently absorbed carbon at the locus of its assimilation in the canopy before its partitioning within the plant for growth. Removal of the carbon assimilates could be affected by an empirical resistance coefficient, which is influenced by the sink strengths of crop organs and/or environmental factors, such as leaf temperatures. Such carbohydrate accumulation in the photosynthetic apparatus could limit new carbon assimilation either because storage sites in the cells are filled or the reactive sites are limited by assimilate back-up (Neals and Incoll, 1968). Carbohydrate accumulation could further act as a barrier for CO_2 diffusion to the reactive sites or radiation attenuation of Rubisco (Connor et al., 2011). Altered radiation attenuation may result from altered extinction and scattering properties due to carbohydrate accumulation. Any mechanism could be based on the ratio of N_P and non-structural carbohydrate contents in the leaves.

5. Conclusions

The model extensions demonstrate that the frequently used equilibrium assumption for the photosynthetic apparatus is not valid under the influences of crop growth and changing environmental conditions, such as atmospheric CO_2 concentrations. It is apparent that canopy acclimation to elevated CO_2 must be described as a dynamic process that allows for the trade-off between resource use for growth and the optimization of photosynthesis. The model can easily be implemented into canopy models that compute photosynthetic rates from the photosynthetic active nitrogen contents in the leaves. It was further shown that the consideration of the effects of leaf temperature on protein turnover can significantly improve model performance. However, due to the few existing studies on the responses of Rubisco chemistry to leaf temperatures, we tested the responses of selected empirical functions that include many degrees of freedom. Therefore, a more detailed knowledge of the species or even variety specific temperature responses of leaf protein turnover could improve photosynthesis and canopy modeling when plant acclimation to changing environmental conditions is the focus.

Acknowledgments

The study was funded by the German Research Foundation (DFG) as part of the Joint Research Project 'Regional Climate Change' (PAK 346) at the Universität Hohenheim and the Helmholtz Zentrum München. We thank Dr. Jürgen Franzaring for providing the [CO_2] data from the mini-FACE experiment in Stuttgart-Hohenheim, Germany.

Appendix A.

Table A.1
Abbreviations, index, parameters, and variables. Units are in brackets. Applied values are given, including the references.

Class	Description [unit] – value (reference)
Abbreviations and index	
N	Nitrogen
i	Canopy layer index
I	Irradiance [W m^{-2}]
L	Leaf area index [m^2 leaf m^{-2} ground]
PAR	Photosynthetic active radiation
$\Upsilon_1, \Upsilon_2, \Upsilon_3$	Temperature functions of different curvature
State variables	
I_0	I above the canopy [W m^{-2}]
I_i	I intercepting leaves of ith canopy layer [W m^{-2}]
I_i^{sh}; I_i^{su}	Shaded (sunlit) leaf fraction of I_i [W m^{-2}]
L_i	Leaf area index of ith canopy layer [m^2 leaf m^{-2} ground]
n_0	N content at the top of the canopy [g m^{-2}]
N_P	Photosynthetic active N; mostly Rubisco enzyme N_P^{-1} [d^{-1}]
$N_{P,i}$	N_P in ith canopy layer [g m^{-2}]
$N_{P,i}^{sh}$; $N_{P,i}^{su}$	N_P in shaded (sunlit) leaves of ith canopy layer [g m^{-2}]
$N_{P,i}^{act}$	Actual N_P in leaves of ith canopy layer [g m^{-2}]
$N_{P,i}^{act,sh}$; $N_{P,i}^{act,su}$	$N_{P,i}^{act}$ in shaded (sunlit) leaves of ith canopy layer [g m^{-2}]
N_P^{tar}	Actual (XN-G) and target (XN-GN) N_P content in leaves [g m^{-2}]
$N_{P,i}^{tar}$	N_P^{tar} in leaves of ith canopy layer [g m^{-2}]
$N_{P,i}^{tar,sh}$; $N_{P,i}^{tar,su}$	N_P^{tar} in shaded (sunlit) leaves of ith canopy layer [g m^{-2}]

Table A.1 (*Continued*)

Class	Description [unit] – value (reference)
N_R	Storage of *N* neither needed for photosynthesis nor for growth [g m^{-2}]
N_X	*N* mainly in structural plant tissues [g m^{-2}]
T_i^{act}	Actual (sunlit or shaded, respectively) leaf temperature of *i*th canopy layer [°C]
W_i	Leaf weight of *i*th canopy layer [g m^{-2}]
Rate variables	
$N_{G\rightarrow P}$	*N* partitioned to leaf for N_P synthesis [g m^{-2} d^{-1}]
$N_{G\rightarrow R}$	*N* that exceeds capacity of N_P synthesis to be stored in N_R [g m^{-2} d^{-1}]
$N^{sh}_{G\rightarrow R,i}$; $N^{su}_{G\rightarrow R,i}$	*N* that exceeds capacity of N_P synthesis in shaded (sunlit) leaves of *i*th canopy layer to be stored in N_R [g m^{-2} d^{-1}]
$N^{syn,sh}_{G\rightarrow P,i}$; $N^{syn,su}_{G\rightarrow P,i}$	New N_P synthesised in shaded (sunlit) leaves of *i*th canopy layer [g m^{-2} d^{-1}]
$N_{P\rightarrow R}$	*N* derived from N_P degradation to be stored in N_R [g m^{-2} d^{-1}]
$N^{sh}_{P\rightarrow R,i}$; $N^{su}_{P\rightarrow R,i}$	*N* derived from N_P degradation in shaded (sunlit) leaves of *i*th canopy layer to be stored in N_R [g m^{-2} d^{-1}]
$N_{R\rightarrow G}$	*N* derived from N_R provided for plant growth [g m^{-2} d^{-1}]
$N_{U\rightarrow G}$	Nitrogen uptake for plant growth [g m^{-2} d^{-1}]
$N_{X\rightarrow G}$	*N* mainly re-mobilized from structural plant tissues provided for plant growth [g m^{-2} d^{-1}]
Parameters	
c_{D,N_P}	N_P degradation constant [d^{-1}] – 0.2 (Thornley, 1998)
c_{G,N_R}	N_R growth constant [d^{-1}] – 1.0 (all N_R available for plant growth within one day)
c_{G,N_P}	Growth constant for synthesis of N_P [d^{-1}] – 0.008 (Thornley, 1998)
n_b	Base value of nitrogen at which leaf photosynthesis is zero [g m^{-2}] – 0.35 (Yin and van Laar, 2005)
m	Number of canopy layers – 10
m_I	Michaelis–Menten coefficient to control impact of inter-acepted PAR on N_P synthesis [W m^{-2}] – 100 (Thornley, 1998)
m_N	Michaelis–Menten coefficient to control impact of amount of *N* available for N_P synthesis [g m^{-2}] – 0.01 (assumed based on Thornley, 1998)
T_0	Minimum temperature for degradation of N_P [°C] – 0.0 (Thornley and France, 2007)
$T_{0'}$	Maximum temperature for degradation of N_P [°C] – 45.0 (Thornley and France, 2007)
T_r	Reference temperature where $f(T_r) = 1$ [°C] – 20.0 (Thornley and France, 2007)
ϑ, υ	Constants to define curvature of temperature response – 1; 2; 3 (Thornley and France, 2007)
Others	
$f(T)$	Effect of the leaf temperature on N_P degradation
$f(T_i^{sh})$; $f(T_i^{su})$	Temperature effect of shaded (sunlit) leaves in *i*th canopy layer on N_P degradation
k	Light extinction coefficient [m^2 ground m^{-2} leaf]
k_{dir}	Direct beam extinction coefficient [m^2 ground m^{-2} leaf]
k_n	*N* extinction coefficient [m^2 ground m^{-2} leaf]
$L_{c,i}$	Cumulative *L* above L_i [m^2 leaf m^{-2} ground]

Table A.2
Genotype specific parameters, units, and values that refer to the crop growth model GECROS (Yin and van Laar, 2005). These parameters are important to run GECROS but were not additionally introduced in this manuscript. Applied values were in the range of the measurements or taken from the literature if necessary. The phenology parameters m_v and m_g were fitted. The values for the constants used in the protein turnover extension module in the XN-GN model were proposed by Thornley (1998) and applied unchanged.

Parameter	Description	Unit	Value	Citation
$Y_{C,V}$	Growth efficiency of vegetative organs	g C g C^{-1}	0.81	Yin and van Laar (2005)
$f_{c,V}$	C fraction in vegetative-organ biomass	g C g^{-1}	0.42	Measured value
w	Leaf width	m	0.012	Bos and Neuteboom (1998)
n_{crit0}	Initial critical shoot N concentration	g N g^{-1}	0.05	Yin and van Laar (2005)
n_{Rmin}	Min N concentration in root	g N g^{-1}	0.005	Yin and van Laar (2005)
n_{Smin}	Min N concentration in stem	g N g^{-1}	0.011	Measured value
S_W	Weight of single seed	g Seed^{-1}	0.042	Measured value
n_{SO}	Standard seed N concentration	g N g^{-1}	0.026	Measured value
H_{max}	Max plant height	m	1.1	Measured value
ρ	Proportionality factor between stem biomass and plant height	g m^{-2} m^{-1}	460	Yin and van Laar (2005)
m_v	Min thermal days for vegetative phase	day	38	Fitted value
m_g	Min thermal days for reproductive phase	day	33	Fitted value
E_{Jmax}	Activation energy of maximum rates of electron transport contributing to Rubisco regeneration	J mol^{-1}	48.270	Yin and van Laar (2005)
β_L	Leaf angle from horizontal	°	25	Simon (1999)
N_{maxup}	Max N-uptake rate	g N m^{-2} d^{-1}	0.6	Yin and van Laar (2005)
n_b	Min specific leaf nitrogen	g N m^{-2}	0.35	Yin and van Laar (2005)
D_{max}	Max root depth	m	1.3	Yin and van Laar (2005)

References

Ainsworth, E., Long, S., 2005. What have we learned from 15 years of free-air CO_2 enrichment (FACE)? A meta-analytic review of the responses of photosynthesis, canopy properties and plant production to rising CO_2. New Phytologist 165, 351–372.

Amthor, J., 2001. Effects of atmospheric CO_2 concentration on wheat yield; review on results from experiments using various approaches to control CO_2 concentration. Field Crops Research 73, 1–34.

Anten, N., Schieving, F., Werger, M., 1995. Patterns of light and nitrogen distribution in relation to whole canopy carbon gain in C_3 and C_4 mono- and dicotyledonous species. Oecologia 101, 504–513.

BassiriRad, H., Gutschick, V., Lussenhop, J., 2001. Root system adjustment: regulation of plant nutrient uptake and growth responses to elevated CO_2. Oecologia 126, 305–320.

Berner, R., 1998. The carbon cycle and CO_2 over phanerozoic time: the role of land plants. Philosophical Transactions of the Royal Society B-Biological Sciences 353, 75–82.

Bertheloot, J., Cournéde, P., Andrieu, B., 2011. NEMA, a functional–structural model of nitrogen economy within wheat culms after flowering. I. Model description. Annals of Botany 108 (6), 1085–1096.

Biernath, C., Gayler, S., Bittner, S., Klein, C., Högy, P., Fangmeier, A., Priesack, E., 2011. Evaluating the ability of four crop models to predict different environmental impacts on spring wheat grown in open-top chambers. European Journal of Agronomy 35, 71–82.

Bloom, A., Burger, M., Asensio, J., Cousins, A., 2010. Carbon dioxide enrichment inhibits nitrate assimilation in wheat and arabidopsis. Science 328 (5980), 899–903.

Borjigidai, A., Hikosaka, K., Hirose, T., Hasegawa, T., Okada, M., Kobayashi, K., 2006. Seasonal changes in temperature dependence of photosynthetic rate in rice under a free-air CO_2 enrichment. Annals of Botany 97, 549–557.

Bos, J., Neuteboom, J., 1998. Growth of individual leaves of spring wheat (*Triticum aestivum* L.) as influenced by temperature and light intensity. Annals of Botany 8, 141–149.

Bose, A., Tiwari, B., Chattopadhyay, M., Gupta, S., Ghosh, B., 1999. Thermal stress induces differential degradation of Rubisco in heat-sensitive and heat-tolerant rice. Physiologia Plantarum 105, 89–94.

Charles-Edwards, D., 1976. Shoot and root activities during steady-state plant growth. Annals of Botany 40, 767–772.

Chen, X., Alm, D., Hesketh, J., 1995. Effects of atmospheric CO_2 concentration on photosynthetic performance of C_3 and CO_4 plants. Biotronics 24, 65–72.

Connor, D., Loomis, R., Cassman, K., 2011. Photosynthesis. In: Connor, D., Loomis, R., Cassman, K. (Eds.), Crop Ecology. 2nd ed. Cambridge University Press, New York, pp. 262–291.

Conroy, J., 1992. Influence of elevated atmospheric CO_2 concentration on plant nutrition. Australian Journal of Botany 40, 445–456.

Davey, P., Parson, A., Atkinson, L., Wadge, K., Long, S., 1999. Does photosynthetic acclimation to elevated CO_2 increase photosynthetic nitrogen-use efficiency? A study of three native UK grassland species in open-top chambers. Functional Ecology 13, 21–28.

Davies, D., 1982. Physiological aspects of protein turnover. In: Boulter, D., Parthier, B. (Eds.), Nucleic acids and proteins in plants. I. Structure, biochemistry and physiology of proteins. Encyclopedia of plant physiology. New Series. Springer Verlag, Berlin, Germany, pp. 189–228.

De Pury, D., Farquhar, G., 1997. Simple scaling of photosynthesis from leaves to canopies without the errors of big-leaf models. Plant Cell and Environment 20, 537–557.

Diaz, C., Lemaitre, T., Christ, A., Azopardi, M., Kato, Y., Sato, F., Morot-Gaudry, J., Le Dily, F., Masclaux-Daubresse, C., 2008. Nitrogen recycling and remobilization are differently controlled by leaf senescence and development stage in arabidopsis under low nitrogen nutrition. Plant Physiology 147, 1437–1449.

Diaz, S., 1995. Elevated CO_2 responsiveness, interactions at the community level and plant functional types. Journal of Biogeography 22, 289–295.

Erbs, M., Manderscheid, R., Jansen, G., Sedding, S., Pacholski, A., Weigel, H.-J., 2010. Effects of free-air CO_2 enrichment and nitrogen supply on grain quality parameters and elemental composition of wheat and barley grown in a crop rotation. Agriculture Ecosystems & Environment 136, 59–68.

Esquivel, M., Ferreira, R., Teixeira, A., 1998. Protein degradation in C_3 and C_4 plants with particular reference to ribulose biphosphate carboxylase and glycolate oxidase. Journal of Experimental Botany 49 (322), 807–816.

Evans, J., Seemann, J., 1989. The allocation of protein nitrogen in the photosynthetic apparatus: costs, consequences, and control. In: Briggs, W. (Ed.), Photosynthesis. Alan R. Liss, New York, pp. 183–205.

Fangmeier, A., Chrost, B., Högy, P., Krupinska, K., 2000. CO_2 enrichtnent enhances flag leaf senescence in barley due to greater grain nitrogen sink capacity. Environmental and Experimental Botany 44, 151–164.

Fangmeier, A., De Temmerman, L., Black, C., Persson, K., Vorne, V., 2002. Effects of elevated CO_2 and/or ozone on nutrient concentrations and nutrient uptake of potatos. European Journal of Agronomy 17, 353–368.

Fangmeier, A., De Temmerman, L., Mortensen, L., Kemp, K.J.B., Mitchell, R., Van Oijen, M., Weigel, H.-J., 1999. Effects on nutrients and on grain quality in spring wheat crops grown under elevated CO_2 concentrations and stress conditions in the European, multiple-site experiment 'ESPACE-wheat'. European Journal of Agronomy 10, 215–229.

Fangmeier, A., Gruters, U., Hertstein, U., Sandhage-Hofmann, A., Vermehren, B., Jäger, H.-J., 1996. Effects of elevated CO_2, nitrogen supply and tropospheric ozone on spring wheat. I. Growth and yield. Environmental Pollutution 91, 381–390.

Farquhar, G., Caemmerer, S., Berry, J., 1980. Biochemical model of photosynthetic CO_2 assimilation in leaves of C_3 species. Planta 149, 78–90.

Feller, U., Anders, I., Mae, T., 2008. Rubiscolytics: fate of Rubisco after its enzymatic function in a cell is terminated. Journal of Experimental Botany 59 (7), 1615–1624.

Feller, U., Fischer, A., 1994. Nitrogen metabolism in senescing leaves. Critical Reviews in Plant Sciences 13, 241–273.

Forrester, J., 1961. Industrial Dynamics. MIT Press, Waltham, MA.

Gayler, S., Wang, E., Priesack, E., Schaaf, T., Maidl, 2002. Modeling biomass growth, N-uptake and phenological development of potato crop. Geoderma 105, 367–383.

Gifford, R., Barret, D., Lutze, J., 2000. The effects of elevated [CO_2] on the C:N and C:P ratios of plant tissues. Plant and Soil 224, 1–14.

Högy, P., Brunnbauer, M., Koehler, P., Schwadorf, K., Breuer, J., Franzaring, J., Zhunusbayeva, D., Fangmeier, A. Grain quality characteristics of spring wheat (*Triticum aestivum*) as affected by free-air CO_2 enrichment. Environmental and Experimental Botany, in press

Högy, P., Fangmeier, A., 2008. Effects of elevated atmospheric CO_2 on grain quality of wheat. Journal of Cereal Science 48, 580–591.

Högy, P., Wieser, H., Köhler, P., Schwadorf, K., Breuer, J., Franzaring, J., Muntifering, R., Fangmeier, A., 2009a. Effects of elevated CO_2 on grain yield and quality of wheat: results from a three-year face experiment. Plant Biology (Stuttgart, Germany) 11 (Suppl. 1), 60–69.

Högy, P., Zörb, C., Langenkämper, G., Betsche, T., Fangmeier, A., 2009b. Atmospheric CO_2 enrichment changes the wheat grain proteome. Journal of Cereal Science 50, 248–254.

Hikosaka, K., Ishikawa, K., Borjigidai, A., Muller, O., Onida, Y., 2006. Temperature acclimation of photosynthesis: mechanisms involved in the changes in temperature dependence of photosynthetic rate. Journal of Experimental Botany 57, 520–526.

Hirel, B., Gallais, A., 2006. Rubisco synthesis, turnover and degradation: some new thoughts on an old problem. New Phytologist 169, 445–448.

Houtz, R., Portis, A., 2003. The life of ribulose 1,5-biphosphate carboxylase/oxygenase - posttranslational facts and mysteries. Archives of Biochemistry and Biophysics 414, 150–158.

Huffaker, R., Peterson, L., 1974. Protein turnover plants and possible means of its regulation. Annual Review of Plant Physiology 25, 363–392.

Hutson, J., Wagenet, R., 1992. LEACHM: leaching estimation and chemistry model: a process-based model of water and solute movement, transformations, plant uptake and chemical reactions in the unsaturated zone. Version 3.0. Technical report. Research Series No. 93-3, Department of Soil, Crop and Atmospheric Sciences, Cornell University, Ithaca, NY.

Imai, K., Suzuki, Y., Mae, T., Makino, A., 2008. Changes in the synthesis of rubisco in rice leaves in relation to senescence and N influx. Annals of Botany 101, 135–144.

Johnson, I., Thornley, J., Frantz, J., Bugbee, B., 2010. A model of canopy photosynthesis incorporating protein distribution through the canopy and its acclimation to light, temperature and CO_2. Annals of Botany 106, 735–749.

Johnsson, H., Bergstroem, L., Bergstroem, P., Jansson, P., Paustian, K., 1987. Simulated nitrogen dynamics and losses in a layered agricultural soil. Agriculture Ecosystems & Environment 18, 333–356.

Kimball, B., Morris, C., Pinter, P., Wall, G., Hunsaker, D., Adamsen, F., LaMorte, R., Leavith, S., Thompson, T., Mathias, A., Brooks, T., 2001. Elevated CO_2, drought and soil nitrogen effects on wheat grain quality. New Phytologist 150, 295–303.

Kimball, B., Pinter, P., Garcia, R., LaMorte, R., Wall, G., Hunsaker, D., Wechsung, G., Wechsung, F., Kartschall, T., 1995. Productivity and water use of wheat under free air CO_2 enrichment. Global Change Biology 1, 429–442.

Körner, C., Bazzaz, F., 1996. Carbon Dioxide, Populations, and Communities. Academic Press, San Diego, CA.

Kropff, M., 1993. Mechanisms of competition for light. In: Kropff, M., van Laar, H. (Eds.), Crop Weed Interaction. C.A.B. International,International Rice Research Institute, Wallingford, Oxfordshire, p. 274.

Kuehny, J., Peet, M., Nelson, P., Willits, D., 1991. Nutrient dilution by starch in CO_2-enriched Chrysanthemum. Journal of Experimental Botany 42, 711–716.

Kull, O., 2002. Acclimation of photosynthesis in canopies: models and limitations. Oecologia 133 (3), 267–279.

Laisk, A., Edwards, G., 2009. Leaf C_4 photosynthesis in silica: the CO_2 concentrating mechanism. In: Laisk, A., Nedbal, L., Gofindjee (Eds.), Photosynthesis in Silico – Understanding Complexity from Molecules to Ecosystems. Springer, Dordrecht, The Netherlands, pp. 323–349.

Makino, A., Mae, T., Ohira, K., 1984. Relation between nitrogen and ribulose-l,5-bisphosphate carboxylase in rice leaves from emergence through senescence. Plant Cell and Environment 25 (3), 429–437.

Meier, U., 1997. Growth stages of mono- and dicogyledonous plants: BBCH-Monograph = Entwicklungsstadien mono- und dikotyler Pflanzen. Blackwell Wiss.-Verl, Berlin, Wien [u.a.], ISBN 3-8263-3152-4.

Mitchell, R., Mitchell, V., Driscoll, S., Franklin, J., Lawlor, D., 1993. Effects of increased CO_2 concentration and temperature on growth and yield of winter wheat at two levels of nitrogen application. Plant Cell and Environment 16, 521–529.

Monsi, M., Saeki, T., 2005. On the factor light in plant communities and its importance for matter production. Annals of Botany 95, 549–567.

Monteith, J., Unsworth, M., 1990. Principles of Environmental Physics, 2nd ed. Edward Arnold, London.

Murthy, R., Dougherty, P., 1997. Effects of carbon dioxide, fertilization and irrigation on loblolly pine branch morphology. Trees – Structure and Function 11, 485–493.
Neals, T., Incoll, L., 1968. The control of leaf photosynthesis rate by level of assimilate concentration in the leaf: a review of the hypothesis. Botanical Review 34, 107–125.
Niu, X., Easterling, W., Hays, C., Jacobs, A., Mearns, 2009. Reliability and inputdata induced uncertainty of the EPIC model to estimate climate change impact on sorghum yields in the U.S. Great Plains. Agriculture Ecosystems & Environment 129, 268–276.
OECD, 02 2012. The OECD environmental outlook to 2050 – key findings on climate change. Online URL http://www.oecd.org/dataoecd/21/30/49089652.pdf (13.09.12).
Peterson, L., Kleinkopf, G., Huffaker, R., 1973. Evidence for lack of turnover of ribulose-di-phosphate carboxylase in barley leaves. Plant Physiology 51, 1042–1045.
Poorter, H., 1993. Interspecific variation in the growth response of plants to an elevated ambient CO_2 concentration. Vegetatio 104/105, 77–97.
Poorter, H., Van Berieo, Y., Baxter, R., Den Hertog, J., Dijkstra, P., Gifford, R., Griffin, K., Roumet, C., Roy, J., Wong, S., 1997. The effect of elevated CO_2 on the chemical composition and construction costs of leaves of 27 C_3 species. Plant Cell and Environment 20, 472–482.
Priesack, E., 2006. Expert-N Dokumentation der Modellbibliothek. FAM-Bericht 60. Hieronymus, München.
Priesack, E., Bauer, C., 2003. Expert-N Datenmanagement Version 3.0, FAM-Bericht 59. Hieronymus, München.
Priesack, E., Gayler, S., 2009. Agricultural crop models: Concepts of resource acquisition and assimilate partitioning. In: Lüttge, U., Beyschlag, W., Murata, J. (Eds.), Progress in Botany 70. Springer-Verlag, Berlin, Heidelberg, Germany, pp. 195–222.
Priesack, E., Gayler, S., Hartmann, H., 2006. The impact of crop growth sub-model choice on simulated water and nitrogen balances. Nutrient Cycling in Agroecosystems 75, 1–13.
Pritchard, S., Rogers, H.H., Prior, S.A., Peterson, C., 1999. Elevated CO_2 and plant structure: a review. Global Change Biology 5, 807–837.
Simon, M., 1999. Inheritance of flag-leaf angle, flag-leaf area and flag-leaf area duration in four wheat crosses. Theoretical and Applied Genetics 98, 310–314.
Simunek, J., Huang, K., van Genuchten, M., 1998. The hydrus code for simulating the one-dimensional movement of water, heat, and multiple solutes in variability-saturated media. version 6.0. Tech. rep., Tech. Rep. U.S. Salinity Laboratory, USDA, ARS.
Smrcka, A., Szarek, S., 1986. Phenotypical temperature adaption of protein turnover in desert annuals. Plant Physiology 80, 206–210.
Stitt, M., Krapp, A., 1999. The interaction between elevated carbon dioxide and nitrogen nutrition: the physiological and molecular background. Plant Cell and Environment 22, 583–621.
Tans, P., 2012. Recent Mauna Loa CO_2. Online URL http://www.esrl.noaa.gov/gmd/ccgg/trends/mlo.html (16.09.12).
Taub, D., Miller, B., Allen, H., 2008. Effects of elevated CO_2 on the protein concentration of food crops: a meta-analysis. Global Change Biology 14, 565–575.
Taub, D., Wang, X., 2008. Why are nitrogen concentrations in plant tissues lower under elevated CO_2? A critical examination of the hypothesis. Journal of Integrative Plant Biology 50 (11), 1365–1374.
Thornley, J., 1998. Dynamic model of leaf photosynthesis with acclimation to light and nitrogen. Annals of Botany 81 (3), 421–430.
Thornley, J., 2002. Instantaneous canopy photosynthesis: analytical expressions for sun and shade leaves based on exponential light decay down the canopy and an acclimated non-rectangular hyperbola for leaf photosynthesis. Annals of Botany 89, 451–458.
Thornley, J., 2004. Acclimation of photosynthesis to light and canopy nitrogen distribution: an interpretation. Annals of Botany 93, 473–475.
Thornley, J., Cannell, M., 2000a. Dynamics of mineral N availability in grassland ecosystems under increased [CO_2]: hypotheses evaluated using the Hurley Pasture Model. Plant Soil 224, 153–170.
Thornley, J., Cannell, M., 2000b. Managing forests for wood yield and carbon storage: a theoretical study. Tree Physiology 20, 477–485.
Thornley, J., France, J., 2007. Mathematical Models in Agriculture: Quantitative Methods for the Plant, Animal and Ecological Sciences, 2nd ed. CABI.
van Vuuren, M., Robinson, D., Fitters, A., Chasalow, S., Williamson, L.J.A.R., 1997. Effects of elevated atmospheric CO_2 and soil water availability on root biomass, root length, and N, P and K uptake by wheat. New Phytologist 135, 455–465.
von Caemmerer, S., Farquhar, G., 1981. Some relationships between the biochemistry of photosynthesis and the gas exchange of leaves. Planta 153, 376–387.
Wallach, D., Goffinet, B., 1989. Mean squared error of prediction as a criterion for evaluating and comparing system models. Ecological Modelling 44, 299–306.
Wang, Y.-P., Leuning, R., 1998. A two-leaf model for canopy conductance, photosynthesis and partitioning of available energy. I: model description and comparison with a multi-layered model. Agricultural and Forest Meteorology 91, 89–111.
Wechsung, G., Wechsung, F., Wall, G., Adamsen, F., Kimball, B., Garcia, R., Pinter, J.R.P., Kartschall, T., 1995. Biomass and growth rate of spring wheat root system grown in free-air CO_2-enrichment (FACE) and ample soil moisture. Journal of Biogeography 22, 623–634.
Wegehenkel, M., Mirschel, W., 2006. Crop growth, soil water and nitrogen balance simulation on three experimental field plots using the OPUS model – a case study. Ecological Modelling 190, 116–132.
Wieser, H., Manderscheid, R., Erbs, M., Weigel, H.-J., 2008. Effects of elevated atmospheric CO_2 concentrations on the quantitative protein composition of wheat grains. Journal of Agricultural and Food Chemistry 56, 6531–6535.
Willmott, C., 1982. Some comments on the evaluation of model performance. Bulletin of American Meteorological Society 64.
Wong, S.-C., 1990. Elevated atmospheric partial pressure of CO_2 and plant growth. II. Non-structural carbohydrate content in cotton plants and its effect on growth parameters. Photosynthesis Research 23, 171–180.
Yamasaki, T., Yamakawa, T., Yamane, Y., Koike, H., Satoh, K., Katoh, S., 2002. Temperature acclimation of photosynthesis and related changes in photosystem II electron transport in winter wheat. Plant Physiology 128, 1087–1097.
Yin, X., Lantinga, E., Schapendonk, A., Zhong, X., 2003. Some quantitative relationships between leaf area index and canopy nitrogen content and distribution. Annals of Botany 91, 893–903.
Yin, X., Schapendonk, A., 2004. Simulating the partitioning of biomass and nitrogen between root and shoot in crop and grass plants. NJAS – Wageningen Journal of Life Sciences 51, 407–426.
Yin, X., Schapendonk, A., Kropff, M., Van Oijen, M., Bindraban, P., 2000. A generic equation for nitrogen-limited leaf area index and its application in crop growth models for predicting leaf senescence. Annals of Botany 85, 579–585.
Yin, X., van Laar, H., 2005. Crop Systems Dynamics. Wageningen Academic Publishers, Wageningen.
Yin, X., van Oijen, M., Schapendonk, A., 2004. Extension of a biochemical model for the generalized stoichiometry of electron transport limited C_3 photosynthesis. Plant Cell and Environment 27, 1211–1222.

4 Evaluation of a ray-tracing canopy light model based on terrestrial laser scans

Published in the Canadian Journal of Remote Sensing/Journal canadien de télédétection. Used with the permission of the Canadian Aeronautics and Space Institute.

Bittner S., Gayler S., Biernath C., Winkler J. B., Seifert S., Pretzsch H. and Priesack E. 2012: The performance of a voxel-based canopy light model based on terrestrial laser scans. *Canadian Journal of Remote Sensing*, 38: 619-628.

Can. J. Remote Sensing, Vol. 38, No. 5, pp. 619–628, 2012

Evaluation of a ray-tracing canopy light model based on terrestrial laser scans

Sebastian Bittner, Sebastian Gayler, Christian Biernath, Jana Barbro Winkler, Stefan Seifert, Hans Pretzsch, and Eckart Priesack

Abstract. The local light regime within the tree canopy is crucial information for modeling water, carbon and nutrient cycling, and vegetation–atmosphere interactions. We tested the performance of a new model to simulate the light environment in the canopy of a juvenile beech stand under controlled light conditions. The canopy architecture was determined using a terrestrial laser scanner to derive a three-dimensional voxel representation. Depending on whether a voxel represents stem biomass, leaf biomass, or air, different attributes of light are assigned to the voxel. The model combines a representation of the canopy as three-dimensional cells (voxels) with a fast ray tracing algorithm that calculates the absorbed fraction of incoming photosynthetic active radiation (PAR). The simulated light regime of the stand was compared with measurements of the PAR regime inside the canopy (model efficiency Nash–Sutcliffe efficiency (NSE) = 0.88, root mean square error (RMSE) = 124 μmol m^{-2} s^{-1}) and at the soil surface (NSE = 0.65, RMSE = 22 μmol m^{-2} s^{-1}). The model needs two input parameters, the edge length of the voxels and the light attenuation coefficient of the voxels. The best simulation results were achieved at a voxel size of 0.03 m. For model calibration, only measurements of the light fraction that reaches the soil surface are needed. The good agreement of the simulated and the measured light regime together with the fast computation by the ray tracing algorithm suggest that the model is also applicable to simulate the light regime of natural forests under variable light conditions.

Résumé. Le régime de la lumière locale au sein de la canopée des arbres est une information essentielle à la modélisation des cycles de l'eau, du carbone et des éléments nutritifs, ainsi que des interactions entre la végétation et l'atmosphère. Nous avons testé les performances d'un nouveau modèle de simulation de l'environnement de la lumière dans la canopée d'un peuplement de jeunes hêtres dans des conditions de lumière contrôlées. L'architecture de la canopée a été déterminée à l'aide d'un scanner laser terrestre permettant de dériver une représentation tridimensionnelle en voxels. Différents attributs de lumière sont affectés au voxel selon que ce dernier représente la biomasse des troncs, la biomasse foliaire ou l'air. Le modèle combine la représentation de la canopée sous forme de cellules tridimensionnelles « voxels » avec un algorithme rapide de lancer de rayon qui calcule la fraction absorbée de rayonnement photosynthétiquement actif « PAR » entrant. Le régime de lumière simulé du peuplement a été comparé à des mesures du régime PAR à l'intérieur de la canopée (efficacité du modèle NSE = 0,88, RMSE = 124 μmol m^{-2} s^{-1}) et à la surface du sol (NSE = 0,65 et un RMSE de 22 μmol m^{-2} s^{-1}). Le modèle nécessite deux paramètres d'entrée: la longueur d'arête des voxels et leur coefficient d'atténuation de la lumière. Les meilleurs résultats de simulation ont été obtenus sur une dimension de voxel de 0,03 m. Seules des mesures de la fraction de lumière qui parvient à la surface du sol sont nécessaires pour l'étalonnage du modèle. La bonne concordance entre le régime de la lumière simulé et celui mesuré en appliquant le calcul rapide par l'algorithme de lancer de rayon montre que le modèle peut être appliqué également pour simuler le régime de la lumière de forêts naturelles dans différentes conditions de lumière.

Introduction

A good estimation of the local light regime within tree canopies is crucial information needed in models of the cycles of water, carbon, and nutrients in forest ecosystems and of the interaction between the vegetation and the atmosphere. In these models, interception and absorption of light are sensible input variables to simulate functions such as transpiration and photosynthesis. Several models are based on a stand-level approach and neglect local

Received 10 May 2011. Accepted 3 August 2012. Published on the Web at http://pubs.casi.ca/journal/cjrs on 20 December 2012.

Sebastian Bittner, Sebastian Gayler, Christian Biernath[1], and Eckart Priesack. Institute of Soil Ecology, Helmholtz Zentrum München, Ingolstädter Landstraße 1, 85764 Neuherberg, Germany.

Sebastian Gayler. WESS – Water & Earth System Competence Cluster, Hölderlinstr. 12, 72074 Tübingen, Germany.

Jana Barbro Winkler. Research Unit Environmental Simulation (EUS), Institute for Biochemical Plant Pathology, Helmholtz Zentrum München, Ingolstädter Landstraße 1, 85764 Neuherberg, Germany.

Stefan Seifert and Hans Pretzsch. Chair of Forest Yield Science, Center of Life and Food Sciences Weihenstephan, Technische Universität München, Hans-Carl-von-Carlowitz-Platz 2, 85354 Freising, Germany.

[1]Corresponding author (e-mail: christian.biernath@helmholtz-muenchen.de).

inhomogeneity of the canopy like gaps or leaf clusters (Bossel, 1996; Hoffmann, 1995) or include an up-scaling from individual trees to consider light inhomogeneities in a parametric way (Oker-Blom et al., 1989; Larsen and Kershaw Jr., 1996). However, as inhomogeneities can have large effects on the local light regime (Castro and Fetcher, 1999; Whitehead et al., 1990) more advanced models use explicit three-dimensional representations of the canopy.

Explicit geometrical models have approached the representation of the canopy in different levels of complexity. The use of three-dimensional virtual trees generated from growth simulation rules such as L-Systems (Allen et al., 2005; Da Silva et al., 2008; Disney et al., 2006; Roupsard et al., 2008; Lamanda et al., 2008; Sinoquet, 2007; Parveaud et al., 2008; Hemmerling et al., 2008) provides information on the position and orientation of leaves and can be used for ray-tracing algorithms, for example by using the leaf orientation for the calculation of scattered light. The disadvantage of complex canopy models is the high demand of input data that are often difficult to obtain.

Therefore, some models approximate the shape of the canopy by simple geometrical bodies (such as ellipsoids, frustrums, or cylinders (Widlowski et al., 2006; Brunner, 1998; Green et al., 2003; Kobayashi and Iwabuchi, 2008; Courbaud et al., 2003; Gayler et al., 2006)) or hulls (Cescatti, 1997; Da Silva et al., 2008). In these models, the leaf area is distributed inside the bodies either constantly or based on physiological observations. The light distribution within the canopy can then be calculated by the radiative transfer equation (Ross, 1981) with the scattering being often neglected leading to a Beer's law of light attenuation (Monsi and Saeki, 1953). An alternative approach to represent the structure of a canopy in a model is to use a discretization of the space into cubical volume elements, called voxels (Kimes, 1984; Cohen and Fuchs, 1987; Gastellu-Etchegorry et al., 2004; Perttunen et al., 2007; Van der Zande et al., 2009), that are either filled by elements of the vegetation or not. Light attenuation within the canopy can then be calculated by tracing the light rays that penetrate the canopy and applying Beer's law for each filled voxel. By decreasing the size of the voxels a more precise determination of the space occupied by the vegetation can be achieved. But, on the other hand, the question arises if the original assumptions leading to the Beer's law of light attenuation are still valid, because the assumption of infinitesimal small phytoelements randomly distributed inside the single voxels does not hold if the voxel size is similar to the leaf size of the plant (Knyazikhin et al., 1997; Myneni et al., 1989; Govaerts and Verstraete, 1998). In this case, the extinction coefficient of the simple exponential formula of light attenuation cannot be referred to physical or geometrical properties of the vegetation. In this study the light attenuation coefficient was interpreted as a voxel-based model input parameter that had to be calibrated to the specific stand.

Light models that describe the canopy by an envelope that attenuates light according to a Lambert–Beer law often include the measured leaf angle distribution and a leaf distribution function in the expression for the light attenuation factor (Baldocchi and Harley, 1995). This is important when the leaves are clumped in old-growth forests and when the expression for the light attenuation factor is derived by physical and geometrical approaches. Here the question arises whether an empirical and constant light attenuation factor used in this study is adequate to simulate the light regime. Analyzing digitalized and simulated tree architectures Sinoquet et al. (2005) could show that the clumping effect should be included in models that work on coarse envelopes of the canopy, but they can be neglected if a voxel representation of the canopy with a small voxel size is used. We found that decreasing the voxel size generally increases the fraction of the inhomogeneity of the spatial leaf distribution accounted for by the space division into voxels with the optimal voxel size similar to the leaf size. Wang (2003) states that a constant light attenuation factor, which is independent of the leaf angle distribution and leaf clumping, is accurate if the model considers the direct and the diffuse radiation separately.

An analytical derivation of the voxel extinction coefficient based on information on the forest structure might be helpful to generalize the model input values to other species and stands without further calibration. However, these structural data are often laborious to obtain and have an uncertainty themselves. Therefore, the use of a single empirical extinction coefficient parameter that can be derived from light measurements or sap flux measurements (Bittner et al., 2012b) could help to advance functional–structural models. This could be the case especially when the light distribution is an input of other submodels such as the photosynthesis of stomatal models and when the principles of light distribution inside canopies are not in the focus of the research.

Because of improvements in the light detection and ranging (LiDAR) technique in recent years, terrestrial laser scanners (TLS) make it possible to retrieve the structural data of forests in high detail. Moorthy et al. (2008) were able to retrieve the leaf area index (LAI), gap fraction, and clumping index from laser scans in a laboratory experiment with a tree of a similar height as the beeches used in our experiment. Structural parameters such as the total LAI and foliage profile have also been retrieved in natural forest stands using TLS (van Leeuwen and Nieuwenhuis, 2010). Estimations of the directional canopy gap probability, the probability that a beam will not intercept a canopy element in a given direction, can be retrieved from TLS data and are used as a measure of the spatial light regime (Jupp et al., 2009; Ni-Meister et al., 2008; Danson et al., 2007; Huang and Pretzsch, 2010). Advances in the interpretation of the TLS data and algorithms for the computing of the retrieved data offer possibilities for applications in functional–structural modeling of the water and nutrient cycle of trees

(Van der Zande et al., 2009; Todd et al., 2003; Van der Zande et al., 2010). Todd et al. (2003) showed that laser scanning is a promising technique for the estimation of light regime by testing the simulations with measurements of photosynthetically active radiation (PAR) at the forest surface of a sugar maple (*Acer saccharum* L.) stand.

The aim of the present study was to evaluate the performance of a modeling approach based on a voxel representation of the canopy. This was based on TLS measurements of trees in combination with a fast ray-tracing algorithm that calculates the attenuation of incoming PAR. In this approach, the space containing the trees is divided into voxels and every voxel that contains at least one point of the TLS point cloud is assumed to be part of the canopy. The ray-tracing algorithm represents the incoming light rays as lines that decrease in intensity according to Beer's law every time an occupied voxel is intersected. To evaluate the accuracy of the simulated light regime, we measured the light distribution in a juvenile beech stand (*Fagus sylvatica* L.) under controlled light conditions in a greenhouse and used our model to simulate the special situation of this experimental setup. The deviation between simulated and measured light regime in the stand was assessed by different statistical criteria. We analyzed the sensitivity of the model with respect to the input parameters of the model, the edge length of the voxels, and the light absorption coefficient. Finally, we analyzed the computational performance of the model and discuss whether the model is transferable to natural adult forests under variable light conditions.

Methods

Experimental setup

Experimental beech stand

Nine containers, each planted with eight 4-year-old beech trees, were set up in a greenhouse in a way that a dense canopy was achieved. The 72 trees occupied a ground area of about 1.25 m $\times$ 1.45 m. The highest tree was 1.07 m tall, and the mean height of the stand was 0.58 m. The stem diameters 0.05 m above the ground varied between 0.0036 m and 0.0113 m. Subsequent to the TLS measurements (detailed in "Terrestrial laser scanner setup") the leaves were collected and the total LAI was determined to be 2.5. Measurements of the leaf angle distribution allowed an estimation of the vertical projection of the leaf area per square metre of 2.2 [m^2m^{-2}].

Lighting and PAR measurements

A grid of nine 400 W metal halide lamps (Osram HQI-TS 400 W/D, Osram GmbH, München, Germany) in combination with projectors (Lightstream Box-type Maxi 721091.784, RZB GmbH, Bamberg, Germany) was installed above the canopy to provide a constant incoming light intensity. The distance of the lamps to the soil surface of the beech stand was 1.35 m.

Under these lighting conditions, PAR was measured using the Li-190 Quantum Sensor (LI-COR Biosciences, Lincoln, Neb.) and the light intensity of the electromagnetic spectrum ranged from 400–700 nm. On the soil surface beneath the canopy we measured the PAR values at 783 positions on a grid layout with a distance of 5 cm between two measurement positions. For a three-dimensional grid layout with a 20 cm distance between the measurement points, PAR was also measured at layers at a distance of 0, 20, 40, and 60 cm from the soil surface at 224 measurement points.

Terrestrial laser scanner setup

To get information about the shape and spatial distribution of leaves and twigs of the sample trees we used a Riegl Z420i terrestrial laser scanner. This scanner has a range measurement standard deviation of 1 cm and a beam divergence of 0.25 mrad. It operates on the principle of time-of-flight measurements, which means it counts the time between sending out a laser impulse and the detection of the returned echo. The scanner is able to scan a panoramic 360° $\times$ 80° field with one setup. The angular spacing between two measurements was set to about 0.06° at a resolution of 0.002°, which resulted in an average point distance of 2 mm in a 2 m distance. To gather a complete three-dimensional point cloud of the beech group scans were made from four positions at ground level and at seven positions from about 1 m above ground level (**Figure 1**). The setup positions were distributed around the tree groups to scan from many directions with a distance of approximately 2–3 m to the center of the tree group. The size of the greenhouse and the minimal distance of the laser scanner to the scene did not allow a perfectly symmetric layout of the scan positions. All scan setup positions were referenced in a local coordinate system using reflectors and reference targets with a positional average standard deviation of less than 4 mm for all coordinate axes. As the scanner is able to detect the first or last returning pulse, the first pulse was used to ensure that small twigs were also detected by the scanner. In addition to the distance measurements, photographic images from a digital camera attached to the scanner were acquired. To be able to simulate the light conditions adequately, the coordinates of the lamps were extracted manually from the laser scans.

Canopy and light model

The canopy model architecture was solely retrieved from TLS measurements using the cloud of three-dimensional points that result from reflections of the laser beam at the surface of the trees. The virtual space was divided into three-dimensional small cubes (voxels) and the canopy was represented by a set of m voxels $V = \{v_1 \dots v_m\}$ containing

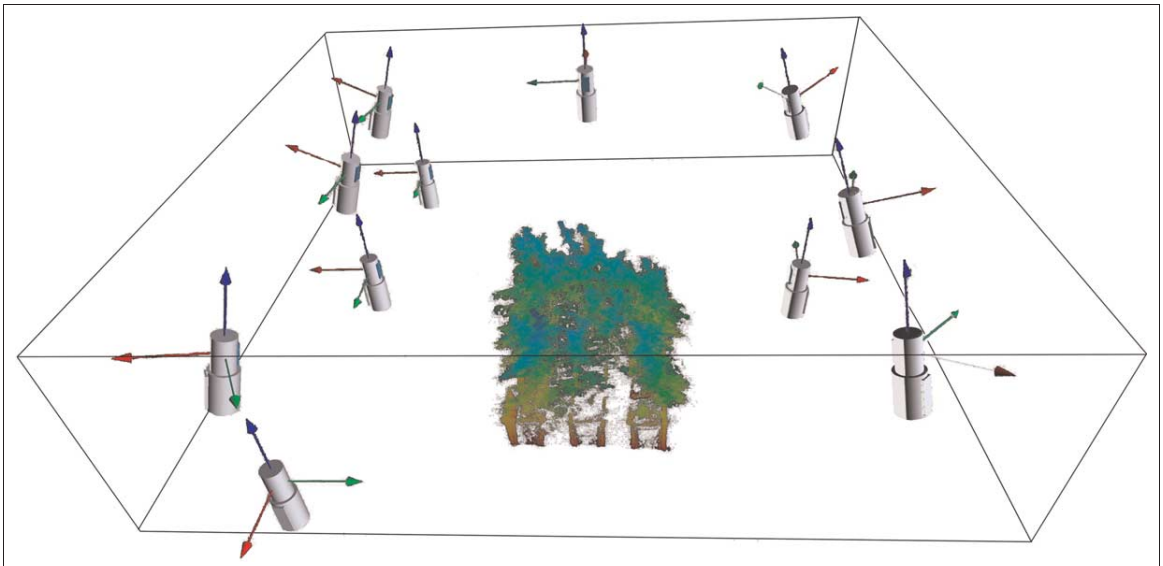

Figure 1. Scanner setup to measure the trees. Multiple positions were used to minimize shadow areas.

at least one point of the TLS reflection points. The number (n) of the voxels that the space is divided into will further be referred as the resolution of the voxel representation. To optimize the memory usage and the computational time (details in "Performance"), the implementation was based on the octree division of space (Wilhelms and Van Gelder, 1992). The space was represented by a three-dimensional cube and is recursively subdivided into eight octants of the same size. The number of voxels equals the number of the smallest cubes that result from the partitioning and is given by

$$n = (2^p)^3, p \in \mathbb{N} \quad (1)$$

where p is the number of subdivisions of the space by the octree algorithm.

The octree division of space optimizes the use of memory by dividing the space into voxels of different size. A three-dimensional region that does not contain any biomass was represented by a large cube with one parameter set, and regions containing biomass were represented by smaller voxels according to the defined resolution.

The incoming light was represented by line segments (R_i) each defined by a starting point (S_i), an ending point (E_i), and a starting intensity (I_0^i). The line segments are herein referred to as rays. Assuming the greenhouse lamps behaved as point light sources, the starting points of the rays were the positions of the lamps. This resulted in a total number of $9 \cdot m$ rays, as the end points of the rays from each of the 9 lamps are the central points of the m voxels that represent the canopy. The light regime was simulated at the positions of the PAR sensors that could be located at voxels not obtained by the canopy. The I_0^i was calculated by setting the position of the lamp into the origin of a coordinate system and then using the solid angle that the voxel i subtended. The azimuth and elevation of the ray were used considering a nonhomogeneous spatial light distribution of the lamps in combination with the projectors given by the retailer in the EULUMDAT format (RZB GmbH, Bamberg, Germany). The coupling with the canopy model was done by calculating the set of voxels $A^i = \{a_j^i\}$ with $j \in [1 \ldots n_i]$ and $a_j^i \in \{v_1 \ldots v_m\}$ that intersect with an arbitrary ray R_i. We applied the Amanatides–Woo algorithm (Amanatides and Woo, 1987) for three dimensions for this step. Then the intersection length d_j^i of the ray R_i and every intersected voxel a_j^i was calculated analytically. The attenuation of light could then be calculated at every position in the canopy using Beer's law

$$I(d) = I_0^i \exp(-k\,d) \quad (2)$$

with the incoming light intensity above the canopy I_0^i [μmol m^{-2}s^{-1}], the attenuation coefficient k [m^{-1}], and the attenuation length d [m] that is the sum of the intersection length of the intersected voxels between the starting point of the ray and the regarded position. Thus, the light intensity I_j^i [μmol m^{-2}s^{-1}] after intersecting the voxel a_j^i is given by

$$I_j^i = I_0^i \exp\left(-k \sum_{c=1}^{j} d_c^i\right) \quad (3)$$

The value for the attenuation coefficient k was kept constant for all voxels in this study. However, the model would be capable of dealing with voxels that are unequally parametrized allowing a division into sun and shade leaves for example.

We further included an optional first-order isotropic scattering of light on leaves and other plant structures. For every canopy voxel, we used Equation (3) to calculate the light that does not transmit the voxel freely and is either absorbed or scattered. The partitioning into absorption and

scattering is given by the scattering coefficient. In that way every illuminated voxel acts as a secondary light source in the scattering model. The targets of the secondary light sources are every voxel of the canopy and the layers that are interesting for the light regime comparison with measurements. The intensity of these secondary light rays are given by the total amount of scattered light by the source multiplied with the solid angle of the target in relation to the voxel scattering the light.

Calibration criteria

Three statistical criteria were used to compare the simulated values of PAR m_i with the n measured values o_i.

Deviations from the measurements are estimated by the root mean square error (RMSE) in total values [μmol m^{-2} s^{-1}] with

$$\mathrm{RMSE} = \sqrt{\frac{1}{n}\sum_{i=1}^{n}(o_i - m_i)^2} \quad (4)$$

The Nash–Sutcliffe efficiency (NSE) is related to the RMSE and defined by Nash and Sutcliffe (1970)

$$\mathrm{NSE} = 1 - \frac{\sum_{i=1}^{n}(o_i - m_i)^2}{\sum_{i=1}^{n}(o_i - \bar{o})^2} \quad (5)$$

where o is the mean value of the observed values. The NSE values are dimensionless and can take values from $-\infty$ to 1.0. A NSE value of 1.0 is given for a perfect match of simulation and observation, if NSE $\leq$ 0, the model is not better than a model that uses the observed mean as a predictor.

The third criterion is the normalized root mean square error (NRMSE). It is given as the ratio of the RMSE to the data range

$$\mathrm{NRMSE} = \frac{\mathrm{RMSE}}{o_{\max} - o_{\min}} \quad (6)$$

with $o_{\max}$ and $o_{\min}$ the largest and lowest observed values, respectively.

Results and discussion

Measured and simulated PAR

The measured PAR intensities at the surface ranged from 6 to 296 μmol m^{-2} s^{-1}. The relative error of the PAR measurements was estimated statistically to be 0.10 and was based primarily on errors of the positioning of the quantum sensor at the grid nodes. Additional errors occurred at positions where the sensor was close to the tree stem, branches, or leaves. At these locations small variations (millimetres) of the sensor position lead to sensible variations of the measured value up to 25%. To elicit effects of data noise due to measurement errors, the measured values were smoothed before the comparison with the simulated values. A Gaussian kernel was used for the smoothing of the values at the ground according to a Gaussian semivariogram model of the measured data. The data were not smoothed for the three-dimensional 0.2 m grid, as the distance between two measurement points was too large with respect to the co-variation length of the local light regime.

The voxel ray tracer was able to reproduce the light regime with canopy depth (**Figure 2**) and at the soil surface with respect to the position of bright spots and shadowed areas (**Figure 3**) as well as the total values of light intensity. The attenuation coefficient was calibrated to $k = 2.1$ m^{-1}. For the 783 measurement points at the soil surface, the model performed with NSE was 0.65, RMSE was 22 μmol m^{-2} s^{-1}, and NRMSE was 0.11. Without smoothing the NSE was 0.56. At the three-dimensional grid NSE was 0.88, RMSE was 124 μmol m^{-2} s^{-1}, and NRMSE was 0.10. Separated into the single layers the NSE values were 0.25 for the layer at soil surface, 0.31 for the layer at 0.2 m height, 0.50 for the layer at 0.4 m, and 0.55 for the layer at 0.6 m. We interpreted the values as a good match of the simulation and the measurement, because in addition to the intrinsic simplifications of the voxel ray tracer approach other factors contributed to a deviation of simulation and measurement: (*i*) PAR measurement errors occurred as discussed above and (*ii*) woody compartments such as stem or branches also contributed points to the laser scan and to the voxel representation of the tree.

The quality of the model could be further increased by separating nongreen voxels from leaf voxels to exclude a transmission of light through woody parts. Applying this correction Moorthy et al. (2008) were able to improve the estimation of LAI from laser scanned data at an experimental setup.

We also analyzed the influence of first-order scattering by keeping the transmissibility of the voxels constant and

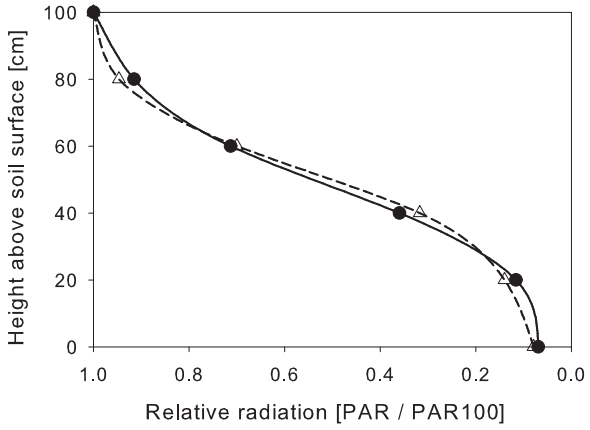

Figure 2. Simulated and measured vertical PAR regime in fractions of the PAR above the canopy 100 cm above the soil surface (PAR100).

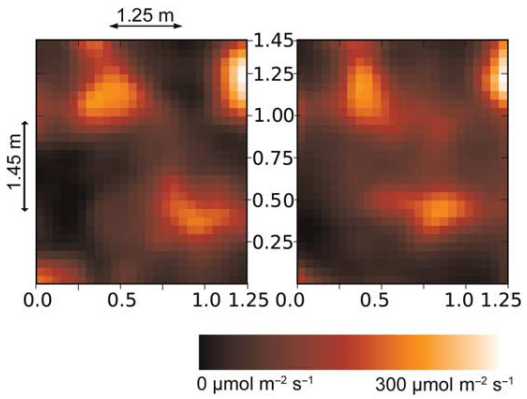

Figure 3. Smoothed measured (left) and simulated PAR values (right) at soil surface beneath the canopy of the artificial beech stand.

assumed a scattering of the light that does not transmit the voxel freely. First-order isotropic scattering increases the simulated light regime at the sensor positions when the transmissibility is kept constant. Using a scattering coefficient of 0.10 (De Pury and Farquhar, 1997) and not changing the value of k, the PAR intensity was increased by 4.3% at the surface in comparison with the calculations without scattering. The RMSE was decreased only marginally at all canopy layers even if k was recalibrated. Because of the minor impact of the isotropic first-order scattering on the modeled light regime as a result of the low PAR scattering coefficient of leaves, we conclude that the simulation of the light regime can be simplified by neglecting the scattering of PAR at the voxels. This is consistent with a study (Wang, 2003) that states that neglecting light scattering is an acceptable simplification for modeling the distribution of PAR within plant canopies. By comparing three different canopy radiation models Wang (2003) concluded that a simple Beer's absorption law can be used to estimate the absorbed visible radiation. However, the situation may be different for old-growth forest stands on days with a high fraction of diffuse sky radiation. It was observed that the relative light intensity below the canopy was higher below the canopy under these conditions because of the effects of scattering. Scattering effects will have a higher impact on the simulated light regime when wavelengths at near-infrared or ultra-violet are simulated because their reflection coefficient is higher than the reflection coefficient for PAR (De Pury and Farquhar, 1997).

Sensitivity analysis

The input parameters of the model are the spatial resolution of the scene, given by the total number of voxels n or the edge length L [m] of the voxels and the light attenuation coefficient k [m^{-1}]. **Figure 4** shows the visualization of the experimental canopy for different resolutions of the voxel space. The sensitivity of the model to the spatial resolution was analyzed by computing NSE between measured and simulated PAR at the soil surface for different values of n. For the resolutions 16^3, 32^3, 64^3, 128^3, 256^3, and 512^3 the NSE values were 0.08, 0.46, 0.64, 0.60, 0.50, and 0.38, respectively.

The model shows an optimum NSE for an edge length of 0.031 m. The decrease for higher L can be explained by an insufficient representation of the canopy by large voxels. Decreasing NSE at high resolutions are due to laser scanner input data errors. Outer trees shaded the laser rays, which resulted in decreasing point cloud densities to the center of the beech stand. These differences of the point cloud density resulted in a different density of voxels in the model only for high resolutions. For low resolutions with larger voxels the effect was leveled out, because a voxel was defined to be part of the canopy if at least one point of the laser scan was inside. The total number of laser scanned points lying inside of a voxel was not included in the model and did not affect the absorption coefficient of the voxel. This simple approach may be improved by the possibility of the model to assign every voxel a distinct absorption coefficient that may be correlated to density of laser scanned points lying in that voxel.

Interestingly, in the region of the optimal value of L the slope of the model efficiency curve was low indicating a robust reaction of the model to changes of L. For values

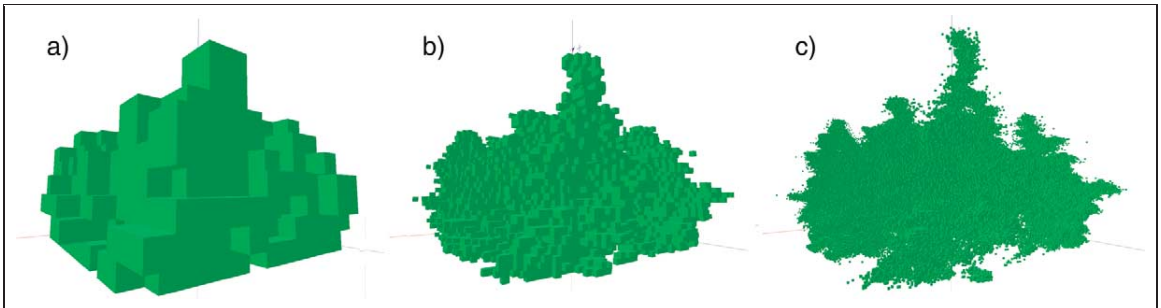

Figure 4. Voxel representation of the artificial beech stand with different resolutions (m, number of voxels representing the space containing the canopy; L, edge length of a single voxel). Visualization with use of the PlantGL framework (Pradal et al., 2009). a) $m = 163$, $L = 12.4$ cm; b) $m = 643$, $L = 3.1$ cm; and c) $m = 2563$, $L = 0.8$ cm.

between 0.008 m and 0.031 m the model efficiency was larger than 0.5. This behavior is a good indication for the transferability of the light model to further applications in natural and adult forests. Obviously the geometry of the canopy can be represented adequately if the intrinsic resolution of the TLS data is not exceeded by the voxel size and, on the other side, if L is small enough to represent the canopy structure with respect to leaf clustering and gaps. A more accurate calibration of L to laborious and expensive field measurements that are not easy to obtain may be not necessary.

For the second input parameter, the attenuation coefficient k, the situation is different. We use k as a calibration parameter of the model and do not give a physical or geometrical description for the calculation of k. The values of k are also dependent on the voxel size L. The calibrated values of k were smaller for large voxels. This can be explained geometrically by the space occupation factor of the canopy in voxel space for different resolutions. For applications of the light model, the parameter k has to be calibrated to the fraction of light reaching the forest soil surface or measurements of other variables related to light regime.

Performance

At a resolution of $n = 512^3$ the canopy occupied about $m = 10^6$ voxels. For every voxel the incoming direct light originating from the nine lamps was calculated resulting in a total number of 9×10^6 rays. On a single processor machine (2.3 Ghz, 2 GB RAM) the computational time was about 4 minutes. At a resolution of $n = 64^3$ the canopy occupied about 3.3×10^4 voxels and the computational time was about two seconds. The algorithm is therefore fast enough to simulate the variable light regime under field conditions that are affected by changes of the sun position and of meteorological factors, such as cloudiness, described by 11 standards for spatial sky luminance models. Moreover, a parallelization of the algorithm can be easily achieved because the calculation of the intersection of a ray and the canopy is independent for individual rays. Including a first-order scattering increases the amount of rays to be of $O(m^2)$ and thus reaching the limit of computational resources when no further simplifications are assumed (Kimes, 1984). In our simulations of first-order scattering we simulated the scattered rays that end at sensor positions to compare the simulations with the measurements.

The largest amount of system memory is occupied by the position and parameters of the voxels occupied by the trees. For each voxel, information such as the absorbed light intensity and the absorption coefficient has to be stored in memory for a fast computation. Increasing resolution of the voxel space increases the amount of voxels. As shown in our experimental setup the fraction of voxels representing the canopy is low. Moreover, typical tree architecture, in particular with older trees, contains large regions with no occupied voxels for example between ground and crown onset or above the canopy. Thus, an octree division of space could optimize the use of memory by dividing the space into voxels of different size. A three-dimensional region that does not contain any element of the plant structure is represented by a large cube with one parameter set, and regions containing biomass are defined by smaller voxels according to the defined resolution. The ray-tracing algorithm could be further optimized by an adaption to nonuniform voxels as discussed in Revelles et al. (2000).

Possible application of the model to old-growth forest stands

Our future goal is to apply the model to old-growth single deciduous trees in natural light conditions. For the application to natural large trees, several further steps must be included in the model. Firstly the distinction between wood and leaf material must be included. This can be done manually (Van der Zande et al., 2006; Huang and Pretzsch, 2010) or automatically if the laser scanner hardware provides additional information on the reflectivity of the surfaces that reflect the laser beam (Côté et al., 2009). Voxels containing woody material will be parametrized to have no transmissivity; the transmissivity of the leaf voxels can be set on a value that reproduces the mean PAR intensity that reaches the forest floor (Bittner et al., 2012a,b).

No laborious light measurements are therefore needed to apply the model in the field. The total intensity of incoming PAR can be provided by meteorological observation stations, and the spatial distribution in the hemisphere can be calculated using daylight distribution models (CIE, 2003). In contrast to the greenhouse light conditions the diffuse radiation of the sky will have to be included next to the direct light from the sun, because the hemisphere is typically fragmented into some hundred parcels and the light rays start at every parcel. This will increase the number of rays in comparison with the nine direct light sources in the greenhouse, but a fast computation on a single processor computer will still be possible.

This study showed that the voxel ray tracing is capable of simulating the PAR distribution in the canopy and the absorption of PAR at every voxel. In functional–structural models of forests this information is important for the calculation of the stomatal conductance of the leaves that depends sensibly on the incoming PAR. Additionally, in photosynthesis calculations the PAR regime is the most important model input. For the estimation of energy fluxes inside the canopy and between vegetation and soil this light model has to be tested and extended to handle the full electromagnetic spectrum of incoming radiation.

Conclusion

Although the model includes a rather complex representation of the canopy retrieved from TLS data, the approach

of the ray-tracing algorithm is simply based on absorption and transmission of radiation. Despite those simplifications, the model was able to reproduce the measured regime of the visible spectrum of light of an experimental greenhouse setup of juvenile beeches. We showed that a voxel ray-tracing algorithm is a promising approach to the simulation of PAR environments in tree canopies.

In comparison with other models, which include a detailed geometrical representation of the canopy, the input parameters are easy to retrieve from laser scans of the canopy. A sensitivity analysis showed that the voxel size should be adjusted in a way that the intrinsic resolutions of the TLS data are not exceeded and should be small enough to represent the canopy structure with respect to leaf clustering and gaps. The light absorption coefficient can be calibrated by using nonspatial input data such as the mean fraction of incoming light that reaches the forest floor. The absorption constant is attached to every voxel and it is easily possible to include an absorption behavior of the leaves that is variable in space. This allows the distinction of sun leaves and shade leaves, which is often related to different physiology or nutrient status, if measurement values for the parametrization are available.

The advantage of a more complex light model such as used in our approach compared with well-known one-dimensional models is given by the spatial resolution of the light distribution within the canopy. Therefore, competition effects of neighboring trees for light or stomatal reactions of single branches and leaves can be simulated in detail by including the spatial heterogenities of the canopy. Performance tests showed that the model is able to deal with variable light input that depends on the time of the day and on meteorological conditions such as clear sky or overcast sky. The algorithm is capable of handling the amount of voxels that are necessary to represent the canopy in a sufficient way. Consequently, the coupling of our approach to a functional–structural tree model that uses the information of the light regime for the estimation of photosynthesis rates and canopy transpiration rates can be directly achieved.

However, as our current approach handles scattering of rays on leaves and other plant structures in a very simple way, the applicability of the model is restricted to PAR simulations. If the model should be used for the simulation of the total spectral intensity of the light including UV and IR, scattering effects have to be analyzed in more detail. The total wavelength spectrum is typically needed for the calculation of the energy balance in a stand as it is required in soil–atmosphere–vegetation transfer models or for simulating the distribution of UV radiation within a stand, which is the most biological reactant radiation and could have influence to the space occupation of trees.

Acknowledgements

This study was conducted in the framework of the following research projects: The role of biodiversity for biogeochemical cycles and biotic interactions in temperate deciduous forests (DFG Research Training Group 1086), Growth and Parasite Defense — Competition for Resources in Economic Plants from Forestry and Agronomy (SFB 607), and Structure and Functions of Agricultural Landscapes under Global Climate Change (PAK 346) all funded by the German Research Foundation (DFG).

References

Allen, M., Prusinkiewicz, P., and DeJong, T. 2005. Using L-systems for modeling source-sink interactions, architecture and physiology of growing trees: the L-PEACH model. *New Phytologist*, Vol. 166, pp. 869–880. doi: 10.1111/j.1469-8137.2005.01348.x.

Amanatides, J., and Woo, A. 1987. A fast voxel traversal algorithm for ray tracing. In: Marechal, G. (Ed.), Proceedings of Euro Graphics '87. Citeseer, Elsevier North-Holland, New York, pp. 3–10.

Baldocchi, D., and Harley, P. 1995. Scaling carbon dioxide and water vapour exchange from leaf to canopy in a deciduous forest. model testing and application. *Plant, Cell & Environment*, Vol. 18, pp. 1157–1173. doi: 10.1111/j.1365-3040.1995.tb00626.x.

Bittner, S., Janott, M., Ritter, D., Köcher, P., Beese, F., and Priesack, E. 2012a. Functional–structural water flow model reveals differences between diffuse- and ring-porous tree species. *Agricultural and Forest Meteorology*, Vol. 158–159, pp. 80–89. doi: 10.1016/j.agrformet.2012.02.005.

Bittner, S., Legner, N., Beese, F., and Priesack, E. 2012b. Individual tree branch-level simulation of light attenuation and water flow of three F. sylvatica L. trees. *Journal of Geophysical Research*, Vol. 117, No. G01037, pp. 1–17.

Bossel, H. 1996. TREEDYN3 forest simulation model. *Ecological Modelling*, Vol. 90, pp. 187–227. doi: 10.1016/0304-3800(95)00139-5.

Brunner, A. 1998. A light model for spatially explicit forest stand models. *Forest Ecology and Management*, Vol. 107, pp. 19–46. doi: 10.1016/S0378-1127(97)00325-3.

Castro, F., and Fetcher, N. 1999. The effect of leaf clustering in the interception of light in vegetal canopies: Theoretical considerations. *Ecological Modelling*, Vol. 116, pp. 125–134. doi: 10.1016/S0304-3800(98)00170-7.

Cescatti, A. 1997. Modelling the radiative transfer in discontinuous canopies of asymmetric crowns. I. Model structure and algorithms. *Ecological Modelling*, Vol. 101, pp. 263–274. doi: 10.1016/S0304-3800(97)00050-1.

CIE. 2003. Spatial distribution of daylight-CIE standard general sky. URL (CIE ISO15469/CIE S011/E-2003, http://www.cie.co.at)

Cohen, S., and Fuchs, M. 1987. The distribution of leaf area, radiation, photosynthesis and transpiration in a Shamouti orange hedgerow orchard. Part I. Leaf area and radiation. *Agricultural and Forest Meteorology*, Vol. 40, pp. 123–144. doi: 10.1016/0168-1923(87)90002-5.

Courbaud, B., de Coligny, F., and Cordonnier, T. 2003. Simulating radiation distribution in a heterogeneous norway spruce forest on a slope. *Agricultural and Forest Meteorology*, Vol. 116, pp. 1–18. doi: 10.1016/S0168-1923(02)00254-X.

Côté, J., Widlowski, J., Fournier, R., and Verstraete, M. 2009. The structural and radiative consistency of three-dimensional tree reconstructions from terrestrial lidar. *Remote Sensing of Environment*, Vol. 113, pp. 1067–1081. doi: 10.1016/j.rse.2009.01.017.

Da Silva, D., Boudon, F., Godin, C., and Sinoquet, H. 2008. Multiscale framework for modeling and analyzing light interception by trees. *Multiscale Modeling and Simulation*, Vol. 7, 910 p. doi: 10.1137/08071394X.

Danson, F., Hetherington, D., Morsdorf, F., Koetz, B., and Allgower, B. 2007. Forest canopy gap fraction from terrestrial laser scanning. *IEEE Transactions on Geoscience and Remote Sensing*, Vol. 4, 157 p. doi: 10.1109/LGRS.2006.887064.

De Pury, D., and Farquhar, G. 1997. Simple scaling of photosynthesis from leaves to canopies without the errors of big-leaf models. *Plant Cell and Environment*, Vol. 20, pp. 537–557. doi: 10.1111/j.1365-3040.1997.00094.x.

Disney, M., Lewis, P., and Saich, P. 2006. 3D modelling of forest canopy structure for remote sensing simulations in the optical and microwave domains. *Remote Sensing of Environment*, Vol. 100, pp. 114–132. doi: 10.1016/j.rse.2005.10.003.

Gastellu-Etchegorry, J., Martin, E., and Gascon, F. 2004. DART: a 3D model for simulating satellite images and studying surface radiation budget. *International Journal of Remote Sensing*, Vol. 25, 73 p. doi: 10.1080/0143116031000115166.

Gayler, S., Grams, T., Kozovits, A., Winkler, J., Luedemann, G., and Priesack, E. 2007. Analysis of competition effects in mono and mixed cultures of juvenile beech and spruce by means of the plant growth simulation model PLATHO. *Plant Biology*, Vol. 8, pp. 503–514. doi: 10.1055/s-2006-923979.

Govaerts, Y., and Verstraete, M. 1998. Raytran: A Monte Carlo ray-tracing model to compute light scattering in three-dimensional heterogeneous media. *IEEE Transactions on Geoscience and Remote Sensing*, Vol. 36, pp. 493–505. doi: 10.1109/36.662732.

Green, S., McNaughton, K., Wunsche, J., and Clothier, B. 2003. Modeling light interception and transpiration of apple tree canopies. *Agronomy Journal*, Vol. 95, 1380 p. doi: 10.2134/agronj2003.1380.

Hemmerling, R., Kniemeyer, O., Lanwert, D., Kurth, W., and Buck-Sorlin, G. 2008. The rule-based language XL and the modelling environment GroIMP illustrated with simulated tree competition. *Functional Plant Biology*, Vol. 35, pp. 739–750. doi: 10.1071/FP08052.

Hoffmann, F. 1995. FAGUS, a model for growth and development of beech. *Ecological Modelling*, Vol. 83, pp. 327–348. doi: 10.1016/0304-3800(94)00101-8.

Huang, P., and Pretzsch, H. 2010. Using terrestrial laser scanner for estimating leaf areas of individual trees in a conifer forest. *Trees – Structure and Function*, Vol. 24, pp. 609–619. doi: 10.1007/s00468-010-0431-z.

Jupp, D., Culvenor, D., Lovell, J., Newnham, G., Strahler, A., and Woodcock, C. 2009. Estimating forest lai profiles and structural parameters using a ground-based laser called 'Echidna (R)'. *Tree Physiology*, Vol. 29, 171 p. doi: 10.1093/treephys/tpn022.

Kimes, D. 1984. Modeling the directional reflectance from complete homogeneous vegetation canopies with various leaf-orientation distributions. *Journal of the Optical Society of America A-Optics Image Science and Vision*, Vol. 1, pp. 725–737. doi: 10.1364/JOSAA.1.000725.

Knyazikhin, Y., Mieben, G., Panfyorov, O., and Gravenhorst, G. 1997. Small-scale study of three-dimensional distribution of photosynthetically active radiation in a forest. *Agricultural and Forest Meteorology*, Vol. 88, pp. 215–239. doi: 10.1016/S0168-1923(97)00036-1.

Kobayashi, H., and Iwabuchi, H. 2008. A coupled 1-D atmosphere and 3-D canopy radiative transfer model for canopy reflectance, light environment, and photosynthesis simulation in a heterogeneous landscape. *Remote Sensing of Environment*, Vol. 112, pp. 173–185. doi: 10.1016/j.rse.2007.04.010.

Lamanda, N., Dauzat, J., Jourdan, C., Martin, P., and Malézieux, E. 2008. Using 3D architectural models to assess light availability and root bulkiness in coconut agroforestry systems. *Agroforestry Systems*, Vol. 72, pp. 63–74. doi: 10.1007/s10457-007-9068-3.

Larsen, D., and Kershaw Jr., J. 1996. Influence of canopy structure assumptions on predictions from Beer's law. a comparison of deterministic and stochastic simulations. *Agricultural and Forest Meteorology*, Vol. 81, pp. 61–77. doi: 10.1016/0168-1923(95)02307-0.

Monsi, M., and Saeki, T. 1953. ber den Lichtfaktor in den Pflanzengesellschaften und seine Bedeutung für die Stoffproduktion. *Japanese Journal of Botany*, Vol. 15, pp. 22–52.

Moorthy, I., Miller, J., Hu, B., Chen, J., and Li, Q. 2008. Retrieving crown leaf area index from an individual tree using ground-based lidar data. *Canadian Journal of Remote Sensing*, Vol. 34, pp. 320–332.

Myneni, R., Ross, J., and Asrar, G. 1989. A review on the theory of photon transport in leaf canopies. *Agricultural and Forest Meteorology*, Vol. 45, pp. 1–153. doi: 10.1016/0168-1923(89)90002-6.

Nash, J., and Sutcliffe, J. 1970. River flow forecasting through conceptual models part I–A discussion of principles. *Journal of Hydrology*, Vol. 10, pp. 282–290. doi: 10.1016/0022-1694(70)90255-6.

Ni-Meister, W., Strahler, A., Woodcock, C., Schaaf, C., Jupp, D., Yao, T., Zhao, F., and Yang, X. 2008. Modeling the hemispherical scanning, below-canopy lidar and vegetation structure characteristics with a geometric-optical and radiative-transfer model. *Canadian Journal of Remote Sensing*, Vol. 34, pp. 385–397. doi: 10.5589/m08-047.

Oker-Blom, P., Pukkala, T., and Kuuluvainen, T. 1989. Relationship between radiation interception and photosynthesis in forest canopies: Effect of stand structure and latitude. *Ecological Modelling*, Vol. 49, pp. 73–87. doi: 10.1016/0304-3800(89)90044-6.

Parveaud, C., Chopard, J., Dauzat, J., Courbaud, B., and Auclair, D. 2008. Modelling foliage characteristics in 3D tree crowns: influence on light interception and leaf irradiance. *Trees – Structure and Function*, Vol. 22, pp. 87–104. doi: 10.1007/s00468-007-0172-9.

Perttunen, J., Sievänen, R., and Nikinmaa, E. 2007. Proceedings of the 5th International Workshop on Functional-Structural Plant Models. Napier, New Zealand, Ch. Assessing the light environment for scots pine in the functional-structural tree model LIGNUM., pp. 59–1–59–5.

Pradal, C., Boudon, F., Nouguier, C., Chopard, J., and Godin, C. 2009. PlantGL: A Python-based geometric library for 3D plant modelling at different scales. *Graphical Models*, Vol. 71, No. 1, pp. 1–21. doi: 10.1016/j.gmod.2008.10.001.

Revelles, J., Urena, C., and Lastra, M. 2000. An efficient parametric algorithm for octree traversal. *Journal of WSCG*, Vol. 8, pp. 212–219.

Ross, J. 1981. The radiation regime and architecture of plant stands. Dr. W. Junk Publ.: The Hague, The Netherlands.

Roupsard, O., Dauzat, J., Nouvellon, Y., Deveau, A., Feintrenie, L., Saint-André, L., Mialet-Serra, I., Braconnier, S., Bonnefond, J., Berbigier, P., Epron, D., Jordan, C., Navarro, M., and Bouillet, J. 2008. Cross-validating sun-shade and 3D models of light absorption by a tree-crop

canopy. *Agricultural and Forest Meteorology*, Vol. 148, pp. 549–564. doi: 10.1016/j.agrformet.2007.11.002.

Sinoquet, H., Sonohat, G., Phattaralerphong, J., and Godin, C. 2005. Foliage randomness and light interception in 3-d digitized trees: an analysis from multiscale discretization of the canopy. *Plant Cell Environment*, Vol. 28, pp. 1158–1170. doi: 10.1111/j.1365-3040.2005.01353.x.

Sinoquet, H., Stephan, J., Sonohat, G., Lauri, P., and Monney, P. 2007. Simple equations to estimate light interception by isolated trees from canopy structure features: assessment with three-dimensional digitized apple trees. *New Phytologist*, Vol. 175, pp. 94–106. doi: 10.1111/j.1469-8137.2007.02088.x.

Todd, K., Csillag, F., and Atkinson, P. 2003. Three-dimensional mapping of light transmittance and foliage distribution using lidar. *Canadian Journal of Remote Sensing*, Vol. 29, pp. 544–555. doi: 10.5589/m03-021.

Van der Zande, D., Hoet, W., Jonckheere, I., van Aardt, J., and Coppin, P. 2006. Influence of measurement set-up of ground-based LiDAR for derivation of tree structure. *Agricultural and Forest Meteorology*, Vol. 141, pp. 147–160. doi: 10.1016/j.agrformet.2006.09.007.

Van der Zande, D., Mereu, S., Nadezhdina, N., Cermak, J., Muys, B., Coppin, P., and Manes, F. 2009. 3D upscaling of transpiration from leaf to tree using ground-based LiDAR: Application on a mediterranean holm oak (*Quercus ilex* L.) tree. *Agricultural and Forest Meteorology*, Vol. 149, pp. 1573–1583. doi: 10.1016/j.agrformet.2009.04.010.

Van der Zande, D., Stuckens, J., Verstraeten, W., Muys, B., and Coppin, P. 2010. Assessment of light environment variability in broadleaved forest canopies using terrestrial laser scanning. *Remote Sensing*, Vol. 2, pp. 1564–1574. doi: 10.3390/rs2061564.

van Leeuwen, M., and Nieuwenhuis, M. 2010. Retrieval of forest structural parameters using LiDAR remote sensing. *European Journal of Forest Research*, Vol. 129, pp. 749–770. doi: 10.1007/s10342-010-0381-4.

Wang, Y. 2003. A comparison of three different canopy radiation models commonly used in plant modelling. *Functional Plant Biology*, Vol. 30, pp. 143–152. doi: 10.1071/FP02117.

Whitehead, D., Grace, J., and Godfrey, M. 1990. Architectural distribution of foliage in 326 individual Pinus radiata D. don crowns and the effects of clumping on radiation interception. *Tree Physiology*, Vol. 7, pp. 135–155.

Widlowski, J., Pinty, B., Lavergne, T., Verstraete, M., and Gobron, N. 2006. Horizontal radiation transport in 3-D forest canopies at multiple spatial resolutions: Simulated impact on canopy absorption. *Remote Sensing of Environment*, Vol. 103, pp. 379–397. doi: 10.1016/j.rse.2006.03.014.

Wilhelms, J., and Van Gelder, A. 1992. Octrees for faster isosurface generation. *ACM Transactions on Graphics*, Vol. 11, pp. 201–227. doi: 10.1145/130881.130882.

Danksagung

Ich möchte mich ganz herzlich bei all jenen Menschen bedanken, die mich auf diesem Weg begleitet haben und so Ihren Teil zum Gelingen dieser Arbeit beigetragen haben.

Mein besonderer Dank gebührt Herrn PD Dr. Eckart Priesack, für das Überlassen dieser Arbeit, für seine vielseitige Unterstützung und die hervorragende Arbeitsatmosphäre in seiner Arbeitsgruppe. Danken möchte ich ihm darüber hinaus für die horizontweitenden Diskurse in die Geschichte, die Theologie und die Philosophie, die ich sehr schätze. Herrn Professor Dr. Jean-Charles Munch danke ich für die Betreuung meines Promotionsstudiums und seine große Unterstützung. Danken möchte ich Herrn Prof. Dr. Urs Schmitthalter für die Übernahme des Prüfungsvorsitzes. Besonders bedanke ich mich bei den Herren Dr. Sebastian Gayler, Dr. Sebastian Bittner und Christian Klein für die gemeinsamen Exkursionen in die Welt des Expert-N, die konstruktive Kritik und die tolle Zusammenarbeit.

Diese Arbeit wurde am Helmholtz Zentrum München im Rahmen des von der Deutschen Forschungsgemeinschaft finanzierten PAK 346 durchgeführt. Ich bedanke mich bei allen Teilnehmern des PAK 346. Besonders bedanken möchte ich mich dabei bei Herrn Prof. Dr. Andreas Fangmeier für seine wohlwollende Unterstützung und ausgezeichnete Kooperation vor und während meiner Dissertation. Ich bedanke mich für die Zusammenarbeit im Rahmen von Pflanzenwachstumsversuchen und der Bereitstellung von Daten bei Frau Dr. Petra Högy und den Mitarbeitern und Mitarbeiterinnen des Fachgebiets Pflanzenökologie und Ökotoxikologie am Institut für Landschafts- und Pflanzenökologie der Universität Hohenheim.

Vielen Dank allen meinen aktuellen und ehemaligen Kollegen und Kolleginnen am Institut für Bodenökologie des Helmholtz-Zentrums München für die stets gute Zusammenarbeit, die außerordentlich gute Arbeitsatmosphäre und die unvergessliche Zeit während und nach der Arbeit. Besonders bedanken möchte ich mich bei Annabel Meyer, Rainer Hentschel, Michael Janott, Peter Hoffmann, Florian Heinlein, Christoph Thieme, Elena Boyko, Dr. Tjaša Gril, Andrés Sauvêtre, Daniela Schacht, Maren Ziegler, Nastasia Wanat, Nguyen Khoi Nghia, Jegan Sekar, Matea Kostrić, Julian Ollivier, Dr. Xia Dong, Dr. Andrea Bannert, Gudrun Hufnagel, Franz Buegger, Dr. Karin Pritsch, und Dr. Christine Klier.

Heiko Fischer danke ich für sein positives Feedback zu dieser Arbeit. Herzlichen Dank an Selma Arnø und Ulrike Bohnet für die Illustration des Einbands.

Von ganzem Herzen danke ich meinen Eltern Lisbeth und Günter Biernath und meinen Bruder Benjamin für ihren stets großen Rückhalt.

Koautorenliste begutachteter Publikationen inklusive deren Zugehörigkeiten

Dr. Sebastian Bittner

Helmholtz Zentrum München, German Research Center for Environmental Health, Institute of Soil Ecology, Modeling Soil-Plant-Atmosphere Systems, Ingolstädter Landstraße 1, D-85764 Neuherberg, Germany.

Prof. Dr. Andreas Fangmeier

Universität Hohenheim, Institute for Landscape and Plant Ecology, Area Plant Ecology and Ecotoxicology, August-v.-Hartmann-Straße 3, D-70599 Stuttgart, Germany.

Dr. Sebastian Gayler

Water & Earth System Science (WESS) Competence Cluster, c/o Universität Tübingen, Center for Applied Geoscience, Hölderlinstraße 12, D-72074 Tübingen, Germany.

Rainer Hentschel

Leibnitz-Zentrum für Agrarlandschaftsforschung (ZALF) e. V., Institute for Landscape Biogeochemistry, Eberswalder Straße 84, D-15374 Müncheberg, Germany

Dr. Petra Högy

Universität Hohenheim, Institute for Landscape and Plant Ecology, Area Plant Ecology and Ecotoxicology, August-v.-Hartmann-Straße 3, D-70599 Stuttgart, Germany.

Peter Hoffmann

Helmholtz Zentrum München, German Research Center for Environmental Health, Institute of Soil Ecology, Modeling Soil-Plant-Atmosphere Systems, Ingolstädter Landstraße 1, D-85764 Neuherberg, Germany.

Christian Klein

Helmholtz Zentrum München, German Research Center for Environmental Health, Institute of Soil Ecology, Modeling Soil-Plant-Atmosphere Systems, Ingolstädter Landstraße 1, D-85764 Neuherberg, Germany.

Prof. Dr. Hans Pretzsch

Technische Universität München, Chair for Forest Growth and Yield, Hans-Carl-von-Carlowitz-Platz 2, 85354 Freising, Germany.

Dr. Stefan Seifert

Technische Universität München, Chair for Forest Growth and Yield, Hans-Carl-von-Carlowitz-Platz 2, 85354 Freising, Germany.

PD Dr. Eckart Priesack

Helmholtz Zentrum München, German Research Center for Environmental Health, Institute of Soil Ecology, Modeling Soil-Plant-Atmosphere Systems, Ingolstädter Landstraße 1, D-85764 Neuherberg, Germany.

Dr. Jana Barbro Winkler

Helmholtz Zentrum München, German Research Center for Environmental Health, Research Unit Environmental Simulation (EUS), Institute for Biochemical Plant Pathology, Ingolstädter Landstraÿe 1, 85764 Neuherberg, Germany.

Lebenslauf

	Christian Jörg Biernath
Geburtsdatum:	02.09.1977
Geburtsort:	Mutlangen
Adresse:	Buchenstraße 9, 85737 Ismaning

Ausbildung und Beruf

1997	Abitur am Limes-Gymnasium Welzheim
1998-1999	Zivildienst im NABU Naturschutzzentrum Wollmatinger Ried
1999-2001	Ausbildung zum Gärtner, Fachrichtung Zierpflanzenbau, Versuchsstation für Gartenbau der Universität Hohenheim
2001-2004	Studium der Allgemeinen Agrarwissenschaften, Universität Hohenheim. Vertiefung: Bodenwissenschaften; Thema der Bachelorarbeit: "Bewertung potentieller Schwermetallbelastungen in Auenböden des Wassertals bei Vișeu de Sus (Rumänien)"
2004-2007	Studium der Allgemeinen Agrarwissenschaften, Universität Hohenheim, Fachrichtung: Pflanzenwissenschaften, Vertiefung: Phytomedizin; Thema der Masterarbeit: "Root Uptake of low Molecular Organic Substances and N by Maize – a $^{14}C/^{15}N$ Tracer Study"
2005/06	Auslandssemester an der University of Wales, Aberystwyth, Vertiefung: Organic

	Farming and the Environment
2007-2008	Doktorand am Institut für Landschafts- und Pflanzenökologie, Universität Hohenheim
2008-2012	Doktorand am Institut für Bodenökologie, Helmholtz Zentrum München

Liste begutachteter Publikationen

Biernath C., Bittner S., Klein C., Gayler S., Hentschel R., Hoffman P., Högy P., Fangmeier A. and Priesack E. 2013: Modeling Acclimation of leaf photosynthesis to increasing atmospheric CO_2 concentration. *European Journal of Agronomy*, 48: 74-87. (**this thesis**)

Bittner S., Gayler S., Biernath C., Winkler J. B., Seifert S., Pretzsch H. and Priesack E. 2012: The performance of a voxel-based canopy light model based on terrestrial laser scans. *Canadian Journal of Remote Sensing*, 38: 619-628. (**this thesis**)

Biernath C., Gayler S., Bittner S., Klein, C., Högy P., Fangmeier A. und Priesack E. 2011: Evaluating the ability of four crop models to predict different environmental impacts on spring wheat grown in open-top chambers. *European Journal of Agronomy*, 35: 71–82. (**this thesis**)

Biernath C., Fischer H. and Kuzyakov Y. 2008: Root uptake of N-containing and N-free low molecular weight organic substances by maize: A $^{14}C/^{15}N$ tracer study. *Soil Biology & Biochemistry*, 40: 2237–2245.